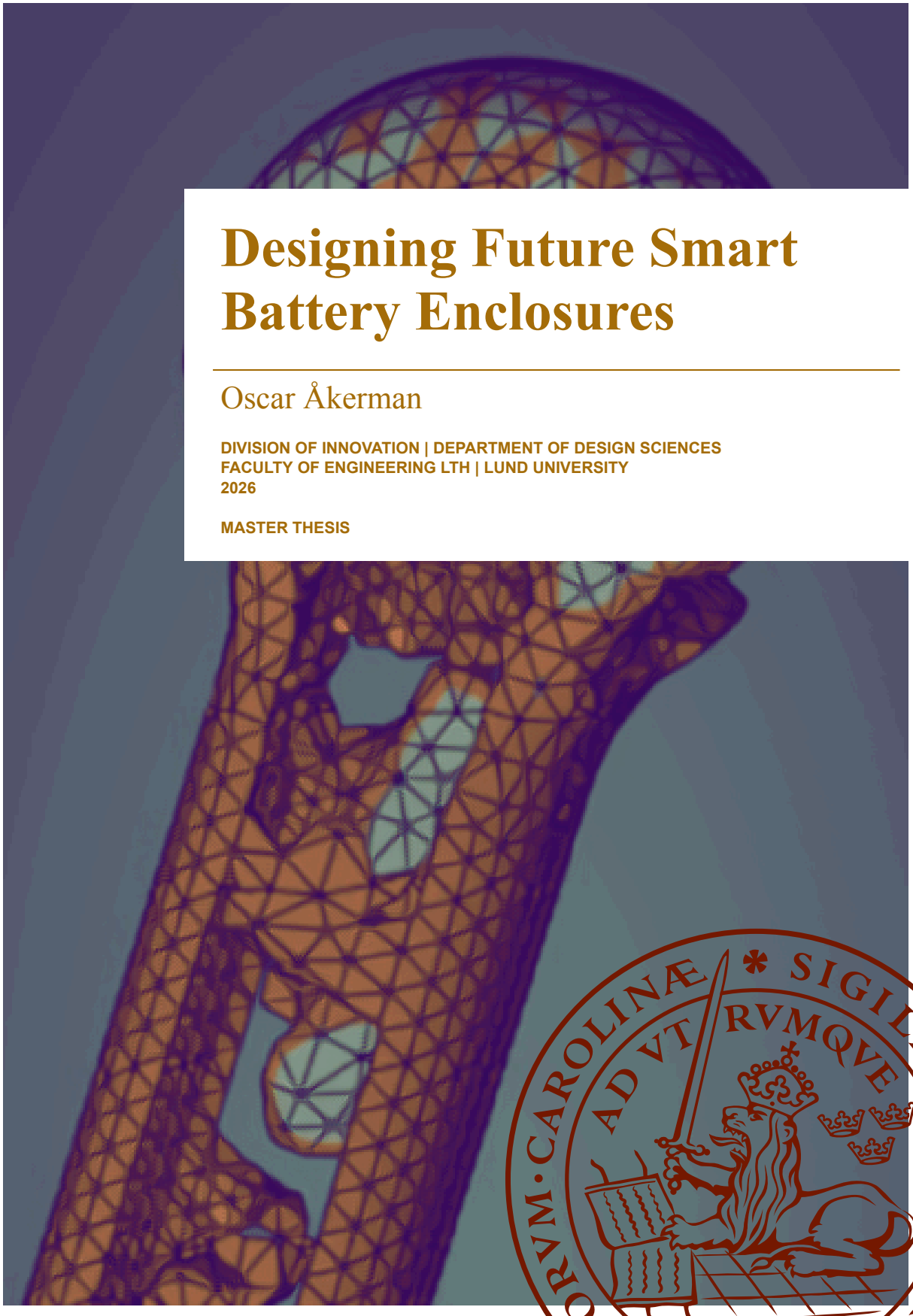

Designing Future Smart Battery Enclosures

Oscar Åkerman

DIVISION OF INNOVATION | DEPARTMENT OF DESIGN SCIENCES
FACULTY OF ENGINEERING LTH | LUND UNIVERSITY
2026

MASTER THESIS

Designing Future Smart Battery Enclosures

Innovation with a design approach

Oscar Åkerman

LUND
UNIVERSITY

Designing Future Smart Battery Enclosures

Innovation with a design approach

Published by
Department of Design Sciences
Faculty of Engineering LTH, Lund University
P.O. Box 118, SE-221 00 Lund, Sweden

Subject: Technical Design (MMKM10)
Division: Innovation
Supervisor: Axel Nordin
Examiner: Jože Tavčar

Abstract

The aim of this project was to explore battery enclosures, specifically for e-scooter batteries, and whether additive manufacturing can be used to enhance existing designs. Furthermore, FEM and topology optimization were explored as tools for optimizing these designs.

A modified Double Diamond approach was used as a guideline for the project. The modified version enters a prolonged optimization phase after the ”discover”, ”define” and ”develop” steps.

The optimization phase consisted of exploration, testing and iteration. Developed concepts were subjected to FE analysis based on UN regulations and IEC standards. Topology optimization was utilized for establishing design principles, which were applied in the iterative ”Master” and ”Maestro” series. In the end, the ”Master 13.7” model was infused with various lattice structures. These latticed models were tested and compared using comparative values. Models for demonstration were ultimately printed using SLS and FDM.

Throughout the project, the only model that narrowly passed all tests was ”Master 13.7”. All ”Maestro” models performed significantly worse. In addition, none of the latticed versions outperformed the original ”Master 13.7”. Nevertheless, the comparative values indicated that the gyroid lattice showed the most promise.

The study concludes that an AM battery enclosure can be designed to pass relevant tests and standards. However, real-life tests are needed in order to determine the validity of these results. Moreover, a business perspective is required in order to evaluate the viability of such a product.

The proposed method of incorporating topology optimization was judged as having questionable usefulness. FEM was, on the other hand, deemed essential to the process.

Keywords: LMT batteries, additive manufacturing, topology optimization, FEM, Double Diamond, lattice structures

Sammanfattning

Målet med detta projekt var att utforska batterihöljen, specifikt för elsparkcykelbatterier, och huruvida additiv tillverkning kan användas för att förbättra de nuvarande designerna. Vidare utforskades FEM och topologioptimering som verktyg för att optimera dessa.

En modifierad ”Double Diamond”-modell användes som guide för projektet. Denna modifierade version inleder en förlängd optimeringsfas efter stegen ”discover”, ”define” och ”develop”.

Denna optimeringsfas bestod av utforskning, testning och iteration. Utvecklade koncept utsattes för FE-analys baserat på förordningar från FN och standarder från IEC. Topologioptimering nyttjades för att etablera designprinciper, vilka användes i de så kallade ”Master”- och ”Maestro”-serierna. I slutändan fylldes ”Master 13.7” med olika gitterstrukturer. De olika gittervarianterna testades och jämfördes med hjälp av jämförande värden. Demonstrationsmodeller printades sedan med både SLS och FDM.

Under hela projektet var det bara ”Master 13.7” som klarade alla tester. Alla ”Maestro”-modeller presterade markant värre. Vidare var det inga gittervarianter som presterade bättre än den ursprungliga ”Master 13.7”. Likväl indikerade de jämförande värdena att gyroid-strukturen hade mest potential.

Studien drar slutsatsen att additivt tillverkade batterihöljen kan designas så att de klarar de relevanta testerna och standarderna. Det krävs dock fysiska tester för att fastställa giltigheten hos dessa resultat. Vidare behövs ett affärsmässigt perspektiv för att utvärdera produktens ekonomiska bärkraft.

Den föreslagna metoden för att inkorporera topologioptimering bedömdes ha tveksam användbarhet. FEM bedömdes däremot vara väsentlig för processen.

Nyckelord: LMT-batterier, additiv tillverkning, topologioptimering, FEM, Double Diamond, gitterstrukturer

Acknowledgements

The following report is my degree project in Mechanical Engineering with Industrial Design at LTH. It was initiated, not as a way of showcasing my knowledge, but rather as a final chance to learn, embracing chaos and uncertainty. So, I will implore whoever is reading this to bear with me on this journey.

I would like to extend my gratitude to Axel Nordin, my supervisor at LTH, for the support, guidance and encouragement throughout the project.

I would also like to thank everyone who helped nudge me in the right direction along the way. Some names that come to mind are David Andersson, Elin Olander, Satabdee Dash and the oddly helpful customer support guy at Cling Systems. Without these people, the project likely would have looked a lot different.

Finally, I would like to thank you, the reader, for taking the time to read a document that is very meaningful to me. It is not only the result of months of hard work, but also the culmination of my five-year degree. I hope you find what you need in this report and that the arduous labour was not in vain.

Lund, March 2026

Oscar Åkerman

Table of Content

List of acronyms and abbreviations

CAD	computer-aided design
EU	European Union
FDM	fused deposition modeling
FEA	finite element analysis
FEM	finite element method
IEC	International Electrotechnical Commission
IP	ingress protection
LMT	light means of transport
MMA	method of moving asymptotes
PA	polyamide
PBF	powder bed fusion
PDE	partial differential equation
SCP	sequential convex programming
SIMP	solid isotropic material with penalization
SLA	stereolithography
SLS	selective laser sintering
TPMS	triply periodic minimal surface
UN	United Nations

1 Introduction

1.1 Background

This master's thesis project was carried out at the Department of Design Sciences, at the Faculty of Engineering, LTH, at Lund University, and it was for the most part done independently. It is part of a research project, initiated by Lund University and University of Glasgow, with the aim of investigating how additive manufacturing and optimization may be applied in battery enclosure design.

More broadly, this particular project is all about experimenting with the use of emerging technologies. Additive manufacturing (AM), electric vehicles, FEM and topology optimization, the subjects that will be touched upon, all have experienced an increase in use as well as availability. This recent increase in availability creates an optimal opportunity to investigate their compatibility with each other.

With regards to electric vehicles, there has been a substantial shift in popularity and sales during the last decade. In 2024, the electric car sales exceeded 17 million globally, which corresponds to a sales share of about 20% [1].

Furthermore, multiple sustainable and electric powered vehicles, such as e-bikes and e-scooters, have been tested during the last decade in major urban areas everywhere [2],[3]. The latter, e-scooters, have especially grown in popularity in Lund, where this project is written. Since they arrived seven years ago, they have been a hotly debated topic among the locals [4].

Such a development, where rental e-scooters grow into an important form of micro-mobility, is one which can be observed in many cities around the world [5],[6]. E-scooters offer flexibility when it comes to short urban trips, while also being low-cost and relatively environmentally friendly [6]. Consequently, many people are substituting taxis, car rides and sometimes even walking, for shared e-scooter transportation [3]. Due to the popular demand, they are receiving huge investments and show substantial growth

in the market, with some estimates forecasting up to $90 billion in revenue in 2030, compared to $3 billion in 2019 [3].

Another technology on the rise is that of additive manufacturing, which has seen a proliferation throughout many different industries, such as automotive, aerospace, medical treatment, art and much more [7]. The technology became commercially available following the introduction of a stereolithography (SLA) machine in 1988. Ever since, the industry has grown exponentially in terms of available systems, materials and technologies [8]. It has been estimated to reach as high as $196.8 billion by 2035 [9], and is overall currently sat at $21.9 billion globally, according to the Wohlers Report 2025 [10].

Meanwhile, the finite element method (FEM) recently celebrated the eightieth anniversary since its conception [11]. The early workings of the FEM can be found as far back as the 1940's [11]. However, the actual FEM software did not begin development until the early 1960's. And it would take about another decade before the two most popular FEM softwares, ABAQUS and LS-DYNA (later ANSYS LS-DYNA), would be released [11],[12]. Currently, FEM is widely used in loads of different industries, as it is able to solve many large and complex problems [11].

The birth of the finite element method also marked a shift in the field of topology optimization, as it resulted in the first numerical procedure for FE-based topology optimization [13]. Topology optimization and structural optimization in general had at that point been limited to pure mathematics, having seen multiple mathematical papers using variational calculus [14]. While the design focus initially was set on cross-sectional areas of simple truss structures [13],[14], the focus eventually, as a result of growth in the field and digitization, shifted towards optimizing general shapes and topologies [13]. After decades of development and innovation, topology optimization has become among the leading and most active fields within design optimization [14].

This project will be an amalgamation of these aforementioned emerging technologies. In spirit, it is an exploration of what is possible when these are used together in the context of a design project.

More specifically, this project will investigate whether it is possible to make use of additive manufacturing in order to enhance and optimize the enclosures of battery packs. The optimization of the design itself will furthermore experiment with the use of FEM and topology optimization as a part of the design process.

This is all done within the context of a partnership with the University of Glasgow, where a priority outcome is the co-development of smart, lightweight, and recyclable energy storage enclosures for drones, EVs, and e-mobility platforms. This partnership will explore AM-enabled nanocomposite structures, combining thermal management, strain and temperature sensing, and EMI shielding functionalities. Advanced materials such as CNT-, MXene-, and graphene-reinforced bio-based polymers, e.g. polyamide (PA) 11, will be employed. Lattice architectures will be tailored via generative design and experimentally validated.

1.2 Purpose

The main purpose of this project is to experiment with the use of additive manufacturing, and determine whether or not it has a place in the world of battery enclosure designs.

The project also investigates how FEM and topology optimization might be used within the context of a design process, given the many variables the problem entails.

Underlying these goals is the hope to create a relatively commercially viable product, which would indicate a promising future for the aforementioned technologies in battery casing design.

1.3 Further Constraints

1.3.1 Context

There are lots of types of light means of transport (LMT) batteries. This made it necessary to pick one to base the project on. Hence, a relatively standard electric scooter battery was decided upon as a basis for the project [15][16]. Subsequently, it is also assumed that this is a lithium-based system, considering that this is the case for most, if not all, such batteries.

The chosen battery is attached to the outside of the scooter framework, unlike some batteries that reside inside the scooter [17]. The latter version would leave little room for improvement which is why it was rejected for this project. More details on the battery can be found in the research chapter.

1.3.2 Necessary Criteria

An important criterion within the development and optimization process was the minimization of mass. This is important for constraining the design from using too much material, which would be an easy way of solving many of the problems. As mentioned in the purpose, the goal is to end up with a relatively commercially usable end product. This means that it should not deviate too much in terms of weight. If the enclosure is to be commercially viable, it is also imperative that relevant regulations are being followed. Adding to this, it is necessary that proper testing against pertinent standards is conducted. The outcome of these tests is a determining factor regarding the success of the project.

1.3.3 Other limitations

Any considerations regarding the functionality of the inner battery pack and its cells will be considered to be beyond the scope of the project. This is mostly due to the lack of access to the desired battery. However, time constraints are also a factor. As a result of this limitation, the battery pack, its cells and its wiring will only be considered in so far as whether or not they will fit. There will be no overcharge testing, discharge testing, short circuit testing or anything like it.

The lack of an actual battery in testing also means that some results will require interpretation, along with a healthy dose of skepticism. Moreover, the use of FEM will further shift the results. The numerical simulations are approximations and therefore cannot be fully trusted.

It should also be noted that there, during this project, was no consideration given to screws or other fastening methods. For this reason, all ideas, computer-aided designs (CADs) and simulations will be assuming the subject to be one piece.

Furthermore, the choice of AM-technology was limited to what was available at the institution. For this reason, the alternatives were immediately narrowed down to stereolithography (SLA), selective laser sintering (SLS) and fused deposition modeling (FDM).

The project had no budget and was funded only by the author.

1.4 Initial Problem Definition

Design an e-scooter battery enclosure, attached to the frame of the e-scooter, in one piece, such that it weighs as little as possible while still being **operational**. The design should be able to be printed effectively using an AM method. **Operational** is defined as possessing the following characteristics:

- Maintaining the usual capabilities of an electric scooter battery
- Following relevant European Union (EU) battery regulations
- Complying with relevant United Nations (UN) regulations
- Passing other relevant test standards*

*An assessment will have to be made regarding what standards are defined "relevant". There are without any doubt plenty to choose from, as well as plenty too many for them all to fit within the scope.

1.5 Structure of this Thesis

This thesis contains eleven chapters outlining the steps and decisions taken within this project. Chapter 1 introduces the project, its purpose and its background. The problem formulation forms the starting point for this project. Subsequently, Chapter 2 describes the chosen methodology (Double Diamond) and how it is utilized. Chapter 3 shows the result of the gathering of information, following the Double Diamond structure. Chapter 4 showcases the chosen design brief which would guide the subsequent design process. The ideation part of the design process is shown in Chapter 5 together with the selection of a few concepts. Chapter 6 shows the following tests of these concepts, along with other tests. Chapter 7 describes the process of iterative improvement of a chosen concept. In Chapter 8, lattices are applied and tested with the intent of improving the concept. Chapter 9 shows the printing results. Finally, Chapter 10 reflects on the project and discusses improvements. Chapter 11 concludes the project.

2 Methodology and approach

2.1 Double Diamond

The project will approximately follow a double diamond design process, as described by the Design Council. This is a widely accepted description of the design process, used and referenced worldwide. The double diamond model, as the name would suggest, consists of two diamond shapes with two phases each [18]. The first diamond can be seen as the process of finding the right problem, while the other is the process of finding the right solution to this problem [19]. Across the four phases the diamonds summarize the convergent and divergent thinking needed for the design process [18]. The phases are shown in Figure 2.1, and explained further below.

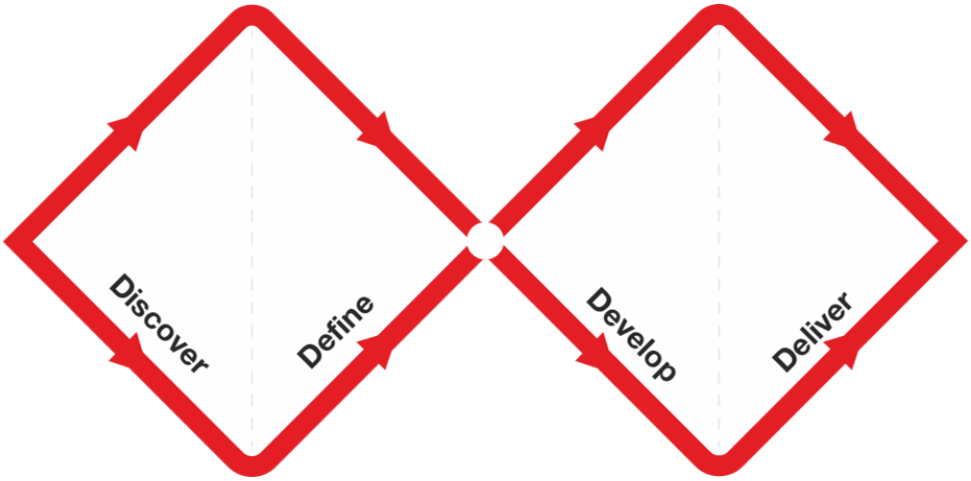

Figure 2.1: Visualization of the double diamond model (Source: the Design Council, https://www.designcouncil.org.uk/our-resources/the-double-diamond/, Creative Commons, CC BY 4.0)

2.1.1 Discover

The “discover” phase is about exploring and questioning the initial challenge through a gathering of information and research. The goal is to get a good understanding of the topic and what needs and challenges it presents. Being a divergent phase, the emphasis is on expanding the thinking to find and explore the fundamental issues [18].

2.1.2 Define

During the “define” phase the different findings are analyzed with the aim of making sense of them. It is now time to converge upon a clear design brief. The design brief should define precisely the problem to be solved, based on the insights from the research [18].

2.1.3 Develop

The “develop” phase concentrates on generating, testing and iterating through multiple solutions. The goal is again to diverge and explore as many different solutions as possible [18].

2.1.4 Deliver

In this phase the best solution is selected [18]. There are many methods of doing this, such as “pros and cons”, intuition, decision matrices and even combining concepts [20]. The final concept is then further refined and prepared for implementation or launch [18].

2.2 Design thinking - why and how?

There are many similar processes to the Double Diamond, such as the IDEO three-phase design model, the Ulrich Eppinger method and the Stanford design school’s five iterative steps. These all share the same foundational design thinking principles: user-centricity, iterative prototyping and creative ideation [21]. Innovation, while chaotic, is in these models divided into a system of spaces, which all need to be passed at some point. These spaces together form a continuous design flow [22]. In short, these models summarize the crucial characteristics of design work [23]. An important part of these models is the concept of iteration. The design

process is not meant to be linear [23]. It is meant for exploration, experimentation and iteration, where there is something new to learn in each attempt [22],[23]. An important function of specifically the Double Diamond model is that it summarizes the convergent and divergent thinking of the design work. This type of thinking is one that has been agreed upon by many theorists on the topic [23]. The Double Diamond is furthermore highly adaptable. It is not meant as a scientific formula, as this would make it limiting and too narrow. It instead favours continuous customization according to current challenges. The skeleton of the model does however still provide a way of assessing the status of the project, which is practical when collaborating with multiple parties [23]. Maybe most importantly though, design models in general enforce the fact that innovation is not necessarily a matter of genius. Rather, it requires hard work together with the right approach. The design processes thus provide the steps such that hard work trumps genius [22].

Design thinking has been recognized as a robust way of tackling complex problems in an ever-changing world [21]. It remains an efficient way of considering people's needs, while recognizing feasibility, business strategy and market opportunity [22]. Despite changes in the field, technology and social context, the manner in which designers work remains roughly the same. For this reason, along with its adaptability, the Double Diamond is highly relevant to this day [23].

2.3 Contextualized within this project

2.3.1 Research and brief

The discovery phase of this project consisted entirely of research and information gathering regarding all related topics. More about the research can be read in the following chapter. Afterwards, all useful insights were assembled into a more specific brief. This brief included all product specifications and target values that were needed for concept generation and evaluation.

2.3.2 Optimization and refinement

The workflow of the optimization process began with brainstorming ideas, as a part of the "develop" phase. Then the most promising ones were selected and CAD:ed. It is at this point the process deviates from the regular Double Diamond, and instead follows the modified one seen in Figure 2.2. Instead of moving towards the "deliver" phase, the rest of the project focused on optimizing according to the brief. This phase was focused on testing and exploring, in the spirit of design thinking.

However, since the timeline of the project still had to be respected as a top priority, there was still a limit to the amount of testing that could be done.

The CADs were subjected to FEA with the appropriate load cases. This, in conjunction with topology optimization, was performed in order to explore and gain information, thus shaping another divergent phase. Furthermore, topology optimization was applied to empty design spaces throughout the process. This gave an idea of what the computer deemed to be the best material distribution for the given problem. Other concepts, such as a simple rectangular model, were tested as well, again with the aim of exploring.

All information was analysed and converged into one concept. This idea could then be subjected to further refinements through iterative improvement, until the brief was fulfilled. This series of improvements was dubbed the "Master" series. At this point, only the shape was considered, saving internal structure for later. FE analysis and optimization were again performed in order to constantly update the pool of information. Besides the main series, another iterative process was done as well, this time with a model based solely on topology optimization. This series was dubbed the "Maestro" series.

The project diverged one final time when lattice structures were tested for the chosen model. These were compared using comparative values and one lattice was acknowledged as the most promising.

A visualization of the whole optimization process can be seen in Figure 2.3. Some of the concepts and processes will be explained later in the project.

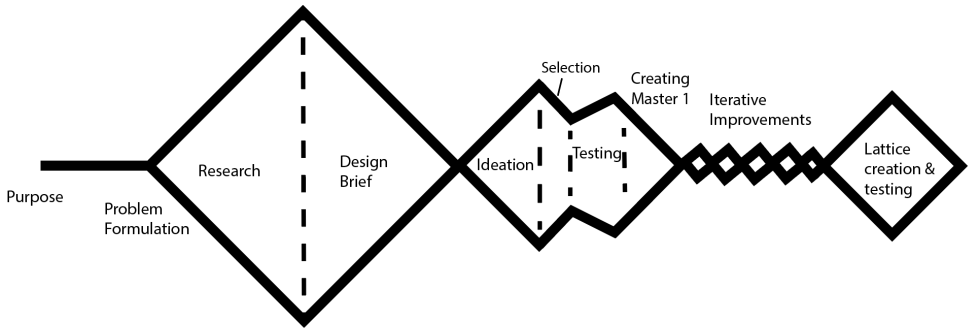

Figure 2.2: Modified Double Diamond model utilized in this project. (Source: Author's own work)

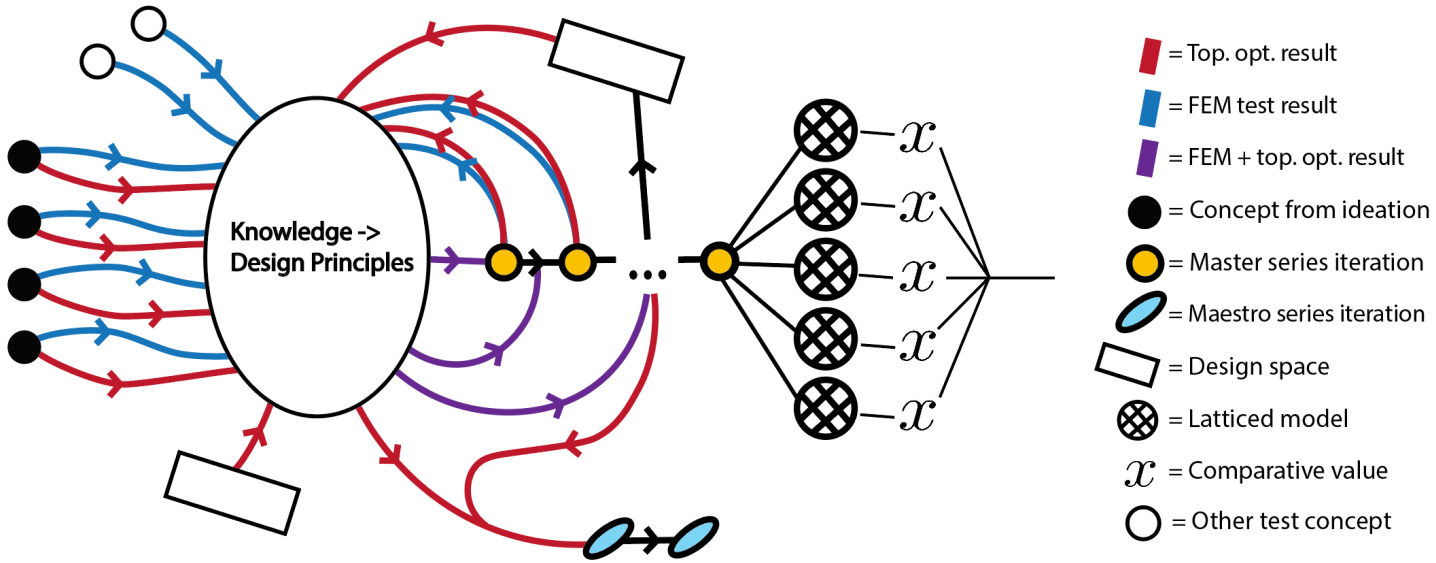

Figure 2.3: Optimization procedure after concept selection. (Source: Author's own work)

3 Theory

3.1 Research Methodology

When beginning the research process, the initial problem to solve revealed three main areas to study: Additive manufacturing (and related materials), batteries along with relevant regulations and topology optimization (in conjunction with FEM). It was crucial to have an underlying understanding of these areas if the project was to be done justice. What will ensue is the result of a comprehensive exploration of these topics. For the most part, research articles, books and official documents were used. Most research articles were discovered through databases such as SCOPUS, ScienceDirect, LUBsearch, FINN, ArXiv and more. Additionally, besides some personally owned course literature, many books (and journals) were accessed through the Springer Nature Link platform.

It should also be noted that a lot of the research was carried out in parallel with the actual project work, even though most of it was completed early on. As new challenges arose, it was important to update and add to the already gathered theory.

3.2 Additive Manufacturing

Additive manufacturing, or AM, is a manufacturing method where an additive process is used, usually by depositing material layer by layer. This allows for the manufacturing of complex geometries [24], in comparison to traditional manufacturing processes where material is subtracted. It also facilitates the manufacturing of products directly from a 3D CAD model, which acts as a geometrical representation [7].

Similar concepts to additive manufacturing can be found as far back as 150 years ago, in the context of topography and photosculpture [25]. However, the conception of modern additive manufacturing could, perhaps more appropriately, be seen as synonymous with a patent by Otto John Munz in 1951 [8]. His technique, involving the selective layerwise exposure of a transparent photo emulsion, is often seen as the origin of the modern stereolithographic technique [25]. Other techniques

surfaced the following decades, and the commercial processes from the late 80s to early 90s would go on to be the foundation for the process variations developed over the following twenty years [8],[25]. The most prevalent methods of AM are FDM, SLA and SLS [26].

A reason for its rapid growth is its ability for flexibility within production, low-cost and short production time (compared to conventional manufacturing). All this while maintaining a high product quality [24]. The technology is moreover able to create these complicated designs with minimum waste [7].

For all of these reasons, additive manufacturing can be, and is, employed in versatile domains, such as medical treatment, art, automotive, aerospace and much more [7].

3.2.1 FDM

Fused deposition modeling, or FDM, is a material extrusion based AM technology [8]. The term is generally used to describe methods where a fine filament of material is being heated and melted at a nozzle, and then extruded onto a platform or onto previously deposited layers [8],[27]. The filament traces out each slice of the model, layer by layer, so that they bond in their semi-liquid state. It is akin to an automatic hot glue gun [8]. For FDM, the continuous filament normally consists of a thermoplastic polymer. The thermoplasticity is essential for this method, as it allows the filament to fuse and then solidify at room temperature [27]. FDM may also be combined with composite filaments, which leads to more robust, rigid and thermally stable results. This is suitable for functional prototypes as well as aerospace and automotive industries, where mechanical performance and longevity are required [26].

Material extrusion technologies generally have low-quality surface finish compared to other AM technologies. Especially visible is the “stair-step” effect arising from sloping surfaces [8]. Other downsides involve weak mechanical properties [27], susceptibility to warping [28], high anisotropy due to the layering, and the need for sacrificial support material in the case of overhangs [8]. There is also a limited number of thermoplastic materials available [27].

On the other hand, FDM machines are the most affordable and easy to use, while not requiring high-cost materials [26]. Furthermore, FDM is relatively high-speed with a simple process [27]. FDM also has the benefit of being able to easily fabricate multi-material parts [26].

Material extrusion is a continuously improving technology, with new machines constantly arriving at the market [8].

3.2.2 SLS

SLS stands for selective laser sintering, and is another AM method. It is a powder bed fusion (PBF) method, which involves spreading and sintering powder material layer by layer [24], see Figure 3.1. It was the first commercialized PBF method, developed at the University of Texas in Austin [29].

The fundamental characteristic of all PBF methods is thermal sources enabling fusion between powder particles. Usually the thermal source is a laser. All PBF methods also include a method for controlling the fusion and a mechanism for adding and smoothing powder layers [30]. The laser scanning, if that is what is being used, does not completely melt the powders. However, they do still fuse on a molecular level due to the elevated surface temperature on the grains [27].

SLS can use a wide range of materials, such as polymers, composites, metals, alloy powder and ceramics [29],[27]. It is particularly associated with the use of polymers and plastics [29],[27], such as Polyamide (PA) 11 and PA 12, which are commonly used. These exhibit low processing temperatures, minimal laser power requirements, and high precision in the final product. The end product, when e.g. PA 12 is semi-crystalline, is robust, has high chemical resistance and low moisture absorption [29]. PA 11 has the added advantage of having high elasticity and being fully isotropic [31]. Additionally, PA 11 is derived from renewable sources, such as castor oil [32]. Polyamide powders are also able to be recycled to various degrees [33].

SLS also has the benefit of high resolution and high quality, while having strong, consistent mechanical properties [27],[31]. Furthermore, it does not require any support structures. The drawbacks are slow printing and it being rather expensive compared to other methods [31].

The speed of SLS is primarily determined by laser power and the thermal characteristics of the material. These in turn affect the speed at which the powder is processed. Since the speeds are highly variable, the technology is adaptable with regards to demands of speed and part quality [26].

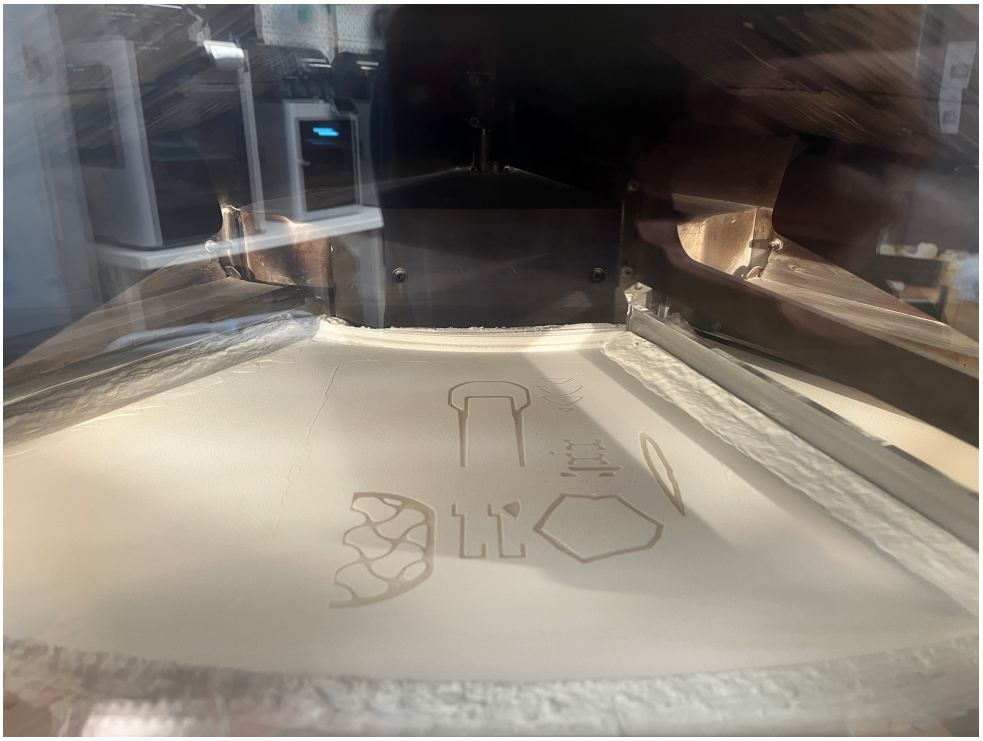

Figure 3.1: Inside of SLS printer during printing, showcasing the powder bed used. (Source: Author's own work)

3.3 AM design considerations and ideas

When designing for additive manufacturing, there are multiple factors that need to be taken into consideration.

3.3.1 SLS holes

If hollowed out parts are created with SLS, leftover unsintered powder will most likely be trapped inside the cavity. For this reason it is often recommended to add a couple of small holes to the model, such that the powder can escape [31].

3.3.2 Anisotropy

For material extrusion systems, such as FDM, there will always be some level of anisotropy. Because of the layering, the material will be more susceptible to

delamination from tearing against the layers. This is due to the plastic itself being stronger than the bond between layers. FDM parts in particular will be susceptible to delamination when under tension, making them more suitable for compression. However, SLS parts will also have some anisotropy [8].

3.3.3 Overhang and support material

Overhanging features might, depending on the method, need to be supported using support material. It is not possible to print in the air when for instance using material extrusion. The support material is sacrificial and will be removed during post processing. Hence, it is important to adapt the design and the printing direction, in order to minimize waste [8].

3.3.4 Ribs

Large surface areas and walls will often be quite vulnerable to distortion during the printing process. Having these areas will also result in an excessively flexible end product, especially at these points. Ribs are a way of increasing the rigidity of the walls, without adding too much material. They are added on the inside, along the walls, thus increasing bending resistance. They can also be hollowed out, further reducing mass [8].

3.3.5 Lattice structures

Lattice structures are cellular structures consisting of unit cells which are repeated in order to form a larger volume [24]. The idea is often to transform a solid structure into a ‘truss’ structure by utilizing a periodic arrangement of interconnected struts, where each period is one unit cell. This can be done by either converting the entire part, or leaving the outer shell, or subdividing the part into lattice areas and solid areas [24],[34]. The result is something like what is seen in Figure 3.2.

There are many types of lattice structures that each have different properties and attributes [24]. Many of these are derived from the crystal structures formed by atoms, ions, molecules or metallic crystal systems, like face-centered cubic (FCC) and body-centered cubic (BCC) [34]. The patterns in the strut arrangements on the other hand can also be arbitrary, instead of periodic [34].

The topological layout of the struts, as well as the loading orientation, is highly significant for how the structure responds globally [34]. By varying cell size, spacing and strut diameter [24],[35], the functional and mechanical properties of

the lattice structure can be influenced and adjusted [34]. This can subsequently be optimized using FEA [24].

The advantage of lattice structures is that part weight is greatly reduced without overtly compromising part strength [24]. This is thanks to lattice structures having a high strength-to-weight ratio, often with capabilities and properties that can be tailored based on the need [34]. The loss of weight additionally leads to lower production time and cost [24].

For these reasons, and many others, lattice structures have been revolutionary in advanced engineering applications [34].

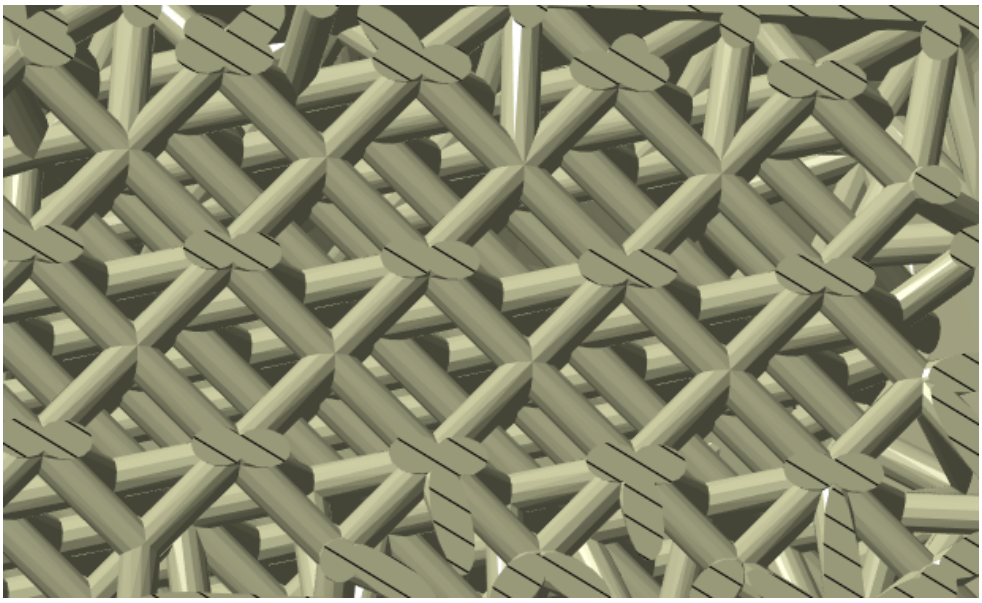

Figure 3.2: A diamond lattice, created in ANSYS Discovery. (Source: Author's own work)

3.3.5.1 Bending-dominated vs Stretching-dominated

The mechanical behavior of lattices can be categorized as either bending-dominated or stretching-dominated. These differ in that stretching-dominated lattices are stiffer while bending-dominated lattices have better energy absorption [36].

Studies have shown that under compression, the behaviour depends on the strut angles which in turn affect the competition between axial compression and beam bending. This goes on to also influence the global behaviour [34]. In fact, the macroscopic deformation properties of the whole lattice are determined by how the struts deform (bending or axial compression) and their topological arrangement. The lattice showcases low strength and high ductility when it is bending-dominated, and the opposite when stretching-dominated [34]. This is due to elastic stiffness,

yield strength and other mechanical properties also being dependent on the amount of bending vs compression a certain topology has [34]. Due to their flexibility, bending-dominated lattices are able to reach a stress plateau more slowly, making them more efficient in absorbing energy [37]. Conversely, stretch-dominated lattices, whose struts hold high tensile or compressive loads, are more susceptible to brittle failure, making them less efficient in absorbing energy [37].

There is a way to predict the behavior of lattice structures based on the connectivity, using the Maxwell criterion [35]. However, it is not always this simple. The density, the orientation and the loading of the lattice can all influence the properties of the structure [37],[38]. For instance, the simple cubic lattice is defined as bending-dominated through its connectivity [39]. However, depending on orientation and loading direction, it has been shown to exhibit stretching-dominated behaviour as well [38],[39].

Another bending-dominated lattice, per definition, is the diamond lattice [40]. This lattice differs from the simple cubic in that it is more compliant (low stiffness) [41]. It has also shown low compressive properties, such as yield stress, plateau stress and energy absorption [41]. Similarly to the cubic, the diamond lattice can show stretching-dominated behaviour as well [42].

Both the simple cubic and diamond lattice have been shown to be effective in reducing peak impact stress [42].

3.3.5.2 TPMS lattices

Triply periodic minimal surface (TPMS) lattices are lattices comprised of periodic surfaces [37]. The geometry of these surfaces is defined by implicit functional equations, resulting in a three-dimensional porous structure [37],[43]. Some examples of TPMS lattices are lidinoid, gyroid and Schwarz [37].

These continuous, non-self-intersecting and smooth surfaces can improve mechanical performance through efficient stress redistribution [43],[44]. In contrast to cellular structures, these lattices lack curvature discontinuities and sharp stress concentrations where high stress concentrations can occur [37].

Other desirable properties exhibited by these lattices include high energy absorption, fatigue resistance, high stiffness-to-weight ratio, uniform deformation under load and more [45],[44]. This makes them promising for use in energy absorbers or lightweight damping components [44].

One of the more widely used TPMS lattice is the gyroid lattice, seen in Figure 3.3, which can be represented using a combination of sine and cosine functions [46]. This lattice has shown considerable potential within engineering through its aptitude for improving energy absorption [45]. The properties of the gyroid lattice, like with the cubic and diamond, also depend on the orientation [45]. Some studies

also suggest that a lower volume fraction and a higher wall thickness increase the energy absorption capabilities [47],[45].

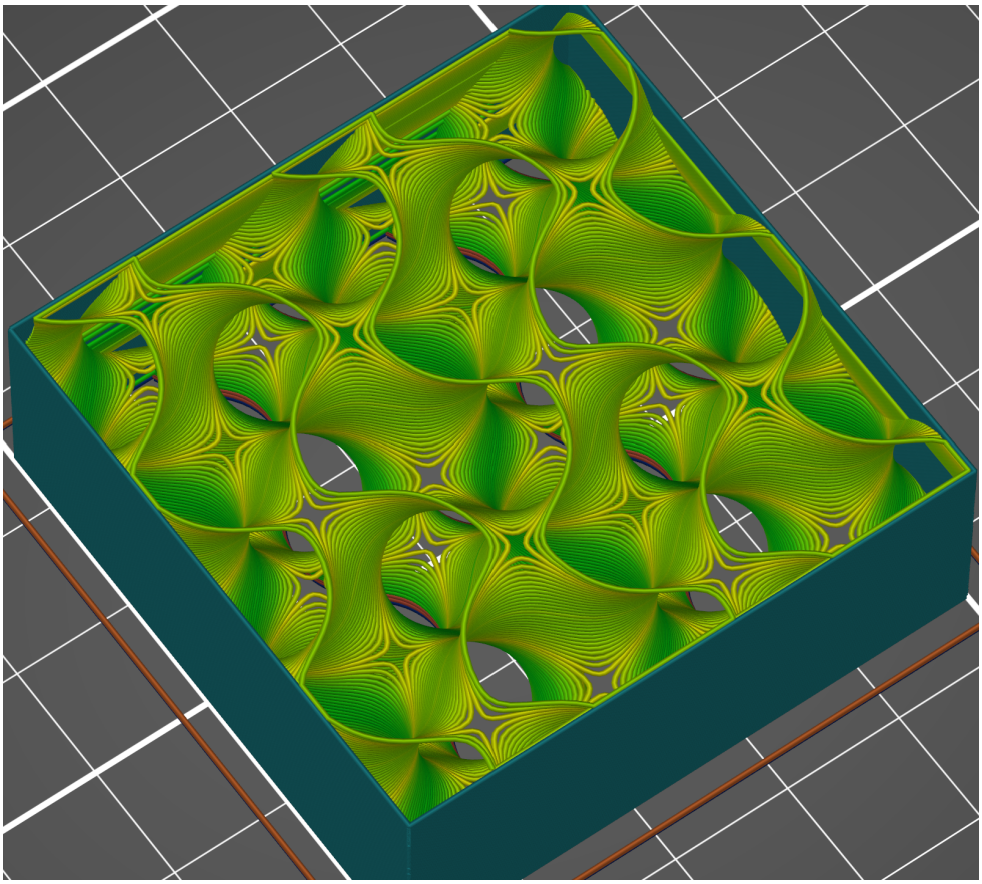

Figure 3.3: Gyroid lattice infill. (Source: Anachronist, https://commons.wikimedia.org/wiki/File:5pctGyroidInfill.png, Wikimedia Commons, CC BY-SA 4.0)

3.4 Materials

For SLS printing, the most common type of material to use is polyamide (also known as nylon). For this project, the focus will be specifically on PA 2200 and PA 1101, which are nylon powders designed for selective laser sintering [31]. These both have good mechanical properties. However, PA 11 is more costly and harder to come by [31].

There are also other materials, such as PEEK, which is also costly and hard to come

by [31].

For FDM, one would use thermoplastics such as PETG, PLA, ABS [28],[8]. PLA is the most common for desktop FDM. All of these have their strengths and weaknesses [28]. Polymers in general are susceptible to cracks due to thermal fatiguing [48].

3.4.1 Material properties

Table 3.1 contains material data for all materials that might be relevant.

Table 3.1: Material data for relevant materials [49],[50],[51],[52],[53].

Material	Density (g/cm^3)	Tensile modulus (MPa)	Poisson's ratio	Tensile strength (MPa)	Melting point (°C)
PA 2200	0,93	1700	$\approx$ 0,4	48	172-180
PA 1101	0,99	1600	$\approx$ 0,4	48	201
PLA (3D-printed)	1,24	3200	0,33	33,1	151,8
ABS (Molded)	1,07	2350	0,36	44,8	234

Notes:

- The Poisson's ratios of PA 2200 and PA 1101 were not found. Instead the Poisson's ratio for nylon 6 was used.
- The ABS values are averages, because the values differ too much depending on the producer.
- For the tensile strength for PLA the worst case stress direction was assumed.

3.5 LMT Batteries

3.5.1 Difference between LMT and EV

When discussing electric scooter batteries, we are not actually talking about EV batteries. In the EU battery regulations [54], Article 3(14), an 'electric vehicle battery' is defined as:

"*...a battery that is specifically designed to provide electric power for traction in hybrid or electric vehicles of category L as provided for in Regulation (EU) No*

168/2013, that weighs more than 25 kg, or a battery that is specifically designed to provide electric power for traction in hybrid or electric vehicles of categories M, N or O as provided for in Regulation (EU) 2018/858." [54]

But the battery in this project is intended to weigh around 1–1.5 kg, and be used for smaller vehicles. For this reason, it instead fits under the definition of an LMT battery, which in [54], Article 3(11), is defined as:

"*...a battery that is sealed, weighs 25 kg or less and is specifically designed to provide electric power for the traction of wheeled vehicles that can be powered by an electric motor alone or by a combination of motor and human power, including type-approved vehicles of category L within the meaning of Regulation (EU) No 168/2013 of the European Parliament and of the Council (1), and that is not an electric vehicle battery.*" [54]

3.5.2 Anatomy of current battery designs

The Li-ion LMT battery has a relatively simple design. It consists of the enclosure which houses a battery pack [55]. The battery pack in turn consists of hundreds of lithium-ion cells connected, in series and parallel, in order to attain the desired voltage [56]. These battery cells are the functional units in the battery [54]. It is within these that one can find electrodes, electrolytes, separators and more [57].

The housing can have various designs, as will be discussed. While finding information on manufacturing methods used is difficult, an educated guess from the author is that injection molding using ABS-plastics is used. The enclosure would in this case consist of a housing and a lid (or two) through which the battery pack can be retrieved [55].

The removable e-scooter batteries usually weigh around 1.5–3 kg, including the battery inside. They are usually elongated, and lean on the rectangular side [15],[16]. However, there are, of course, a variety of ways in which e-scooter batteries are designed. Some have the battery in the scooter deck, some have it externally mounted and others have the battery hidden within the frame [17].

Other essential aspects of the battery are vents, an attachment mechanism, labeling and charging ports, among other things. The vent is needed in order for the battery to be able to release any gas generated by the battery cells [54].

The attachment mechanism is used in this project to denote the manner in which the battery is attached to its corresponding vehicle. In the case of this project, that would be the mechanism used to attach the battery to the frame of the e-scooter.

An overview of the components can be viewed in Figure 3.4.

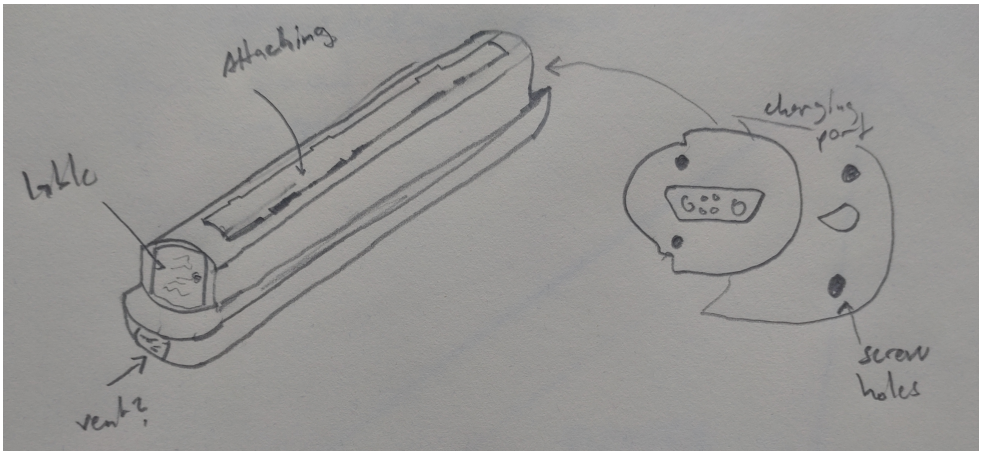

Figure 3.4: Sketch of an HX X8 Electric scooter battery and its components. (Source: Author's own work)

3.5.3 Regulation and testing

The LMT battery has various regulations that have been established by different authorities. The aim is, for one, to classify transported goods [58]. However, it is also to ensure the safety of the battery and the end user, while maintaining a certain quality of the battery [54].

3.5.3.1 EU

The EU battery regulations, among other things, aim to lay down "*requirements on sustainability, safety, labeling, marking and information to allow the placing on the market or putting into service of batteries within the Union. It also lays down minimum requirements for extended producer responsibility, the collection and treatment of waste batteries and for reporting.*" [54].

While there is plenty of information in these regulations, only a few are relevant to this project. For one, it demands the interoperability of chargers. Recital 41 in [54] states:

"*The interoperability of chargers for specific categories of batteries could reduce unnecessary waste and costs for the benefit of consumers and other end-users. It should be possible therefore to recharge LMT batteries and rechargeable batteries that are incorporated into specific categories of electrical and electronic equipment, by making use of common chargers that allow interoperability within each category of batteries. This Regulation should therefore require the Commission to assess how to introduce harmonised standards for common chargers for those categories of batteries, excluding charging devices for categories and classes*" [54]

The EU regulations also demand the removability and replaceability of the battery pack, something which is brought up in Article 11 in [54]. It states that:

"*Any natural or legal person that places on the market products incorporating portable batteries shall ensure that those batteries are readily removable and replaceable by the end-user at any time during the lifetime of the product. That obligation shall only apply to entire batteries and not to individual cells or other parts included in such batteries.*" [54]

This could mean that the final design has to have some sort of lid or disassembly method which allows for the retrieval of the battery pack. It is defined further by saying that:

"*A portable battery or LMT battery shall be considered readily replaceable where, after its removal from an appliance or light means of transport, it can be substituted by another compatible battery without affecting the functioning, the performance or the safety of that appliance or light means of transport.*" [54]

There are also some regulations for labeling, maintenance and other essential requirements that are beyond the scope of the project [54].

3.5.3.2 UN Manual of tests and criteria

The UN has established different tests, criteria and procedures for the classification of dangerous goods. This manual has been updated regularly ever since its conception in 1984 [59].

The part relevant to this project is section 38.3, which will henceforth be referred to as "UN 38.3". This section contains tests for the classification of lithium metal, lithium ion and sodium ion batteries [59]. These tests are aimed towards promoting safety when transporting batteries [58]. There are eight tests (T.1-T.8). However, only a few of these have any relevance to the enclosure itself. The tests regarding the cells themselves, charging and discharging are beyond the scope of the project. The relevant tests, T.2, T.3 and T.4, consist of a thermal test, a vibration test and a shock test [58].

The tests are created for both full batteries and battery cells. This is the reason the acceptance criteria also mention ignition and leaking [59]. The important criteria for this project are that the battery cannot rupture or disassemble.

3.5.3.2.1 Logarithmic sine sweep

The vibration test includes something called a logarithmic sweep test. A regular sine sweep test is a method of analysing frequency response where sinusoidal excitation is applied across a range of frequencies. This is done in order to understand the behaviour of the object and find any natural frequencies in that range [60].

A logarithmic sweep test is when a logarithmic frequency progression is used, meaning the same amount of time is spent in each octave. This results in more time being spent at lower frequencies, which is necessary for accurately capturing low-frequency behaviour, seeing as these cycles take longer to complete [61].

3.5.3.3 IEC

The International Electrotechnical Commission (IEC) is an organization that publishes international standards for technologies related to electricity and electronics [62].

SS-EN 62133-2 is an IEC standard, adopted by both SIS and CENELEC, containing "*Safety requirements for portable sealed secondary cells, and for batteries made from them, for use in portable applications*" [63]. This is the second part of the standard and it contains specifications for lithium systems [63]. It is also this standard which will be used most during this project, as it is more directed towards smaller LMT batteries, such as electric scooter batteries.

Compared to the UN 38.3, SS-EN 62133-2 is more about the safety during operation and use, while UN 38.3 focuses more on transport safety [58],[63].

The SS-EN 62133-2 standard contains a shock test and a vibration test with similar or identical instructions to the ones in UN 38.3. This is due to the UN taking a lot of tests from the IEC recommendations [59],[63]. SS-EN 62133-2, however, also contains a drop test, which would be highly relevant for the battery enclosure. During this test the battery is dropped from 1 m onto a concrete or metal floor, after which a visual inspection is performed [63].

Another test from the SS-EN 62133-2 standard is the one regarding case stress during high ambient temperature. The aim of this test is to assure that the enclosure does not physically distort and expose internal components as a result of the high temperature [63].

3.5.3.4 IP testing

Another thing possible to test is ingress protection (IP). IP testing tests an enclosure's ability to prevent the intrusion of dust or liquids. This is important because most electronics will deteriorate if this happens [64]. Both IP rating and testing have been developed by the IEC and are explained in great detail in IEC 60529 [65]. However, it is not mentioned as necessary in either of the previously mentioned standards [63],[59]. It is only referred to in a commission notice from the EU, but never said to be a legal requirement [65]. It is more so a method of further testing the safety of the product, especially if it is designed to operate in wet environments [64]. It is in this project considered optional during the testing phase, while some considerations are be made during development.

3.5.3.5 Humidity testing

Similarly, humidity testing is not necessary according to either the EU or the UN. However, there are IEC standards for this as well, e.g. SS-EN 60068-2-78 [66]. This will, however, be considered completely outside the scope of this project due to a lack of equipment. It is also highly dependent on materials, something this project places little (if any) focus on.

3.5.3.6 ISO

It should be noted that there are also ISO standards regarding lithium batteries. For instance, there is ISO 17546 which covers design and verification requirements for lithium ion batteries for space vehicles [67]. Due to the limited scope of the project, there are only so many tests that may be accounted for. For this reason, the IEC standards are prioritized as these are the ones referenced by both the UN and the EU [59]. Furthermore, batteries are an electro-technical product category, which specifically falls under IEC's scope [62]. For these reasons, the ISO standards will be ignored in this project.

3.5.4 Summary of relevant tests

To summarize the tests and standards, Table 3.2 shows all aforementioned tests which will be considered. '-' means that the standard does not have the test, while 'X' means that it does.

Table 3.2: Summary of all tests and their origins

Test	UN 38.3	IEC 62133-2
Drop test/free fall	-	X
Shock test	X	X
Vibration test	X	X
Temp. cycling	X	Only cell level
Thermal abuse	-	X

3.6 FEA and FEM

Finite element analysis (FEA) is a way of predicting an object's behaviour based on calculations made with the finite element method [68]. This method is a numerical technique used in engineering and applied mathematics, that allows for solving differential equations in an approximate manner [69]. Characteristically, FEM involves dividing the region which the differential equations preside over into smaller solvable units, finite elements [69],[70]. It is subsequently possible to make approximations for each finite element (instead of approximating the whole domain) which, after patching everything together, enables the approximation of the entire body's behaviour [69]. Plenty of examples of FEM can be viewed in Chapter 6.

The essential part of this method is the discretization of the system, which is an important simplification of the solution domain. The problem is most often not ideal, which means it needs to be idealized in this way, within whichever computational platform is used [70]. After this, the relevant governing equations may be applied to each unit with the intent to solve for unknown parameters. Then, in order to finally obtain the solution, numerical methods may now be implemented [70].

The advantage of FEA is, for one, the ability to assess geometries that would otherwise be too complex to calculate [68]. Most problem domains have properties which are non-smooth, something this method is able to handle. This makes the FEM capable of solving most practical problems [70]. It is also advantageous to be able to approach complicated partial differential equations (PDEs), such as the ones arising from problems within fluid dynamics, electromagnetism and the like, numerically. The fact of the matter is that solving these problems analytically is oftentimes not feasible. Hence, it is a more viable route to instead use a numerical method, arriving at an approximate solution [70]. Since it also is done purely on a computer, without the need for physical prototypes, the FEM has the ability to save both time and money [70].

With that said, FEM still has its limitations. These limitations are encountered within extreme cases, such as overly stiff elements, too high deformation, fracturing or material losses, etc. The consequence is usually loss of accuracy, numerical errors or substantially increased computation time. In the worst case, the computation fails completely [70].

3.6.1 Creating the FE formulation

The basic steps in creating the FE formulation are described as follows, in *Introduction to the finite element method* by Ottosen, N.S. and Peterson, H. [69].

1. Establish strong form formulation of the problem.
2. Obtain the weak form of the problem.
3. Make an elementwise approximation over the entire body of the unknown function
4. Choose the weight function v using the Galerkin method.
5. (Other steps depending on the situation (e.g. constitutive relations))

Once the formulation is established, it can straightforwardly be calculated numerically [69].

The strong form of the problem is the initial boundary value problem. It consists of differential equations which can be formed directly from the context or the governing equations [69]. These equations are often not possible to solve, and so, in the FE approach the strong form is formulated into an equivalent form known as the weak form [71]. These equations are identical, in that one implies the other [69]. One could say that the weak form is the integral form of the governing equations, and it acts as an intermediary version of the original equations. It is needed because the original equations are not always easy to integrate [70]. In fact, it is called "weak" since it relaxes requirements, needing only equality in terms of integrals. Another way of describing it is that it lowers any smoothness requirements, requiring only first derivatives instead of second derivatives [72]. All this makes the weak form more general, and more manageable than the strong form, despite them being mathematically equivalent [69].

3.6.1.1 Approximation using the Galerkin method

The weight function is an arbitrary function. It is used when obtaining the weak form from the strong form. However, since the weight function is integrated in the weak form, a solution needs to be found for the weak form which holds for all weight functions [69].

In the FE method, the most convenient method of obtaining the weight function has proven to be the Galerkin method, established by Galerkin in 1915. This is a "weighted residual method" (similar to the least squares method) and its strength lies in the fact that a symmetric coefficient matrix K (or stiffness matrix) arises when combined with the weak form. Furthermore, it is applicable to any differential equation [69].

The Galerkin weak form-based FE formulation was formulated first in 1964. This was done by Theodore H.H. Pian who utilized the Hu-Washizu variational principle [11].

3.6.1.2 Meshing

As stated before, the FEM is built on dividing the problem domain into a number of smaller elements, also known as the mesh [70],[68]. These elements are furthermore connected via nodes and they are used in the FEM solver to get an approximate solution [69]. An example of a meshed model can be viewed in Figure 3.5.

The earliest form of mesh discretization can be found in a paper published by A. Hrennikof in 1941. In this paper, the solution domain was discretized into a mesh of lattice structure [11].

Since the early beginnings of FEM, many different element types have been conceived. And new elements are still being researched to this day, with the aim of improving their efficiency and robustness [11].

The choice of element requires sophisticated assessment. For instance, one needs to consider the number of nodes in the element, as well as directional influence (in the case of triangular elements), which both can have a significant impact on the accuracy [12].

Selecting the type of elements and the resulting mesh can be considered the first step in the FE analysis. While there is a lot of nuance to the decision, it can at least be stated that the accuracy of the analysis increases as the element size decreases. For this reason it is common practice to have small elements in regions where the unknown varies swiftly [69]. In fact, in an efficient solution scheme, it is necessary that few elements are used in regions where the function varies slowly and many where it varies rapidly. This comes from the fact that as the number of elements increases, so does the computational cost, seeing as the number of equations increases as well. Hence, generating unnecessary detail suggests wasted computational effort, which highlights the need for a balance between the computational effort and the level of detail [70].

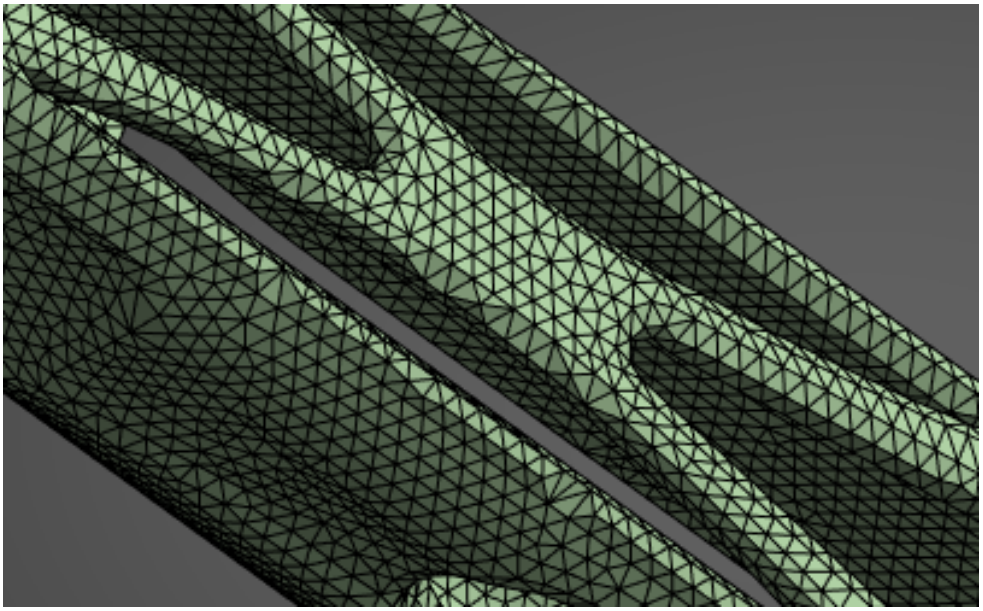

Figure 3.5: Example of a meshed model. (Source: Author's own work)

3.6.1.3 FE formulation for this project

In the case of this project, most of the simulations will deal with static problems using three-dimensional elasticity. This means that inertial forces are neglected. For the steps, refer back to previous sections. The following formulations are based on *Hållfasthetslära: allmänna tillstånd* by Ottosen, N.S. et al. (2007) [73] and *Introduction to the finite element method* by Ottosen, N.S. and Peterson, H. (1992) [69].

In the three-dimensional case, the equilibrium between the body forces in the region and the traction forces along the surface S grants that:

$$\int_S \mathbf{s}\, dS + \int_V \mathbf{b}\, dV = 0 \tag{3.1}$$

Using $\mathbf{s} = \mathbf{Sn}$, where $\mathbf{S}$ is the stress tensor, and then applying the Gauss divergence theorem leads to the following expression:

$$\tilde{\boldsymbol{\nabla}}^T \boldsymbol{\sigma} + \boldsymbol{b} = 0 \tag{3.2}$$

This can be seen as the strong form of the problem. Following the steps in section 3.6.1, the final formulation becomes:

$$\mathbf{Ka} = \mathbf{f}_b + \mathbf{f}_l + \mathbf{f}_0 \tag{3.3}$$

where:

$$\begin{cases} \mathbf{K} = \int_V \mathbf{B}^T \mathbf{D} \mathbf{B} \, dV \\ \mathbf{f}_b = \int_{S_h} \mathbf{N}^T \mathbf{h} \, dS + \int_{S_g} \mathbf{N}^T \mathbf{t} \, dS \\ \mathbf{f}_l = \int_V \mathbf{N}^T \mathbf{b} \, dV \\ \mathbf{f}_0 = \int_V \mathbf{B}^T \mathbf{D} \varepsilon_0 \, dV \end{cases} \tag{3.4}$$

Here **K** is the stiffness matrix, **a** is the displacement vector, $\mathbf{f}_b$ is the boundary vector due to boundary conditions, $\mathbf{f}_l$ is the load vector, $\mathbf{f}_0$ is the initial strain, **D** is the constitutive matrix and **B** is a strain-displacement matrix. (3.3) is then further simplified into:

$$\mathbf{Ka} = \mathbf{f} \tag{3.5}$$

where $\mathbf{f} = \mathbf{f}_b + \mathbf{f}_l + \mathbf{f}_0$.

And finally, by using only the degrees of freedom belonging to element e, the result becomes:

$$\mathbf{K}^e \mathbf{a}^e = \mathbf{f}^e \tag{3.6}$$

for each element, where:

$$\begin{cases} \mathbf{K}^e = \int_{V_\alpha} \mathbf{B}^{eT} \mathbf{D} \mathbf{B}^e \, dV \\ \mathbf{f}_b^e = \int_{S_{h\alpha}} \mathbf{N}^T \mathbf{h} \, dS + \int_{S_{g\alpha}} \mathbf{N}^T \mathbf{t} \, dS \\ \mathbf{f}_l^e = \int_{V_\alpha} \mathbf{N}^{eT} \mathbf{b} \, dV \\ \mathbf{f}_0^e = \int_{V_\alpha} \mathbf{B}^{eT} \mathbf{D} \varepsilon_0 \, dV \end{cases} \tag{3.7}$$

These are calculated for each element and then assembled into the full stiffness matrix **K**. Subsequently, displacements, stresses and more can be calculated [69].

3.6.2 FEM programs

Most finite element modeling environments are comprised of three main components. These are the: pre-processor, simulation engine and the post-processor [70]. The pre-processor, as the name suggests, handles what happens before the simulation, such as discretization, material model, boundary conditions along with other specifications. In ANSYS this is done within ANSYS Workbench. The simulation engine then performs the numerical calculations, according to what we've seen. In ANSYS' case this is done with ANSYS LS-DYNA [70]. Finally, there is the post-processing, which includes further calculations (e.g. internal forces or stresses), displaying plots and more [70].

3.6.2.1 Static and dynamic Analysis

Static analysis is a computational mechanics approach used when the conditions are static, i.e. will not (considerably) change over time. It usually refers to a system with a steady load that is in equilibrium, or approaching equilibrium [68],[70].

Most forces vary with time, causing the structural response to also vary with time [73]. However, since statics are characteristically slow, and often completely time invariant, the effect of changing time is not important [73],[70]. For this reason inertial forces can be neglected for these systems (as is seen in the FE formulation above) [12].

Dynamic analysis, on the other hand, is used when there are changes over time, which is highly consequential from the perspective of mechanics [68]. If the time variation is rapid enough, the inertial forces become important and the load is considered dynamic [73].

In dynamic problems, the structural behaviour, as well as the displacement and internal forces, will be significantly time-dependent. They are no longer described by constant values, but by functions dependent on time. This further complicates the FE formulation, since inertial forces, damping forces and kinematic relations are suddenly relevant [12].

Dynamic analysis requires a substantially higher computational effort compared to static analysis [12].

There are many engineering areas where dynamic loads are encountered, for example shock loads on structures, earthquakes, vibrations in machines, car designs, musical instruments, fluttering airplane wings etc [73].

3.6.2.2 Implicit and explicit Analysis

When using the FEM, the notion of a simulation being implicit and explicit often shows up. The difference lies in what time integration method is being used [70].

In implicit methods, the behaviour of the system at the current time t and a future time $(t + \Delta t)$ is known. It furthermore requires that the system of linear equations is solved completely [70]. Implicit methods are best suited for static analyses, however they can in some cases be used for dynamic problems as well [74]. Their solvers are robust and mostly achieve good convergence with small errors [70].

Explicit methods, on the other hand, use an explicit time integration approach [70],[75]. This requires a prediction of future behaviours of the system, coming directly from the current behaviours. These methods are commonly used for impact problems and dynamic problems, such as drop tests, vehicle crashes and material failure. In other words, it is suitable for nonlinear time-dependent behaviour over a short duration [75]. The explicit solvers do converge to their solutions rapidly. However, they are also more error-prone when compared to implicit methods. These errors will increase if the time steps used are too large [70].

3.6.2.3 Modal analysis

Modal analysis is used in order to find natural frequencies, also known as eigenfrequencies, also known as modes. With these it is possible to predict the vibration of the structure which in turn affects performance [68].

More generally, modal analysis is used in order to find inherent dynamic characteristics, such as natural frequencies, damping factors and mode shapes. This is called the modal data and it is used for creating a mathematical model, known as the modal model [76].

The analysis is made possible by how the vibration response of a linear time-invariant dynamic system is able to be conveyed in the form of a linear combination of natural modes of vibration [12]. The natural modes are a set of harmonic motions, and they are inherent to the dynamic system. They are determined by the physical properties of the structure, i.e. the mass, stiffness and damping [12].

Modal analysis requires linear system behaviour as well as constant mass and stiffness matrices [12].

3.7 Topology Optimization

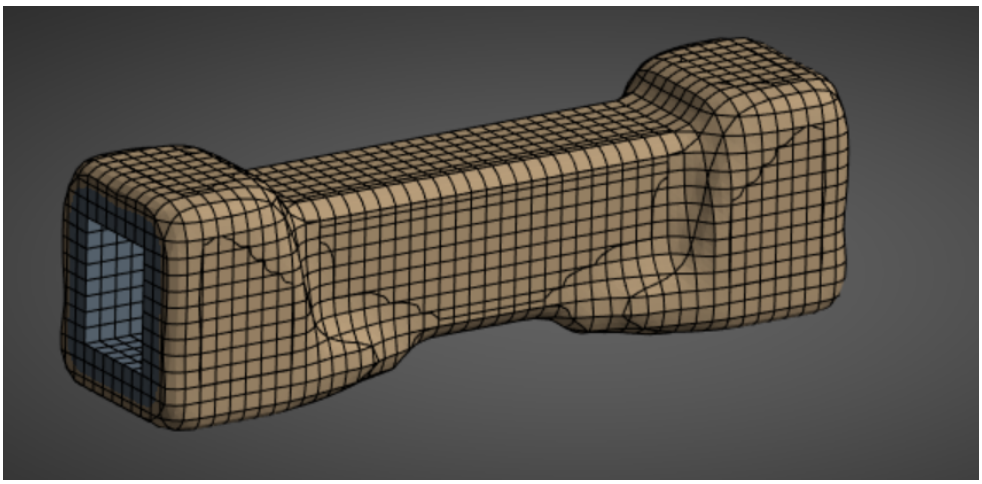

Figure 3.6: Example of topology optimization in ANSYS. (Source: Author's own work)

Topology optimization is one of the basic classes of structural optimization, which in turn denotes geometrical optimization problems regarding mechanical structures. Other classes are size and shape optimization [77]. Topology optimization is a way of optimizing how material is placed within a certain design domain. The goal is to find a subdomain Ω filled with material in such a way that it satisfies the given criteria [78]. An example of topology optimization in ANSYS can be viewed in Figure 3.6.

Topology optimization is a subfield within structural optimization which has gained notable popularity recently. Its multitude of applications has made it a highly investigated field, with hundreds of scholars working on it currently [13]. The first paper on the topic is considered to be Mitchell's optimization paper, published in 1904 [13]. Apart from this, there were other studies on optimizing topology performed in the early twentieth century. These featured layouts being described in terms of densities of fields of stringers at the plastic limit, using variational calculus [14]. In more recent years optimizing shape and topology has gained more attention. One of its main challenges is to establish a workable problem [13]. Early developments of topology optimization can be attributed to people such as N. Kikuchi, M.P. Bendsøe, G. Cheng and O. Sigmund [11]. As of 2007, it was among the leading fields within design optimization [14].

3.7.1 Formulation and terminology

A structural optimization problem is often presented as in (3.8) below [77].

$$P \begin{cases} \min\limits_{x} \;\; C = f(\mathbf{v}, \mathbf{x}) \\ \text{s.t.} \quad \begin{cases} g(\mathbf{v}, \mathbf{u}) \leq 0 \\ h(\mathbf{v}, \mathbf{u}) - 1 \geq 0 \\ 0 \leq x_e \leq 1, \qquad \forall e \in [1, ..., n_{elm}] \end{cases} \end{cases} \tag{3.8}$$

The objective function C above is the function used to assess the designs. For each design, C returns some value. The aim is often to minimize this value.

The design variables **x** contain variables describing the design. These are the variables that are adjusted during the optimization, in order to minimize or maximize the objective function.

The state variables **v** describe the response of the structure, like displacement or stress. These are often a function of the design.

The bottom three expressions are conditions that need to be met. ”s.t.” stands for ”subject to”. So this is read as ”minimize C subject to these constraints” [77].

3.7.1.1 Objective function

The optimization problem formulation most often involves the minimization of compliance. The compliance is defined as $\mathbf{F}^T\mathbf{u}$, where **F** is the force vector and **u** is the nodal displacement vector. Minimizing this will subsequently lead to a lower displacement, especially in nodes where the forces are high [77].

It is also possible to use a stress criterion, aiming to minimize stresses. If a local stress constraint is used, stress limits are applied at specific elements on the model, while a global stress constraint applies an upper bound that has to be satisfied by all elements [79],[80]. Local stress constraints are cumbersome, as they tack on a large number of constraints to a likely already large optimization problem [79]. This issue may be ameliorated by using a more relaxed formulation. The complexity can also be kept low by strategically dividing the relevant design elements into clusters [80]. On the other hand, when using global stress constraints only one constraint is being used, which saves an enormous amount of computational effort [79].

Another common design goal is maximizing the fundamental eigenvalue, in the case of dynamic loads [79].

3.7.2 General Structural optimization method

The structural optimization process is an iterative one and each iteration can be described using the following steps. These steps are taken directly from *An Introduction to Structural Optimization* by Peter W. Christensen and Anders Klarbring (2009) [77]:

1. Start with an initial design $\mathbf{x}^0$. Set the iteration counter k = 0.
2. Calculate the displacement vector $\mathbf{u}(\mathbf{x}^k)$ for the current design by performing FEA: $\mathbf{K}(\mathbf{x}^k)\mathbf{u}(\mathbf{x}^k) = \mathbf{F}(\mathbf{x}^k)$.
3. For the current design $\mathbf{x}^k$, calculate the objective function $g_0(\mathbf{x}^k)$, the constraint functions $g_i(\mathbf{x}^k)$, i = 1, . . . , l, and their gradients $\nabla g_i(\mathbf{x}^k)$, i = 0, . . . , l.
4. Formulate an explicit, convex approximation $(SO)^k_{nf}$ at $\mathbf{x}^k$ of $(SO)_{nf}$.
5. Solve $(SO)^k_{nf}$ by a nonlinear optimization algorithm to give a new design $\mathbf{x}^{k+1}$.
6. Put k = k + 1 and return to step 2 unless a stopping criterion is satisfied.

3.7.3 Specifically for topology optimization

In topology optimization specifically, the design variables **x** represent non-dimensional densities in each element, where $0 < x_i < 1$. This value is related to the physical density ρ through $\rho_i = x_i\bar{\rho}$ where $\bar{\rho}$ is the actual density. As a result, $x_i = 0$ means nothing is there and $x_i = 1$ means fully occupied [77],[79]. The design variable is then used to interpolate the material properties, through $E_i = E_i(x_i)$, which in turn affects the FE formulation through the constitutive matrix **D**, see (3.7). As a result, x_i now controls the stiffness of each element since $\mathbf{K}_i = \mathbf{K}_i(\mathbf{D}_i(E_i(x_i)))$. Now that the material distribution has been linked in, the same optimization steps described before can be followed [81].

3.7.4 Optimization algorithms

In order to complete the optimization, it is usually necessary to reformulate the SO-problem into an explicit, convex approximation (see step 4). The new problem will be convex, separable and solvable [77].

The approximations typically involve some type of linearization of the non-linear function, with the help of sensitivities (or gradients) [77].

There are many different nonlinear optimization algorithms that are commonly used. The one used in ANSYS is called Sequential Convex Programming (SCP), made by Zillober, which is an extension of the method of moving asymptotes (MMA) developed by Svanberg. The MMA method is a programming algorithm which is well suited for non-linear optimization problems [80]. It utilizes the sensitivity information (of the involved functions) at the current iteration, as well as previous ones, in order to create a sequence of convex separable subproblems [79]. This is done by linearizing the current design $\mathbf{x}_k$ in the intervening variables U_j and L_j. These are the so called "moving asymptotes" which are changed in between iterations in order to control the "conservatism" of the approximation [77],[82]. If chosen carefully, these will improve the speed of convergence [79].

Solving the linearized problem, while being simpler, merely yields an approximate solution. This convex approximation is at least locally accurate, meaning it will at least point in the right direction (compare this to classical gradient descent) [83]. For this reason, iteration is a must, since it gives time for convergence on an optimal solution. The subproblems are solved, using e.g. a dual method, and the solution assumes the role of the design variable in the following iteration [79].

The MMA method was introduced by Svanberg in 1987 and has since proven to be a popular and reliable optimization tool [84]. The SCP method is an improved version by Zillober [85], adding a line search method along with a merit function (augmented Lagrangian merit function) in order to stabilize the algorithm and prove global convergence [80], [85]. The line search and the merit function are used in order to evaluate whether the current step leads to the optimal solution. The ones that do not improve convergence are rejected [80].

The difference in performance between SCP and MMA is most often rather insignificant, and both methods might even coincide at most iterations. The reason for this is that structural design problems usually are endowed with good starting points, leading to both methods preferring the same step-length [85]. SCP does, however, handle large infeasibilities better. During such problems MMA tends to go back and forth a lot [85].

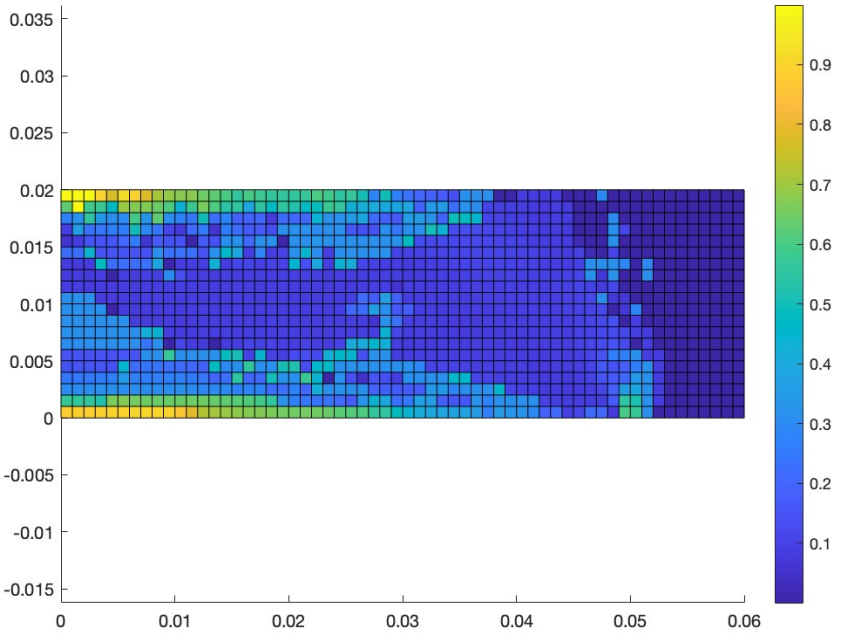

Figure 3.7: Topology optimization results without SIMP-scheme or filter, created in MATLAB. Colors show the design values x in the elements. (Source: Author's own work)

3.7.4.1 SIMP

The solution granted from the methodology above alone will be blurry and have a large amount of undecided areas, see Figure 3.7. In order to get a more defined solution, the Solid Isotropic Material with Penalization (SIMP) method is applied. The idea is to introduce a penalty exponent p, causing intermediate design values to be even lower. Consequently, these values, which are less economical, will be avoided. The resulting structure will become more "confident", with elements having either full stiffness or no stiffness at all [77],[79]. A simple SIMP scheme can be seen in (3.9).

$$E_i(x_i) = x_i^p E_0, \;\; x_i \in]0, 1] \tag{3.9}$$

where E_0 is the elastic modulus of fully solid material [81].

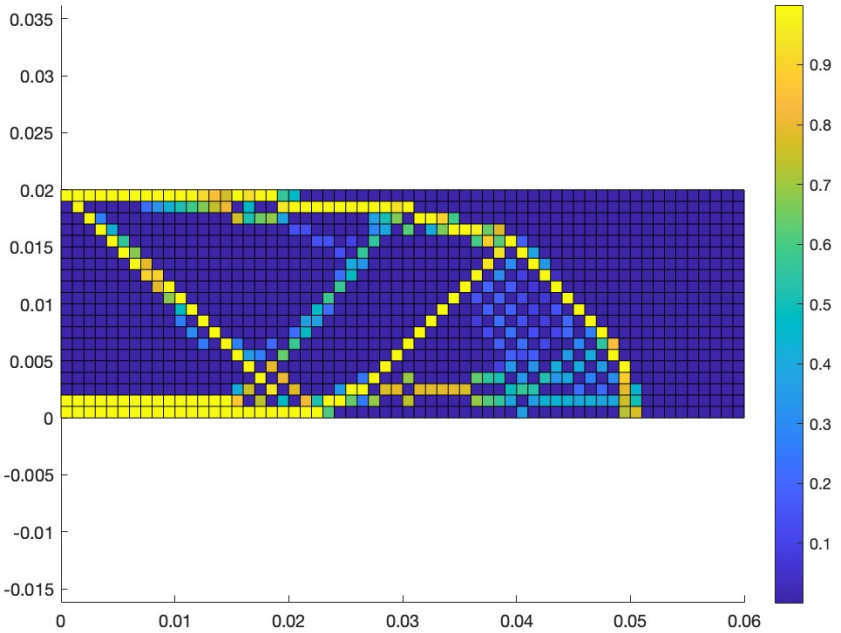

Figure 3.8: Topology optimization result using SIMP-scheme but no filter, created in MATLAB. Colors show the design values x in the elements. (Source: Author's own work)

3.7.4.2 Filter

When using the techniques above the result often turns out like a checkerboard pattern, due to the FEM discretization, see Figure 3.8. While this result is not necessarily incorrect, it is unusable for the real world. Furthermore, it makes the result heavily dependent on the chosen mesh. For this reason, there is often a filter applied [77],[79]. While there are many different filter techniques that can be applied, most of them consist of taking some weighted average of neighboring design values. The effect of the filter can be viewed in Figure 3.9.

It has also been proven useful to filter the sensitivities (the gradients), as a way of further ensuring mesh independency [79],[85]. Here again, a weighted average would be used, but in this case using the neighboring element sensitivities. Such a filter can also act as a local stress constraint [79].

ANSYS utilizes both a SIMP scheme and a filter [86].

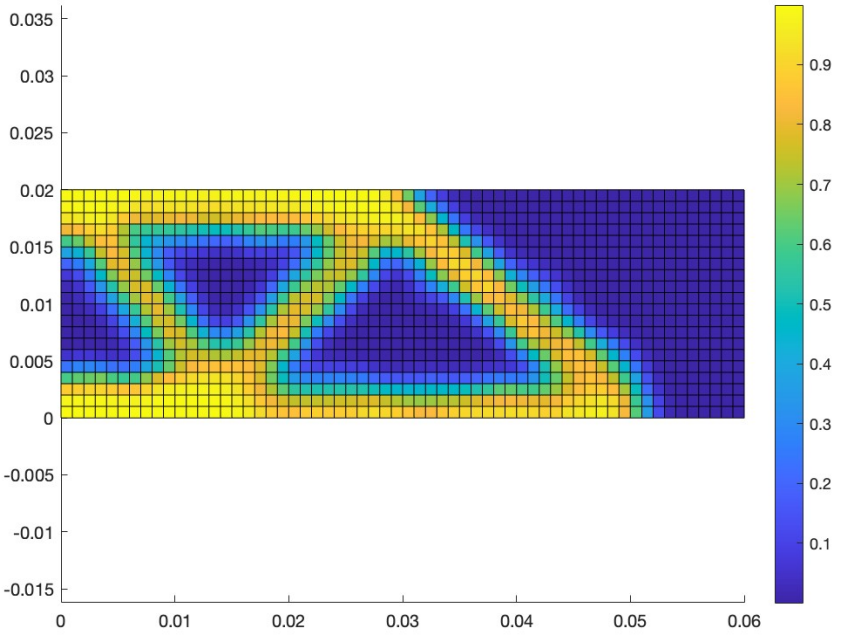

Figure 3.9: Topology optimization result using both SIMP scheme and filter, created in MATLAB. Colors show the design values x in the elements. (Source: Author's own work)

4 Developed Design Brief

After the initial research, a brief was constructed in order to constrain the work into a manageable task. The brief is:

Design an e-scooter battery enclosure, simplified into one part (screws and lids not considered), attached to the frame of the e-scooter, such that it weighs as little as possible while still being of **acceptable quality**.

Acceptable quality is defined as possessing the following characteristics:

- Maintaining the usual capabilities of an electric scooter battery, including attachment mechanism, charging port and vents.
- Covering the whole battery (considering IP rating)
- Including components required according to EU regulation.
- Passing drop-, shock-, vibration-, thermal cycling- and thermal abuse tests, in accordance with UN 38.3 and IEC 62133-2*

Furthermore, the design should be able to be **effectively** printed using SLS. **Effectively** is used merely to discourage the development of impossible and unrealistic designs. SLS was chosen as the better option over FDM. This was partially due to mechanical properties and partially due to SLS being more suitable for the Glasgow partnership.

In order to properly think the design shapes through, there needs to be an idea of what shape the protected battery cells have. Hence, a “standard battery pack” had to be decided upon. This battery pack had the shape of a rectangular prism, with the measurements 60x75x435.6 mm. This was based on other battery packs found on the market. This battery was not included in the FE simulations. This is further explained in section 6.2.

*During FE analysis, the battery is considered to have passed if the stress does not exceed the tensile strength of the material during the simulation. For PA 2200 and PA 1101 the tensile strength is 48 MPa, see Table 3.1. The tests will be described more in-depth in the following chapter.

4.1 Detailed test instructions

These instructions are an amalgamation of the tests as described in UN 38.3 and IEC 62133-2. When they both have differing tests, UN 38.3 was prioritized since it is actually required in many countries, unlike IEC. Aspects of the tests that are irrelevant to the project have been omitted. The way they are described here is the way they will be considered for the rest of the project.

Drop/free fall
This is the free fall test, based on IEC 62133-2:

The aim of the drop test is to ensure that dropping the battery does not cause an explosion or a fire.

Test instructions:

- Conduct at 20 °C ± 5 °C
- Drop battery three times, with impact in random orientations, from a height of 1 m. Drop onto concrete or metal floor.
- After a 1 h rest, visually inspect the damage.

The battery is accepted if there is ”no fire and no explosion” [63].

Shock
This is the shock test, based on UN 38.3:

The aim of the shock test is to assess the robustness against cumulative shocks.

Test instructions:

- Secure the battery to the testing machine using a rigid mount, supporting all mounting surfaces (20 °C ± 5 °C).
- Subject the battery to a half-sine shock with an acceleration of 150 g and pulse duration of 6 ms (since mass < 12 kg). The battery is subjected to three shocks in negative direction and three shocks in positive in each of the three perpendicular mounting positions (x-direction, y-direction and z-direction). This totals 18 shocks.

The battery is accepted if there is ”no leakage, no venting, no disassembly, no rupture and no fire” [59].

Vibration
This is the vibration test based on IEC 62133-2:

The aim of the vibration test is to ensure that vibrations during transport do not cause leakage, fire or explosion.

Test instructions:

- Secure battery to the platform of a vibration machine, without distorting it too much.
- Subject the battery to sinusoidal vibration with a logarithmic sweep. The waveform goes from 7 Hz to 200 Hz and back, with this cycle taking 15 minutes. The idea is to simulate vibrations faced during transport.
- Repeat the cycle 12 times over 3 h for each of the perpendicular mounting directions. One of these directions has to be perpendicular to the terminal face.

The battery is accepted if there is ”no fire, no explosion, no rupture, no leakage or venting” [63].

Temperature cycling
The temperature cycling test, as described in UN 38.3:

The aim of this test is to assess battery seal integrity under extreme, rapid temperature cycling.

Test instructions:

- Store battery for at least six hours at a temperature of 72 ± 2 °C.
- Then, maximum 30 minutes later, store the battery at a temperature of -40 ± 2 °C. This is done for six hours.
- Repeat this procedure for 10 cycles.
- Finally, store the battery at ambient temperature (20 ± 5 °C) for 24 hours.

The battery is accepted if there is ”no leakage, no venting, no disassembly, no rupture and no fire” [59].

Thermal abuse
This is the thermal abuse test based on IEC 62133-2:

The aim of this test is to ensure that internal components are not exposed during use at high temperature.

Test instructions:

- The battery is placed in an oven with circulating air at a temperature equal to 70 °C ± 2 °C.
- The battery is to stay in the oven for 7 h and then return to room temperature.

The battery is accepted if there is no physical distortion of the case which results in exposure of internal components [63].

5 Ideation

5.1 Design ideas

After the brief had been established, the ideation process started. In this process, as many ideas of shapes and designs as possible were considered. In order not to stifle the creativity too much, the brief was ignored for some of the first sketches. Only after a while were ideas conceived specifically with the brief in mind. Some initial sketches can be seen in Figure 5.1.

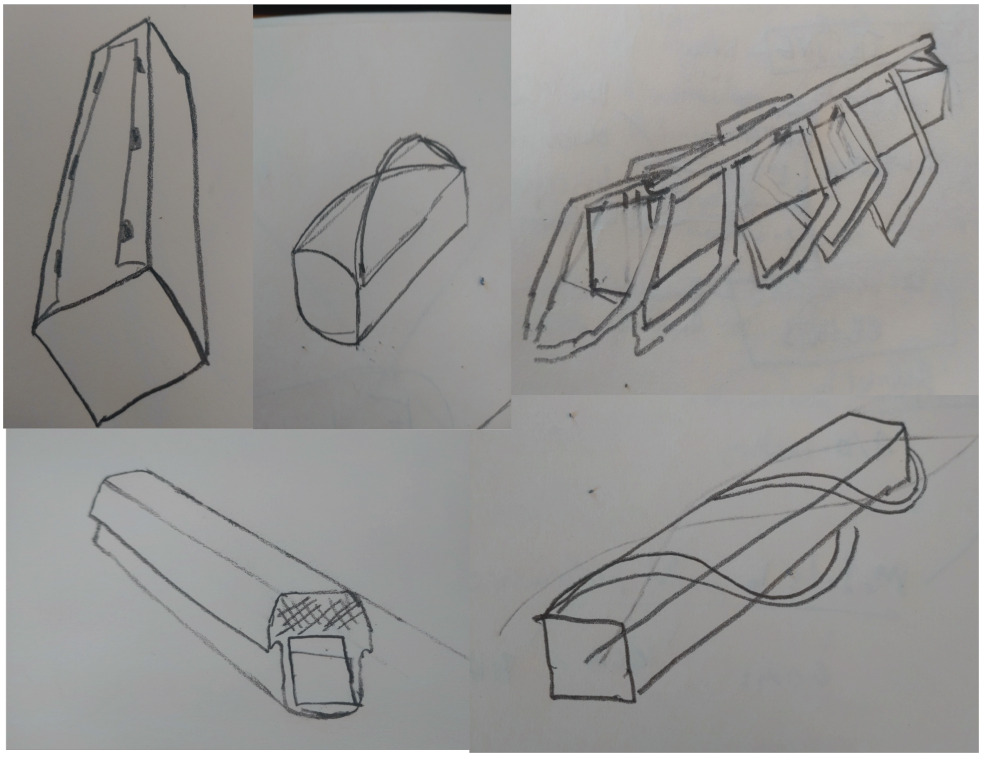

Figure 5.1: Initial sketches of some creative concepts. (Source: Author's own work)

5.2 Concept Selection

The concepts were selected primarily based on how the author deemed that they would perform in the different tests. However, it was also important to choose varying concepts with different ideas behind them. Furthermore, some ideas could be disqualified immediately, based on the IP test criterion. In the end, four concepts were chosen, the sketches of which can be seen in Figures 5.2–5.5 below.

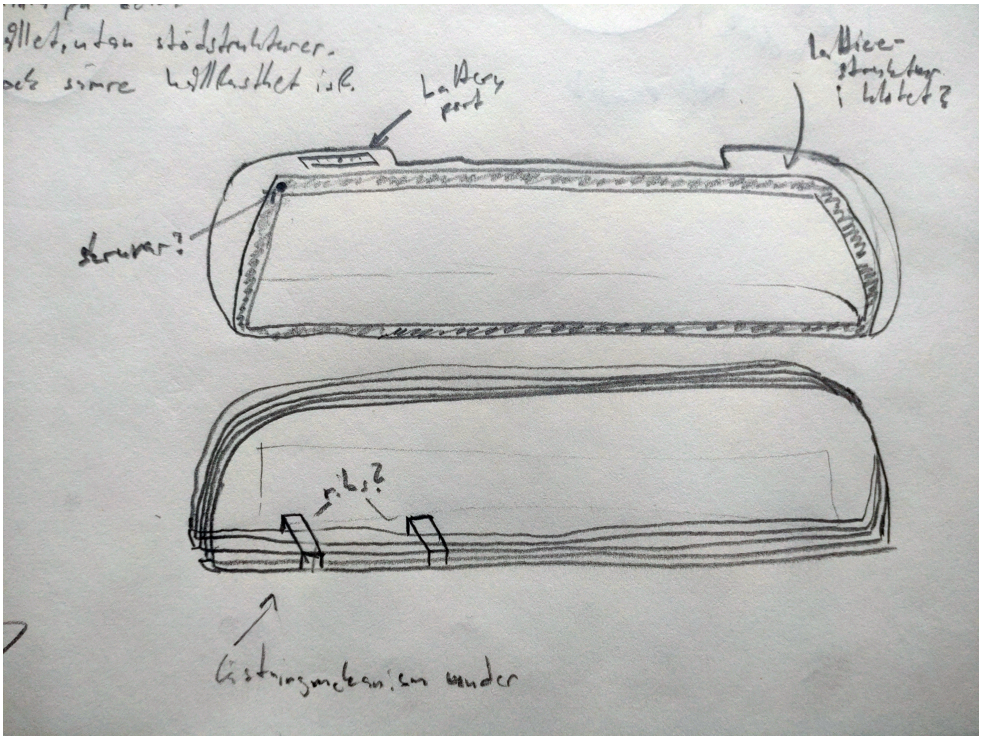

Figure 5.2: Initial sketch of the concept ”Genius”. (Source: Author’s own work)

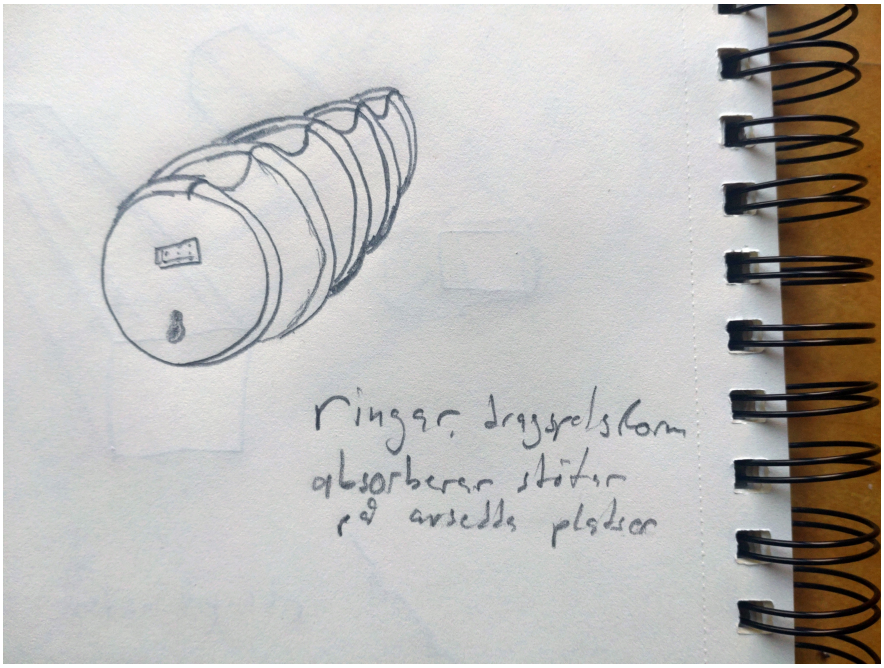

Figure 5.3: Initial sketch of the concept ”Dragspel”. (Source: Author’s own work)

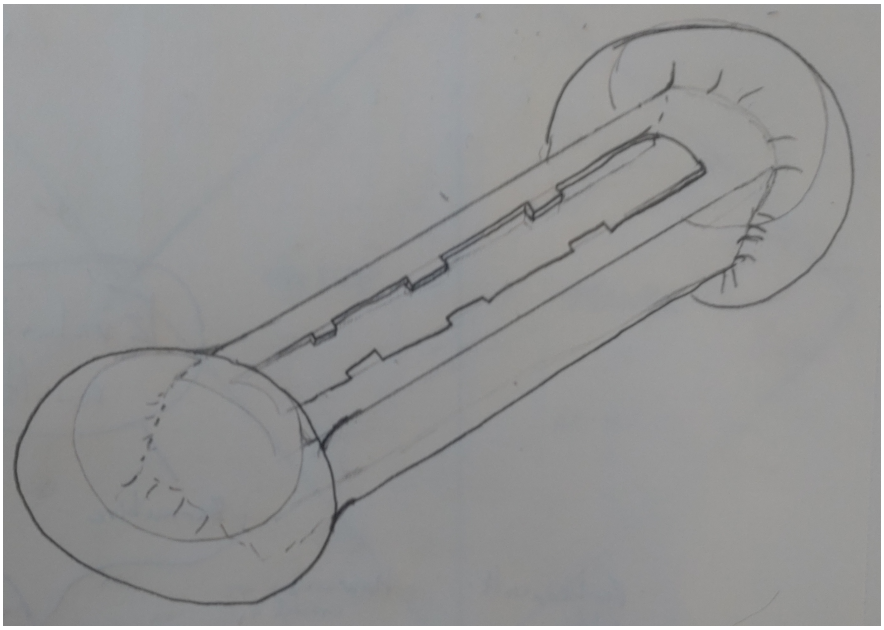

Figure 5.4: Initial sketch of the concept ”Dumbbell”. (Source: Author’s own work)

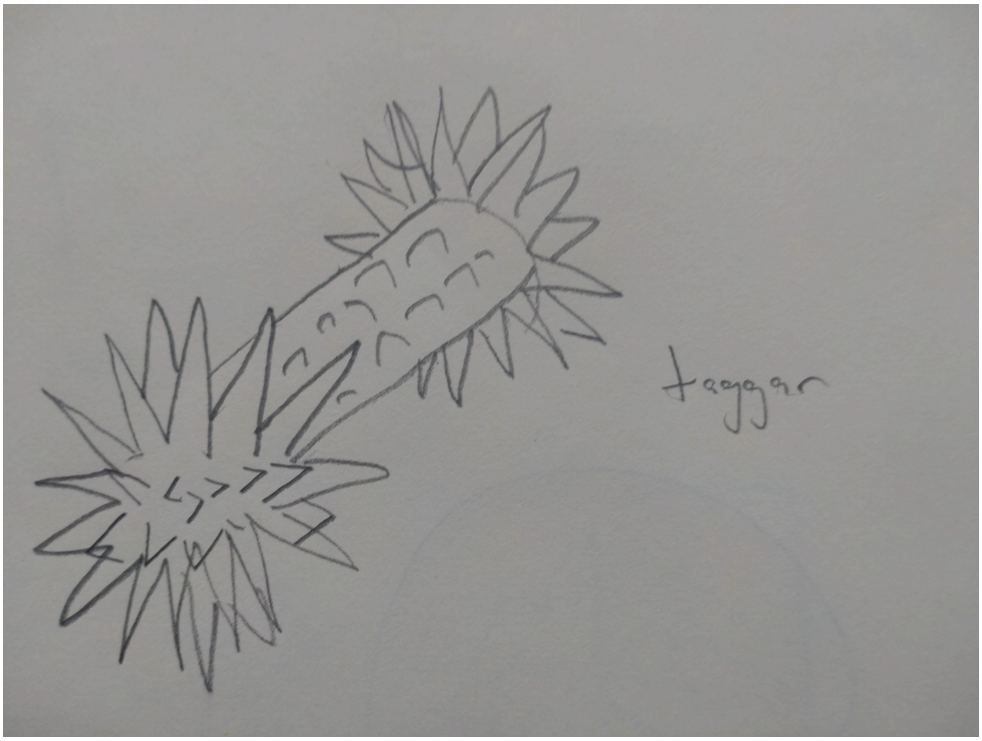

Figure 5.5: Initial sketch of the concept ”Spikes”. (Source: Author’s own work)

5.3 Common ideas and concepts

5.3.1 Implications from the brief

Following the creation of the “standard battery pack”, it is easily observed that if the goal was to only minimize weight, the same geometry but hollowed out would be ideal. The complications arise from the other criteria, making it necessary to add material to certain places. Here the concepts of ingress protection and humidity play an important role in what is and isn’t possible. Had the mechanical and thermal tests been the only ones taken into consideration, then it would have been possible to have complex hollowed out rib-like structures. However, this is not feasible in terms of making a viable product. Electric scooters are regularly subjected to dirt and water, while being outside in the Swedish climate. To ignore this completely would be silly. Hence, all concepts feature full protection (in terms of shape).

5.3.2 Ideas

Other similar ideas were used across multiple concepts. For instance, many designs have more material on the short side of the battery. This idea comes from the drop test. It should be more likely for an oblong shape to make first contact at the outskirts, during the tests. Hence, it would make sense to reinforce these parts. For the same reason, the corners are rounded here, with the aim of distributing the load more evenly, and not getting the forces too concentrated, during impact.

Another idea utilized in some concepts is the idea of diverting the force to more advantageous areas. For instance with the “dragspel” or the “spikes”, the geometries are designed in such a way that the forces act in the most reinforced places. On the other hand these reinforced areas would probably be the first to break, and rather quickly at that.

5.3.3 Simplifications

The essential parts in the battery autonomy were not included. However, the shape of the designs did include surfaces to place these on.

It should also be noted that during this project no consideration was given to screws or other fastening methods. For this reason all ideas, CADs and simulations will assume that the subject is one piece.

Finally, all concepts have some level of symmetry. Symmetry is a good way of simplifying the evaluation, seeing as the shock test and drop test can be applied in multiple directions.

6 Simulations

6.1 CAD

The models were then CAD:ed in Autodesk Fusion. Here the standard battery pack was first modeled, see Figure 6.1. Then the designs were subsequently modeled around this, according to the sketches seen in the previous section. Importantly, extra thickness was added to the models. This was in order to give the future topology optimization a proper design space to optimize. These first designs were more about finding the right outside shape, rather than calculating any internal dimensions or thickness. The initial CADs can be viewed in Figures 6.2–6.5.

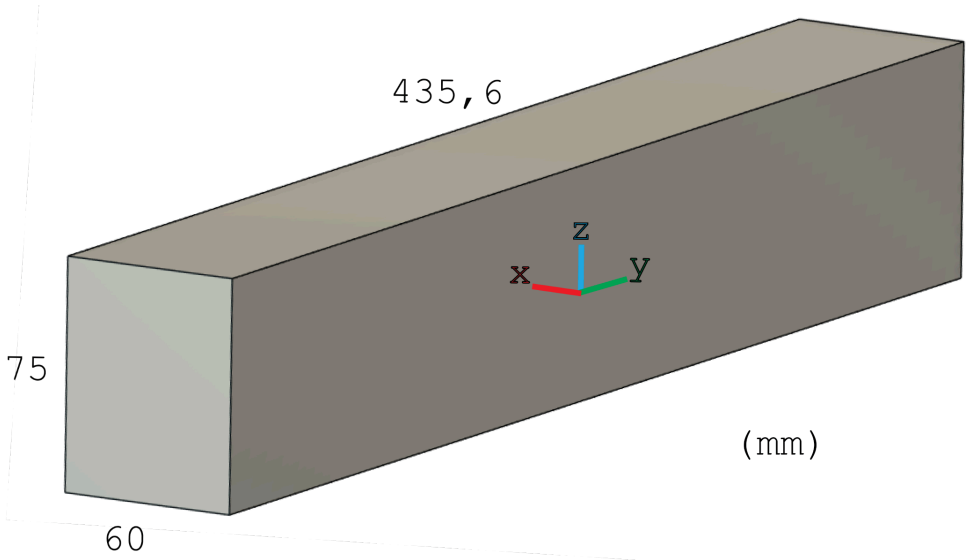

Figure 6.1: Standard battery pack. (Source: Author's own work)

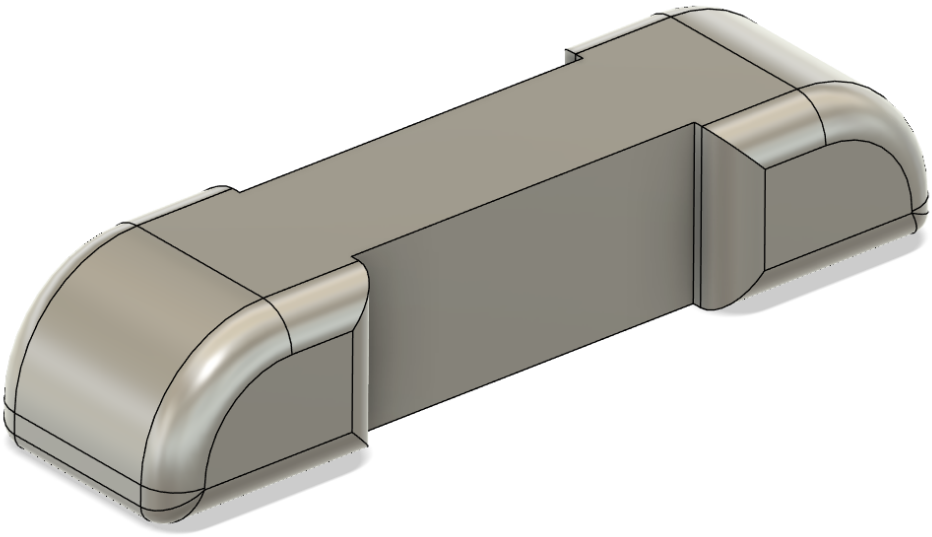

Figure 6.2: CAD of ”Genius” concept. (Source: Author’s own work)

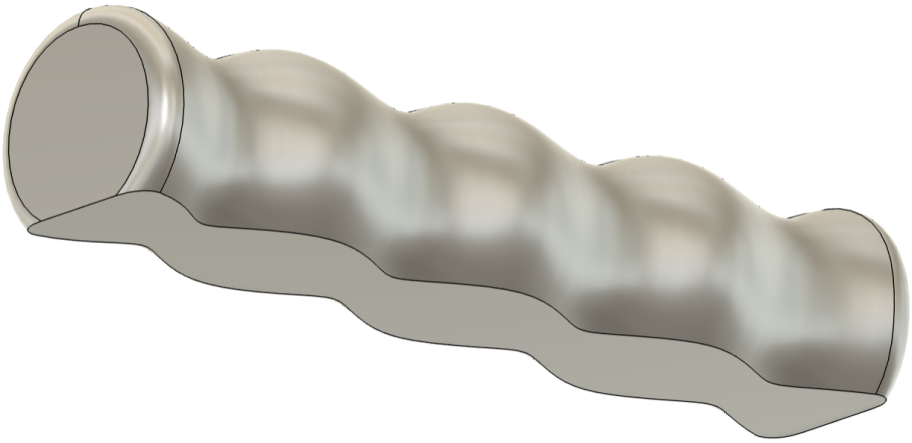

Figure 6.3: CAD of ”Dragspel” concept. (Source: Author’s own work)

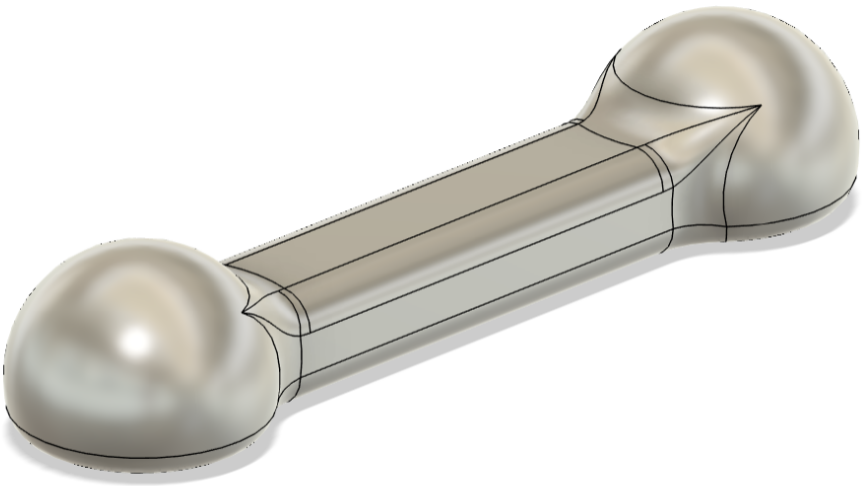

Figure 6.4: CAD of ”Dumbbell” concept. (Source: Author’s own work)

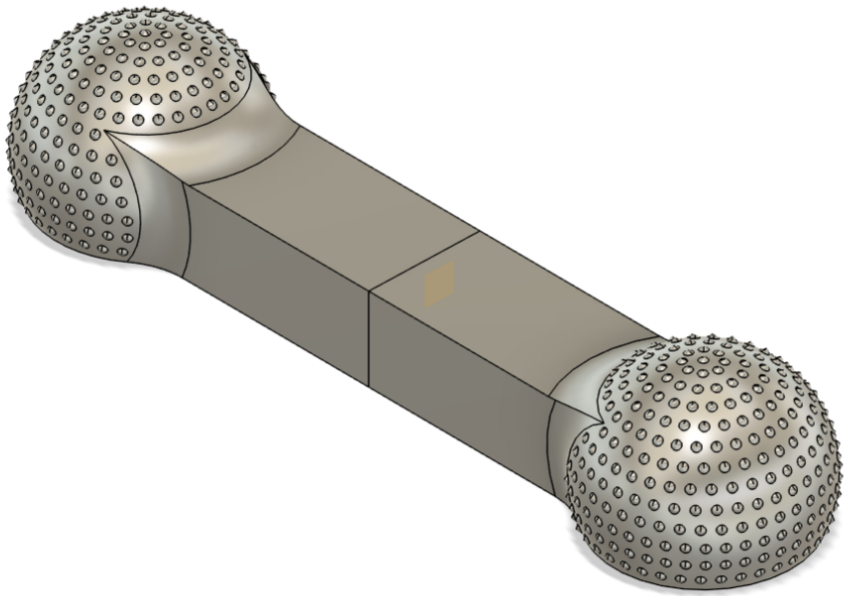

Figure 6.5: CAD of ”Spikes” concept. (Source: Author’s own work)

6.2 General simulation information

For the simulations, ANSYS 2024 R2 was used. The FE analyses and the topology optimization were done in ANSYS Mechanical.

The material was modeled based on PA 2200, using values from Table 3.1. All other parts, such as walls and floors, were assumed to be structural steel, which was mentioned as an appropriate material in the drop test instructions.

A major simplification made was to not include the battery or its mass in the simulations. This was primarily done due to its weight not being found. However, another difficulty lay in simulating its placement and movement within the inner cavity. This would also require an approximation of the material properties of the battery, which would substantially complicate the task. And so, in order to keep things simple, the battery and its weight were excluded from the simulations. How this impacts the project is discussed in Chapter 10.

Anisotropy was not considered for the simulations. While it is possible to do this in ANSYS, it is a lot of work for not that much insight, especially when designing for SLS.

For all simulations, the von Mises stresses were measured. These were of interest since they could be compared to the tensile strength of the material, in order to evaluate the durability of the design.

Another thing worth mentioning is that super fine meshing was not deemed important in the initial tests. More important was just getting a relatively correct value that might be compared to other designs. Furthermore, knowing “where” the stresses occur gives plenty of information on its own, especially when looking to improve the design. Exact values are more important when trying to verify the design, which is relevant later. Meshing could nevertheless not be disregarded completely at this point, especially when faced with singularities, something which will be expanded upon later.

6.2.1 Template workflow

Making so many simulations in a short period of time was made possible through the use of a ”template workflow”. This method, like the name suggests, involved making a template for each test. When the geometry eventually was changed, ANSYS guided the process of recreating the set-up. This method meant that there was no need for creating a new workbench project for each new test.

6.2.2 Drop test

The drop test instructions specify that the battery should be dropped from a height of 1 m, onto a concrete or metal floor.

When simulating this, an assumption had to be made regarding the orientation during impact. In reality, this would be random, however it is not feasible to simulate for every possible scenario. The assumption eventually made was that the enclosure most likely would land at a corner.

Carrying out the FEA, the CAD was oriented in the manner decided, and placed close to a rectangular plate, simulating the floor. Then, using explicit dynamics, the model was set to an initial velocity calculated based on the 1 m height it was dropped from (neglecting wind resistance). The analysis used 1 step with a 1–2 ms end time. This was enough to capture the impact since the model was so close to the floor. The set-up can be viewed in Figure 6.6. More specific settings can be viewed in Appendix B.

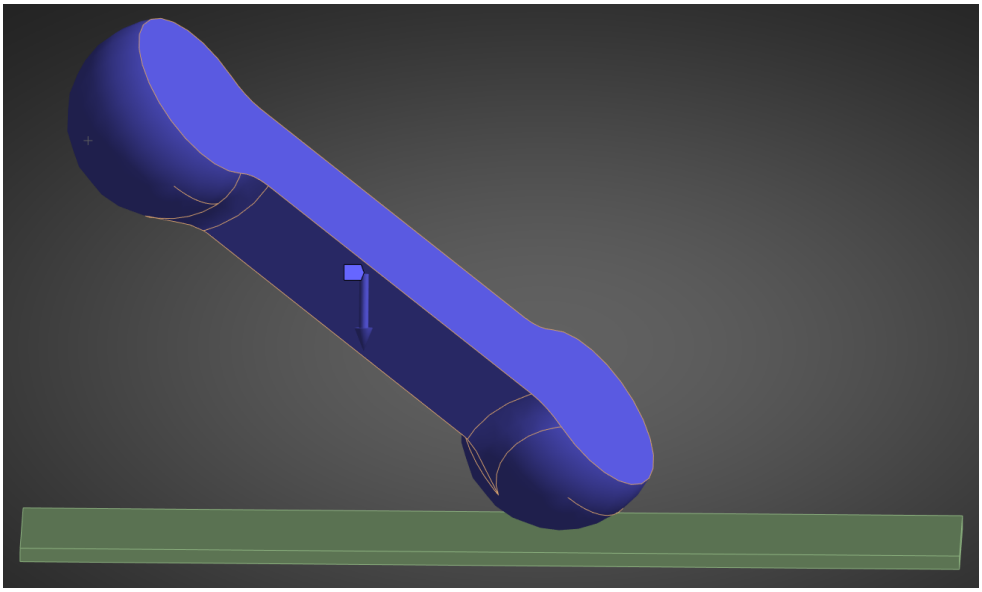

Figure 6.6: Drop test set-up. (Source: Author's own work)

During these tests, the contact force was also calculated and graphed using ANSYS' built-in function, see Figure 6.7.

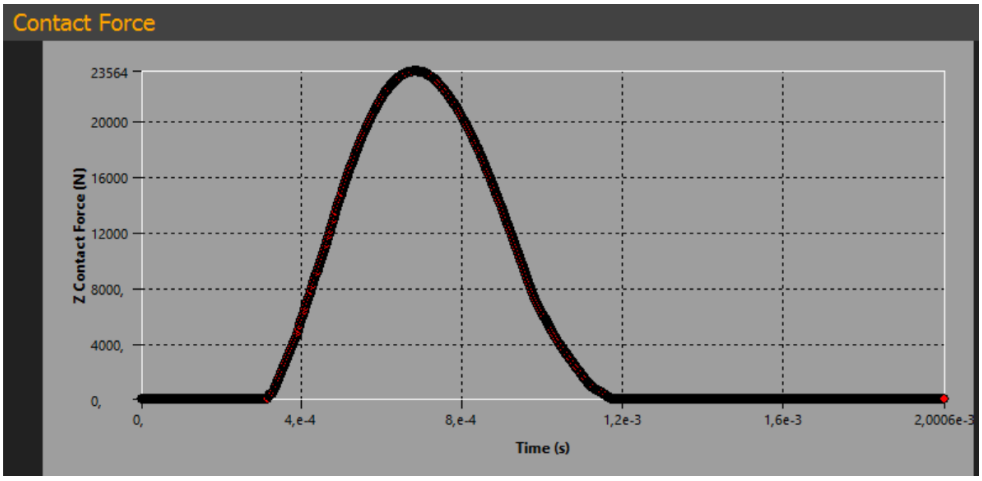

Figure 6.7: Contact force curve. (Source: Author's own work)

6.2.2.1 Drop test issues

The problem encountered with the drop test is that it is not possible to do topology optimization on an explicit dynamic analysis in ANSYS Mechanical. This makes the results obtained from this analysis unusable for further improvement. Another issue that arises with this analysis is that of a singularity. A singularity is a point in the mesh where the stresses do not converge, instead increasing towards infinity as the mesh is refined further and further [87]. In the case of the drop test, this occurs at the point load, at the point of contact. This point can be seen in Figure 6.8.

The problem regarding topology optimization can be solved by instead moving into a static structural analysis. This does, however, require that the model has a fixed support. This has to be there in order to limit the displacements due to acceleration, which static analysis cannot handle. It was deemed most appropriate to place the supports in the inside hole. This way there is not too much torque on the model. Also, for the subsequent topology optimization, having the support inside will not interfere too much. Placing the support at the point furthest away from contact was also experimented with.

The issue of measuring stress was hard to avoid. This issue was tackled by measuring at different mesh sizes and then comparing these values, accepting that they might not be entirely accurate. At this stage of the project, this is fine since it was merely about comparing options. During testing, meshing with 10 mm, 2 mm and 1 mm mesh at the contact point was used, with the hope of convergence.

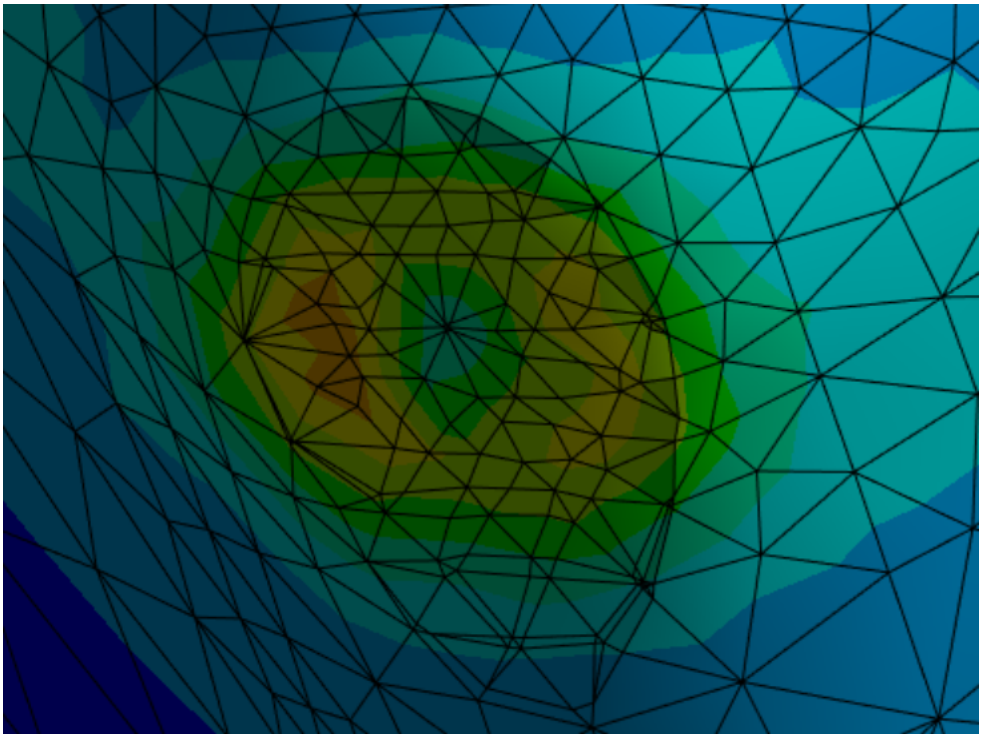

Figure 6.8: Drop test ”Genius” close-up. 2 mm mesh. (Source: Author’s own work)

6.2.3 Shock test

The shock test instructions specified a shock in the shape of a half-sine wave, with a pulse duration of 6 ms. Also, there is a maximum acceleration of 150 g. This can be described as:

$$150 * 9,80665 * sin((acos(-1) * time)/0,006) \tag{6.1}$$

For this test, the enclosure was placed between two plates. Then one of the plates was assigned as fixed support, while the other parts were subjected to acceleration according to the test specifications. The acceleration had to be applied as a function based on (6.1).

This could be done in a static analysis, since all the parts are in contact with each other during this part of the shock test. Figure 6.9 shows what one of these simulations looked like.

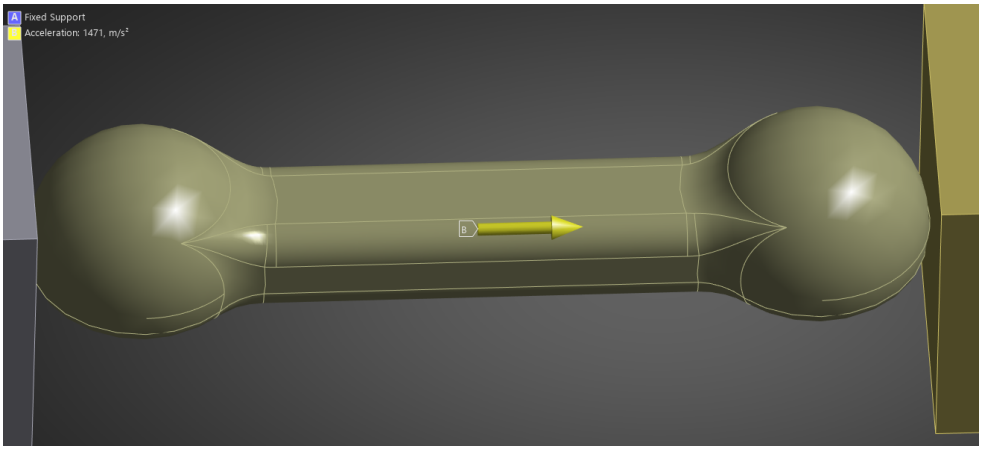

Figure 6.9: Shock test set-up with ”dumbbell” model. (Source: Author’s own work)

The shock test was done in three different directions (x, y, z). These directions are also defined in Figure 6.1. Whenever directional stresses are mentioned in this report, e.g. ”y-direction stresses”, it is assumed that it is in the context of the shock test.

6.2.4 Vibration test

In order to test for vibration, there was no need to simulate a full logarithmic sine sweep test. Instead, the program is simply allowed to find the natural frequencies of the structures. The test is passed if there are no modes within the 7–200 Hz range.

The method used within ANSYS was to apply a modal analysis on the model, in order to find the modes (or the natural frequencies). The aim is transport safety, so no fixed support was used.

6.2.5 On the topic of thermal simulations

There will also be no thermal simulations, with respect to the two thermal tests. For one, the shape of the model barely has any impact on these tests. However, more importantly, material data, such as melting temperature, was deemed sufficient for this project. Furthermore, attempting to simulate the actual thermal test and getting an accurate result was deemed too complicated. This is discussed further in section 10.1. All other tests are done at 20°C, as is specified in the test instructions.

6.3 Simulation results

The following table, Table 6.1, contains all FE simulations made in ANSYS at this stage. The drop test contains three values, each for different mesh sizes at the contact point. The shock test contains stresses for each of the three directions x, y, z. These directions are also defined in Figure 6.1.

Table 6.1: Concept testing results

Concept	**Mass (kg)**	**Drop test (MPa) (10mm/2mm/ 1mm)**	**Drop test(contact force)(10mm) (N)**	**Shock test (MPa)**	**Closest mode (Hz)**
Real Product	0,35985	21,686/ 98,087/ -	2450,8	x:5093,1 y:506,99 z:728,04	733,04
Simple rect-angular	0,281	23,865/ 84,011/ 116,06	1295,3	x:39,759 y:37,456 z:54,027	261,75
Genius	0,638	22,662/ 64,697/ 73,028	2926,3	x:336,96 y:171,07 z:25,235	396,53
Dragspel	0,978	30,335/ 59,603/ 102,47	6258,6	x:284,01 y:27,703 z:383,35	451,28
Dumbbell	2,661	40,718/ 38,302/ 45,504	23564	x:83,943 y:58,874 z:133,52	189,94
Spikes	2,632	-/ -/ 304,39	19399	-	-

In the spirit of design thinking, other tests were made outside of the developed ideas. These tests, which were deemed relevant by the author, had the aim of further gathering information. One such test involved simulating a model inspired by current products. This way, information is gathered regarding how other e-scooter batteries might perform in these tests. As can be seen in Figure 6.10 and in Table 6.1, the stresses were quite high in these tests compared to other concepts.

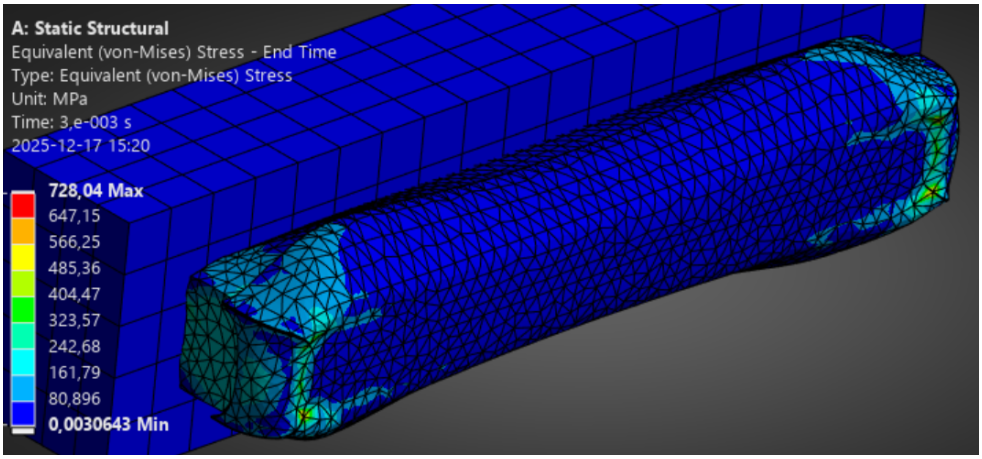

Figure 6.10: ”Real product” model, based on the HX X8 e-scooter battery. z-direction shock test. One wall hidden. (Source: Author’s own work)

It needs to be made clear that this model is merely a rough translation based solely on a picture. Furthermore, a different material to the original was most likely used.

Another test the author thought was relevant was simulating a simple rectangular model, see Figure 6.11. While not passing all tests, it did have comparatively low stresses. As can be seen in Table 6.1, it outperformed all the concepts on most metrics.

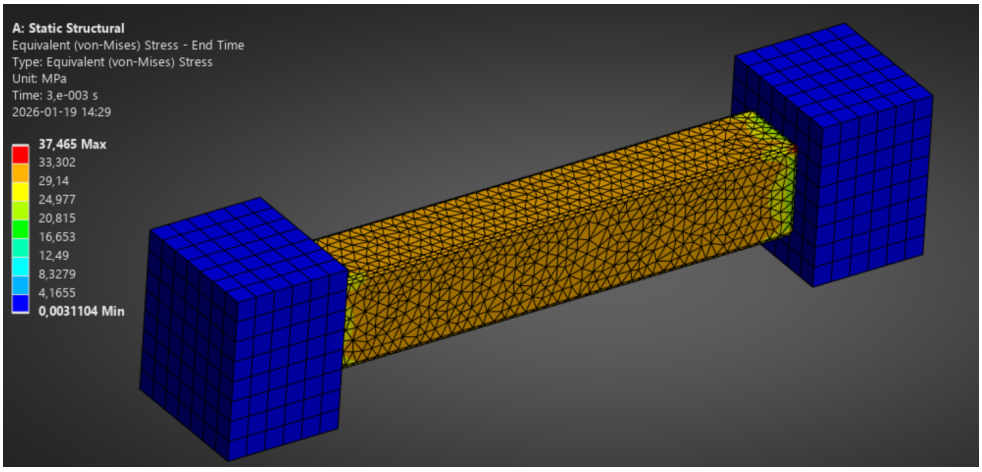

Figure 6.11: y-direction shock test of ”Simple rectangular” model. (Source: Author’s own work)

The ”Genius” model showcased the lowest stresses of all in the z-direction. Its highest stresses were in the x direction, see Figure 6.12.

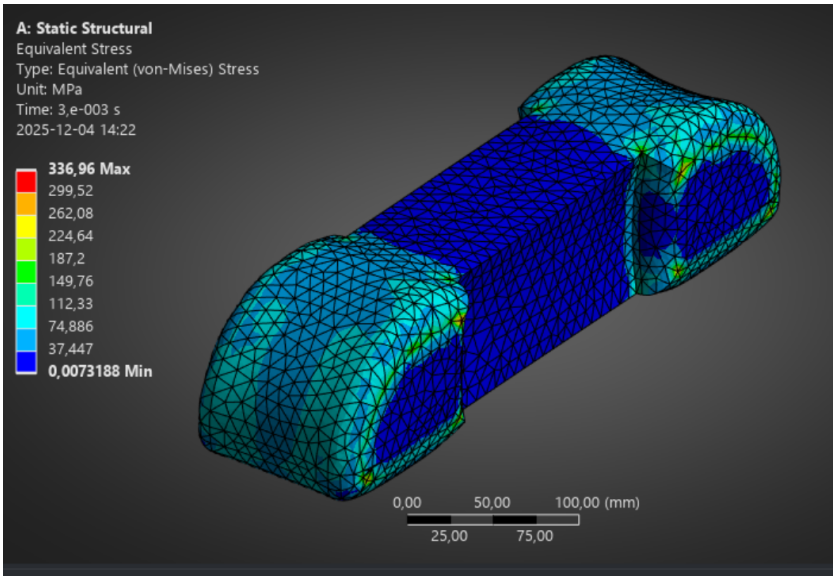

Figure 6.12: x-direction shock test of ”Genius” model. Both walls hidden. (Source: Author’s own work)

The ”Dragspel” model showcased the lowest stresses of all in the y-direction, see Figure 6.13. In this test, stresses were evenly distributed in the crevices. Its highest stresses were in the x-direction.

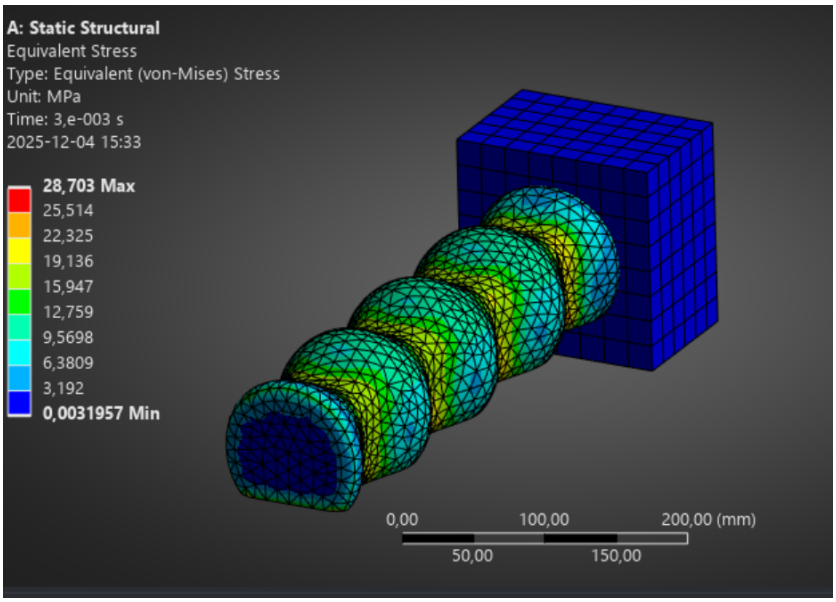

Figure 6.13: x-direction shock test of ”Dragspel” model. One wall hidden. (Source: Author’s own work)

The ”Dumbbell” model had the lowest drop test stresses of all at the finer mesh sizes. ”Dumbbell” was however the only concept that failed the modal test.

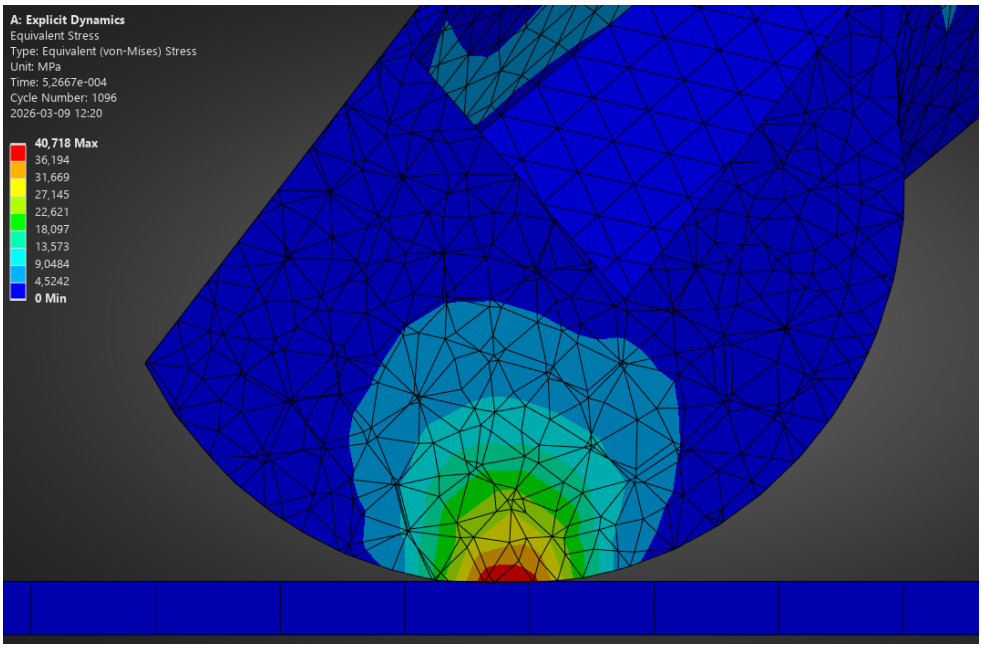

Figure 6.14: Drop test of ”Dumbbell” model. Sectioned view. (Source: Author’s own work)

”Spikes” was tested mostly with the intent of making a point, which can be read about in the discussion. Due to the high level of detail in the drop test contact point, see Figure 6.15, it was concluded that a coarser mesh than 1 mm would be nonsensical. The shock- and modal tests were not conducted due to ”Spikes” already being discarded as a concept after the drop test.

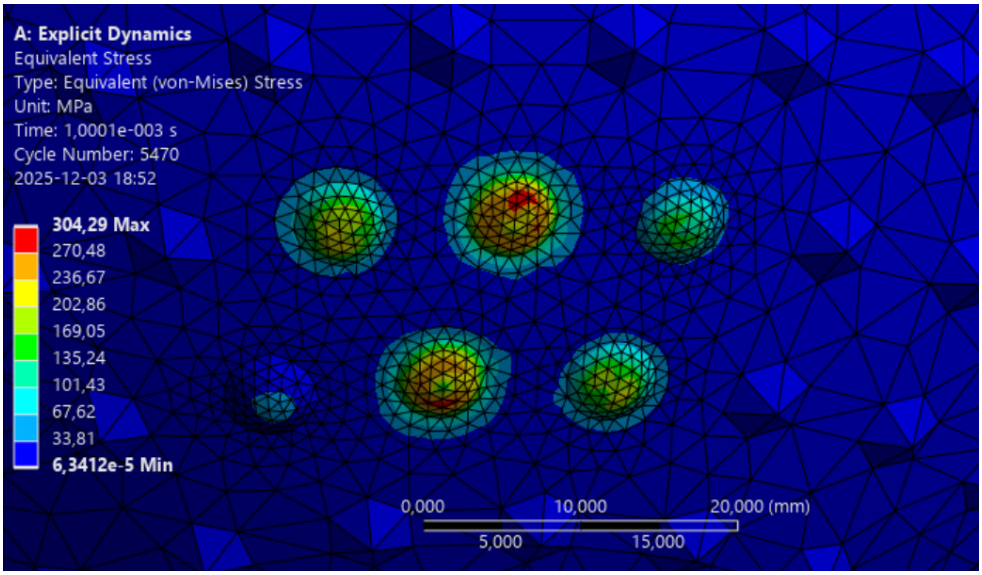

Figure 6.15: Close-up view of contact point in ”Spikes” drop test. Floor hidden. (Source: Author’s own work)

6.4 Topology optimization

After every FEM simulation, the opportunity of performing topology optimization was seized. This was also done in ANSYS Mechanical. Since the acceptance criteria for many of the tests were ”no rupturing”, it was considered most relevant to optimize for the minimization of stress. However, compliance was also, at times, used as goal function. More specific settings can be viewed in Appendix B.

6.4.1 Drop test optimization

For the drop test optimization, a separate static analysis was made with a constant force. The furthest point from the force was chosen as support. This can be seen in Figure 6.16 with the grey spot up top where the program wants to keep material.

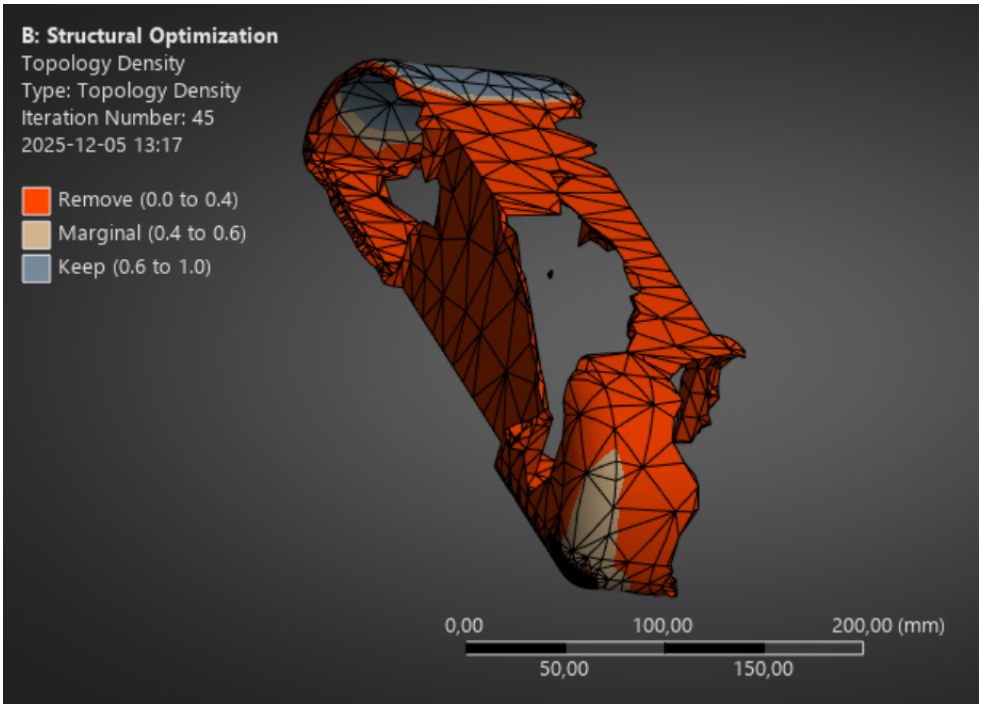

Figure 6.16: Drop test topology optimization of ”Genius” model. (Source: Author’s own work)

6.4.2 Shock test optimization

For the shock tests, topology optimization could be directly applied to the already created FEM set-ups. Figures 6.17–6.19 show three results which would prove influential for the rest of the development.

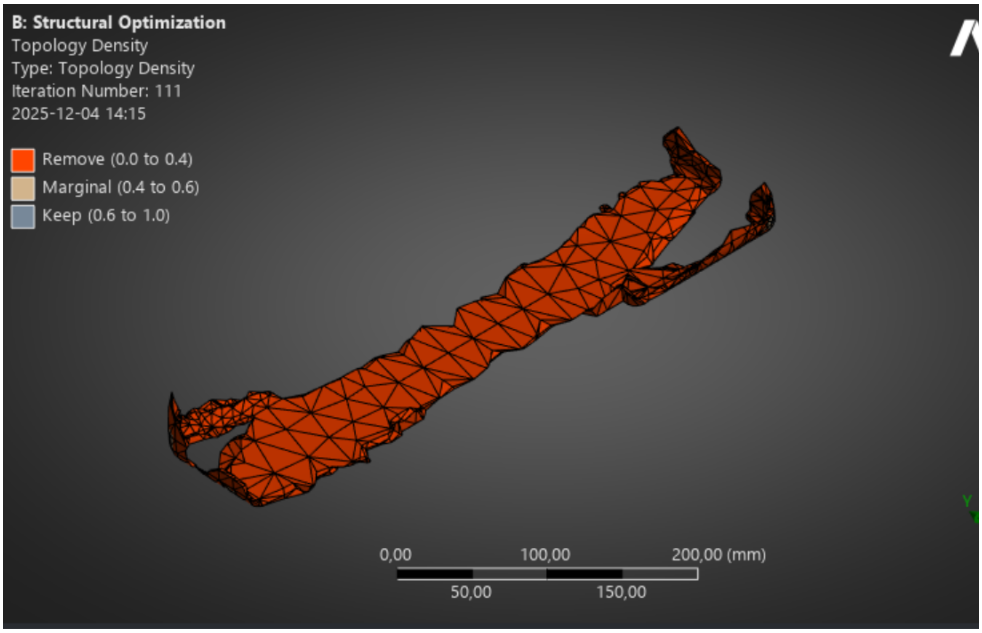

Figure 6.17: y-direction shock test topology optimization of ”Genius” model. (Source: Author’s own work)

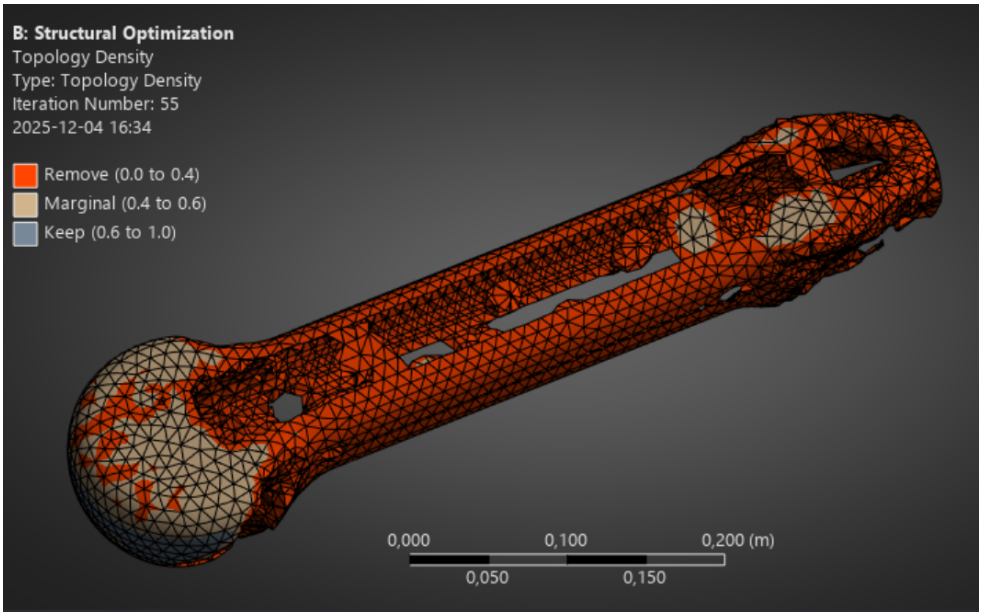

Figure 6.18: y-direction shock test topology optimization of ”Dumbbell” model. (Source: Author’s own work)

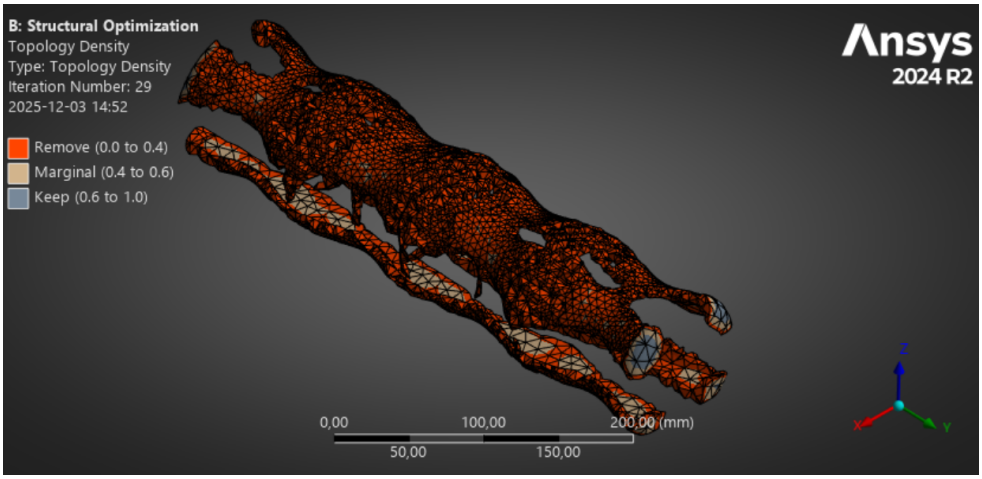

Figure 6.19: y-direction shock test topology optimization of ”Dragspel” model. (Source: Author’s own work)

6.4.2.1 Modal optimization

Finally, it is also possible to optimize for maximum natural frequency. This produced the result seen in Figure 6.20. The author evaluated this result as being undecipherable.

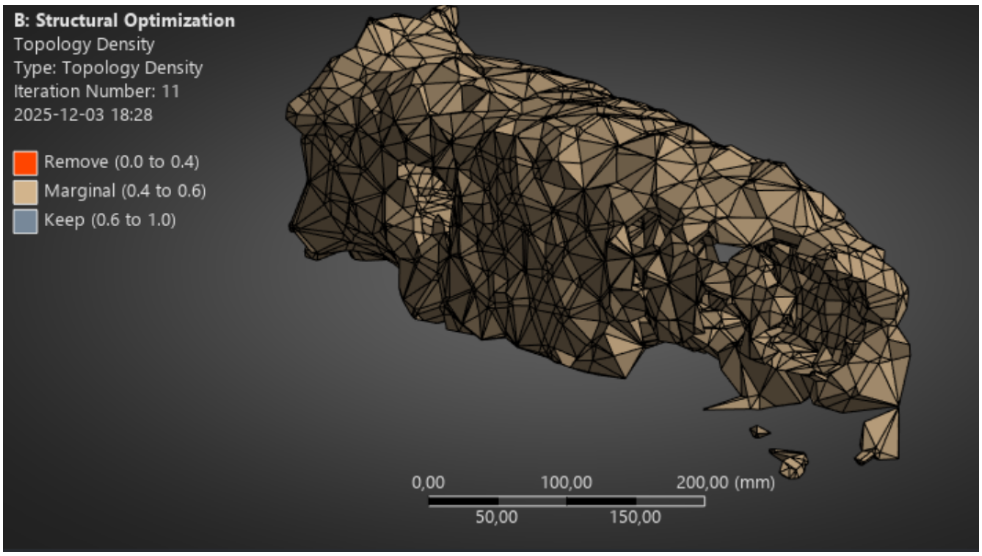

Figure 6.20: Topology optimization, maximizing the natural frequency of a design space. (Source: Author’s own work)

6.4.3 Design space optimization

On top of these topology optimizations, tests were also made using a complete design space. This gave the program access to all material within a rectangular domain.

6.4.3.1 Drop test - different corners

Applying the same drop test procedure, the results in Figure 6.21 and Figure 6.22 were obtained. One had a drop test at only one corner, while the other applied the force at all corners.

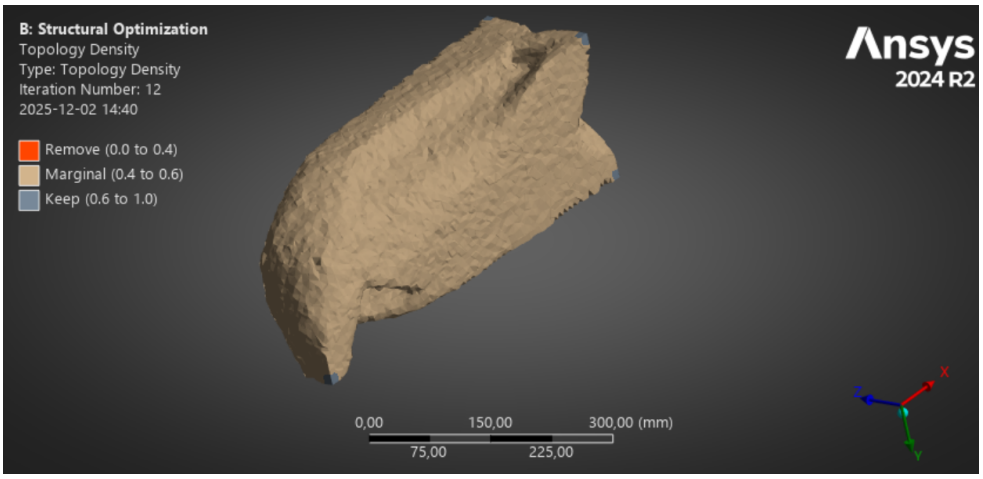

Figure 6.21: One corner drop test optimization of design space. (Source: Author's own work)

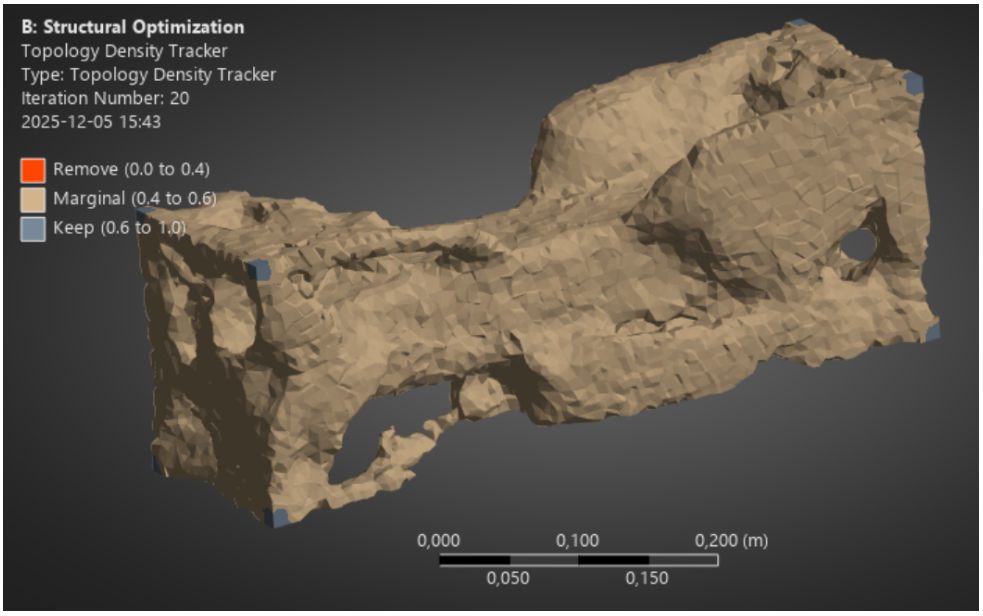

Figure 6.22: All corners drop test optimization of design space. (Source: Author's own work)

6.4.3.2 All shock tests

Using the same shock test procedure as before, but for the design space, yielded the result seen in Figure 6.23. The same test in x- and z-direction resulted in similar geometries, including the slight concavity.

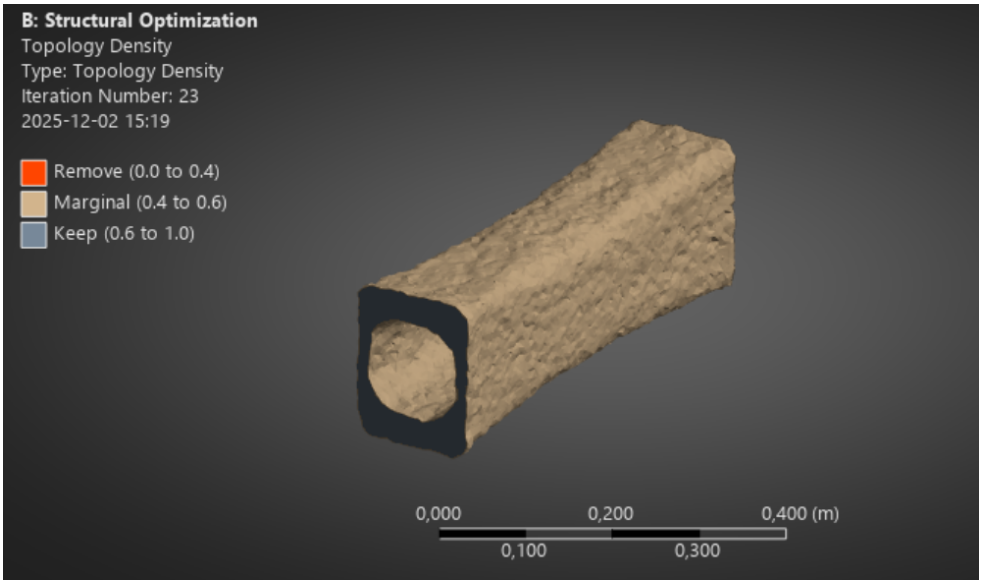

Figure 6.23: Design space y-direction shock test optimization. (Source: Author's own work)

Furthermore, ANSYS allows for topology optimization of multiple FEM set-ups at the same time. This means that multiple FE analyses are made at each iteration. This was utilized for optimizing the design space for all shock tests at once, minimizing stress. The set-up can be viewed in Figure 6.24, where all three shock tests are applied to the design space. The resulting tesseract-like geometry can be viewed in Figure 6.25.

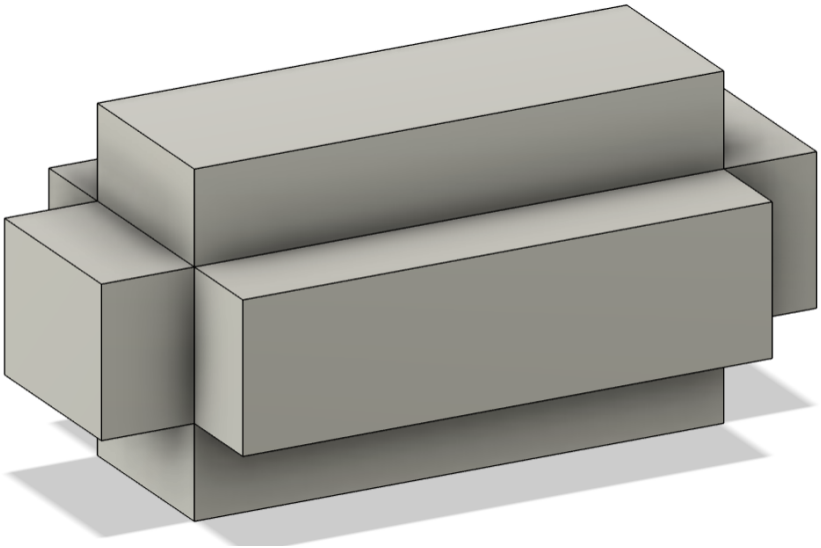

Figure 6.24: All shock tests set-up in Autodesk Fusion (the design space is on the inside). (Source: Author's own work)

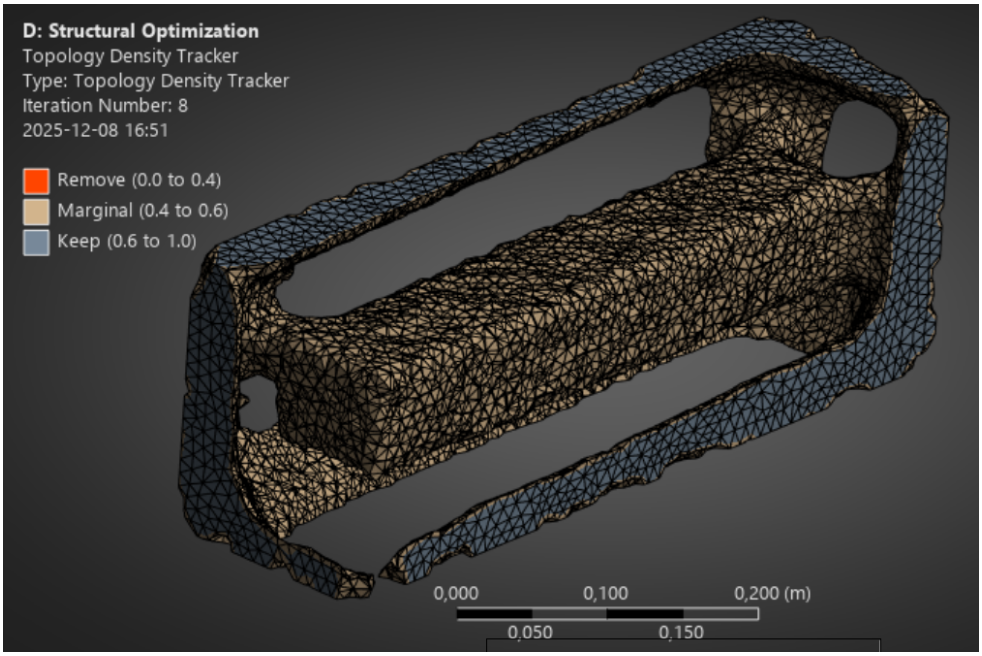

Figure 6.25: All shock tests optimization result. (Source: Author's own work)

6.4.4 Limitations

One limitation of the topology optimization program is that material cannot be removed wherever the force is applied, or at places where supports are set up. This is reasonable as the program would otherwise have to constantly update these, without having the same context the user has. Nevertheless, it does lead to some additional thinking required when analysing the results.

In the case of the drop test, there will always be material at the force application, leading to the spike seen in Figure 6.21. This does not mean that the spike is the ideal form. However, ignoring the spike itself, it does give an idea of what the support behind the contact point might look like.

6.4.5 Some specific settings

For most of the optimizations, a penalty factor of p=3 was used. This is the default setting in ANSYS and was accepted as a reasonable number. However, when the results sometimes gave a very vague shape, the penalty factor was increased up to p=5.

The problem also calls for a response constraint to be set up. This comes in the

form of penalizing too much mass. For these optimizations a ranged response constraint was used, setting the retained mass at 30–80 %. In some cases, when a distracting amount of mass was kept, the maximum was 50 %, and sometimes even 30 %. For instance, the “all shocks test” had a maximum mass of 50 %, so that the program was forced to make some hard hitting decisions.

Like mentioned before, it was deemed most relevant for this project to minimize stress. Hence, the equivalent von Mises stress was chosen as the goal function. Even so, the opportunity to also do an optimization minimizing compliance was seized, seeing as this would waste very little time with the project already open. This way even more information could be obtained regarding the behaviour of the model.

It can also be of note that stress optimizations required on average about 40–50 iterations in order to converge sufficiently. A few times there were problems with the optimization taking too long to converge. This was solved by loosening the requirement for the program to consider it converged.

6.4.6 Other information

The colors in the topology optimization images inform whether or not the material in question “should” be removed or not. However, since these limits are somewhat arbitrary, it is a valid strategy to also investigate the red material close to the limits. This will still give information regarding shape and how the material is prioritized.

7 Iterative improvements and testing

7.1 Choice of design

After all tests, the decision was not to choose one singular design. Rather, all conclusions, insights and general information were gathered in order to form design principles. Some of the most important ones were that:

- A rounded contact point is beneficial for the drop test
- A large contact area is beneficial for the shock test
- An accordion-like structure can distribute stresses more evenly

This, together with pen and paper, was applied in order to design one ”Master” design, see Figure 7.1.

This concept combined the accordion-like function of ”Dragspel”, while still attempting to maintain rounded ends, like ”Dumbbell”. Furthermore, the ”Master” concept features large contact areas during all shock tests.

This was subsequently CAD:ed and tested, see Figure 7.2.

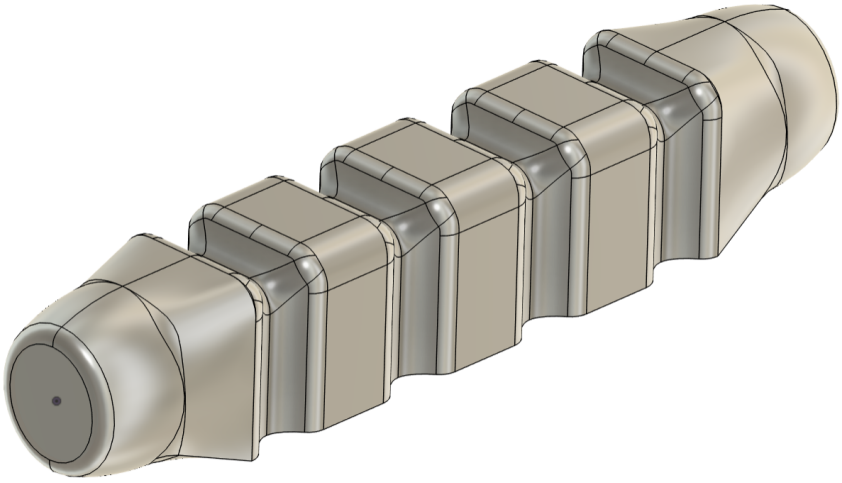

Figure 7.1: ”Master 1” CAD (Source: Author’s own work)

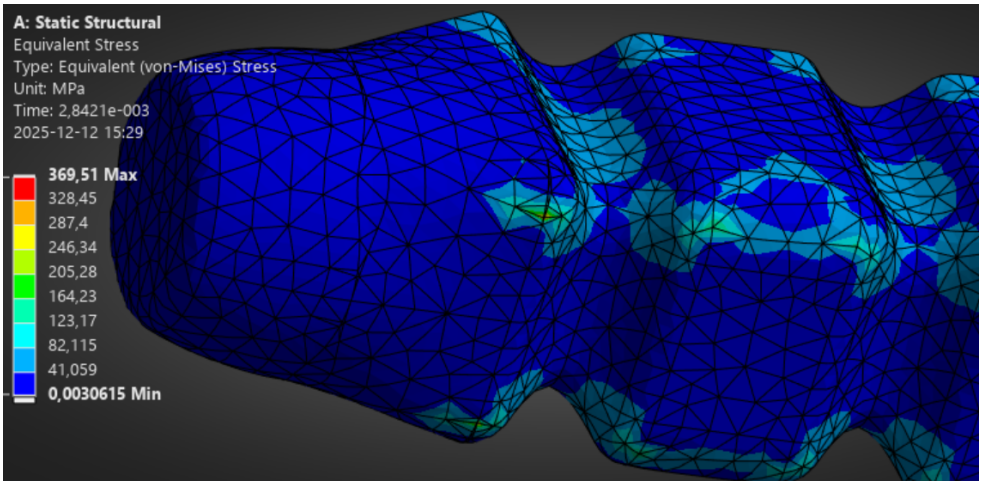

Figure 7.2: ”Master 1” z-direction shock test. Walls hidden. (Source: Author’s own work)

As can be seen in Figure 7.2, the resulting stresses were higher than many of the concepts it was based on.

Subsequently, the author decided to completely abandon this idea and create a new concept, ”Master 2”.

This marked the beginning of the ”Master” series.

7.2 The ”Master” series

The ”Master 2” concept was more similar to the ”Dumbbell” model. In comparison to ”Master 1”, it was more compact, while still attempting to maintain large contact areas for the shock tests. The tunnel between the ends featured a slight concavity, inspired by previous topology optimizations, see Figure 6.23. ”Master 2” can be viewed in Figure 7.3.

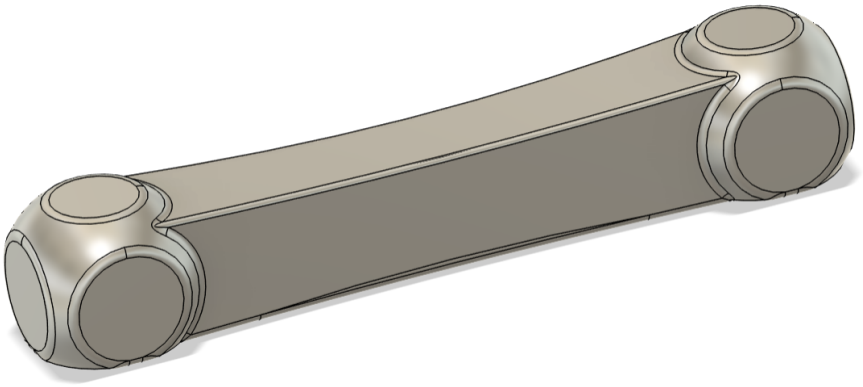

Figure 7.3: ”Master 2” CAD. (Source: Author’s own work)

This test showed stresses below 48 MPa in all tests except the drop test and the shock test in y-direction, see Table 7.1. The shock test in y-direction showed high stresses from bending, as can be viewed in Figure 7.4.

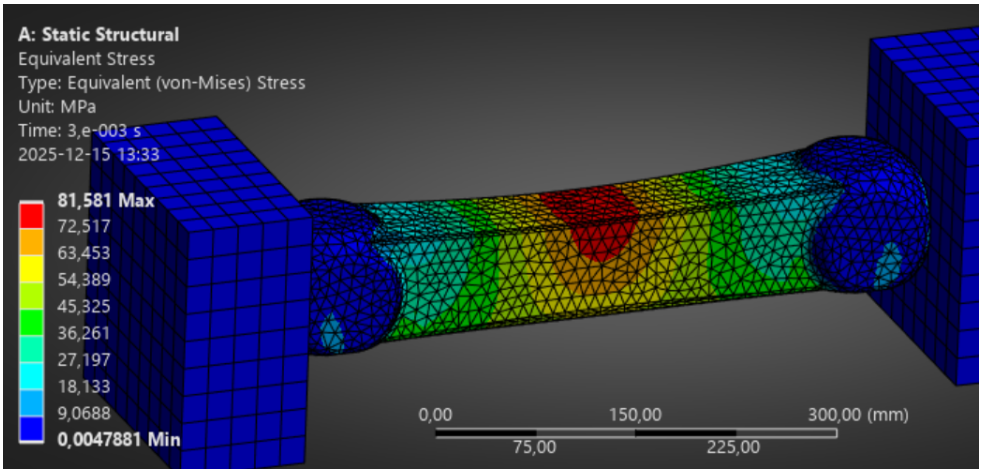

Figure 7.4: ”Master 2” y-direction shock test. (Source: Author’s own work)

What followed was a quest with the singular aim of minimizing the stress in y-direction, as can clearly be seen in Table 7.1. The process involved adding X-shaped reinforcements, see Figure 7.5, inspired by topology optimization results seen in Figure 6.17 and Figure 7.11. The shape and size of the reinforcements were experimented with in iterations 3–13.5, focusing on reinforcing high stress areas.

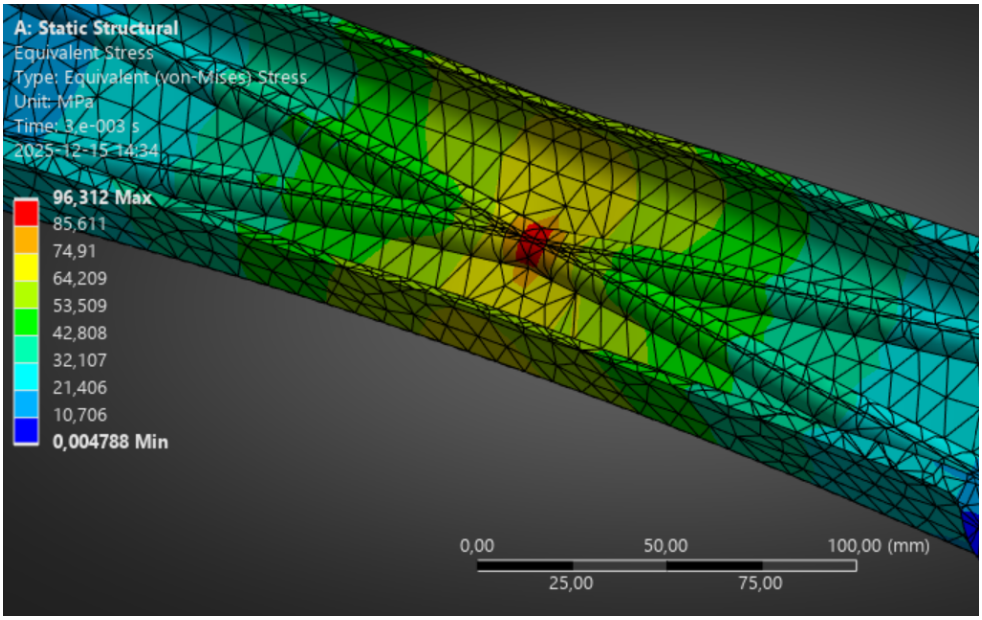

Figure 7.5: ”Master 3” stress point. Section view. (Source: Author’s own work)

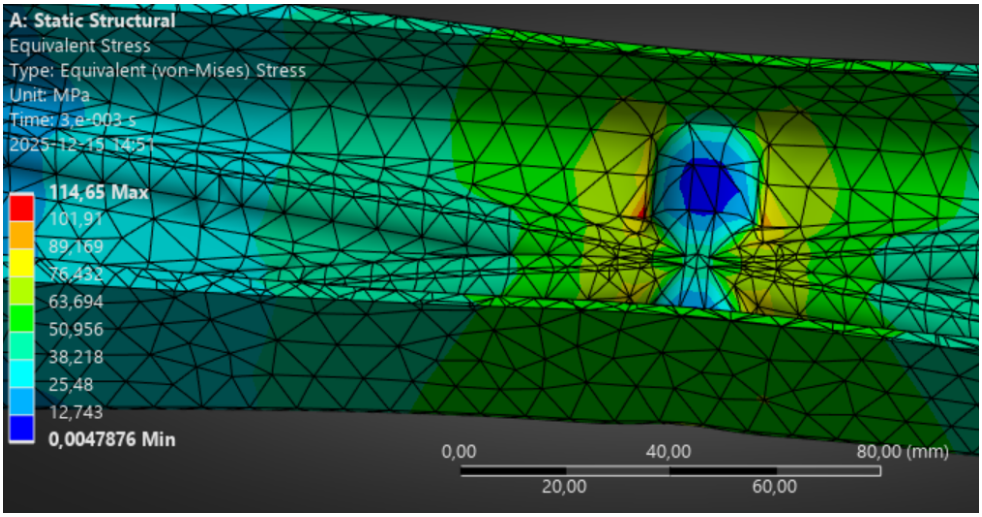

Figure 7.6: ”Master 4” stress point. Section view. (Source: Author’s own work)

Finally, after adding more smooth reinforcements, not only up top but along the sides of all walls, the result in Figure 7.7 below was achieved. It is called Master 13.5 because it was not different enough from the original Master 13.

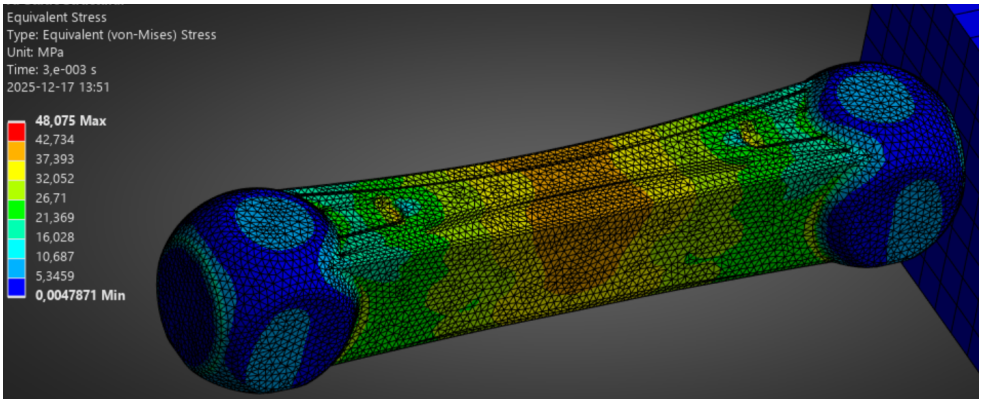

Figure 7.7: ”Master 13.5” y-direction shock test. One wall hidden. (Source: Author’s own work)

This model was subsequently subjected to all tests, and was used as a benchmark for comparing following iterations. The testing revealed z-direction stresses of 56,754 MPa. The following iterations (Master 13.6–13.7) featured slight alterations in the height of the balls, which finally led to the result in Figure 7.8 below. ”Master 13.7” also had lower drop test stresses than 13.5.

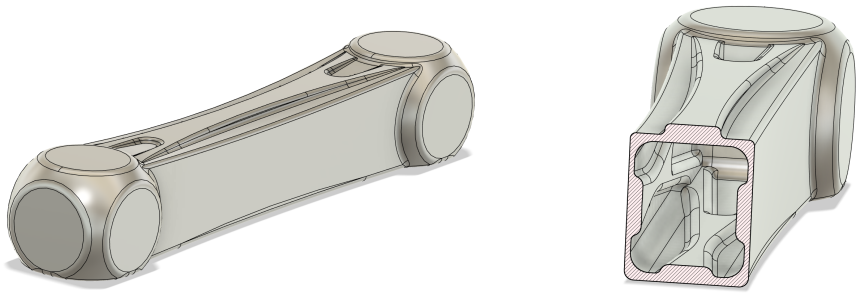

Figure 7.8: Left. ”Master 13.7” CAD. Right. ”Master 13.7” section view. (Source: Author’s own work)

This ended up being the best performing concept of the whole Master series. The whole Master series can be viewed in Table 7.1.

Table 7.1: Results of the ”Master” series

Iteration	Mass (kg)	Drop test (MPa) (10mm/2mm/ 1mm)	Drop test(contact force)(5mm) (N)	Shock test (MPa)	Closest mode (Hz)
Master 1	0,710	18,836/ 30,704/ 63,934	2485,7	x:190,35 y:125,11 z:369,51	198,96
Master 2	1,490	21,508/ 53,372/ 60,532	16805	x:27,246 y:81,581 z:37,196	233,99
Master 3	1,554	- / - / -	-	x:- y:84,209 z:-	-
Master 4	1,563	- / - / -	-	x:- y:114,65 z:-	-
Master 5	1,604	- / - / -	-	x:- y:78,269 z:-	-
Master 6	1,607	- / - / -	-	x:- y:84,303 z:-	-
Master 7	1,612	- / - / -	-	x:- y:80,445 z:-	-
Master 8	1,399	- / - / -	-	x:- y:90,535 z:-	-
Master 9	1,618	- / - / -	-	x:- y:70,838 z:-	-
Master 10	1,692	- / - / -	-	x:- y:54,433 z:-	-
Master 11	1,593	- / - / -	-	x:- y:55,207 z:-	-
Master 12	1,603	- / - / -	-	x:- y:53,003 z:-	-
Master 13	1,711	- / - / -	-	x:- y:48,099 z:-	-
Master 13.5	1,682	54,428/ 60,448/ 79,165	17845	x:33,066 y:48,075 z:56,754	235,99
Master 13.6	1,674	- / - / -	-	x:- y:- z:85,206	-
Master 13.7	1,675	53,122(5mm)/ 42,863/ 49,606	17746	x:33,889 y:46,176 z:47,314	236,7
Master 14	1,678	- / - / -	-	x:- y:52,463 z:-	-
Master 14.5	1,679	- / - / -	-	x:- y:57,162 z:-	-
Master 15	2,724	42,421(5mm)/ 65,067/ 54,091	20457	x:56,248 y:20,463 z:114,11	338,46

7.2.1 Other tests

After ”Master 13.7”, a few other tests were made with the intent to lower y-direction stresses even further. This had mixed results. ”Master 14–14.5” had points of high stress, which can be seen in Figure 7.9. ”Master 15” was created due to the author not wanting to give up on the accordion idea. This iteration showed very promising y-direction stresses, see Figure 7.10, while on the other hand having high stresses on all other tests, see Table 7.1.

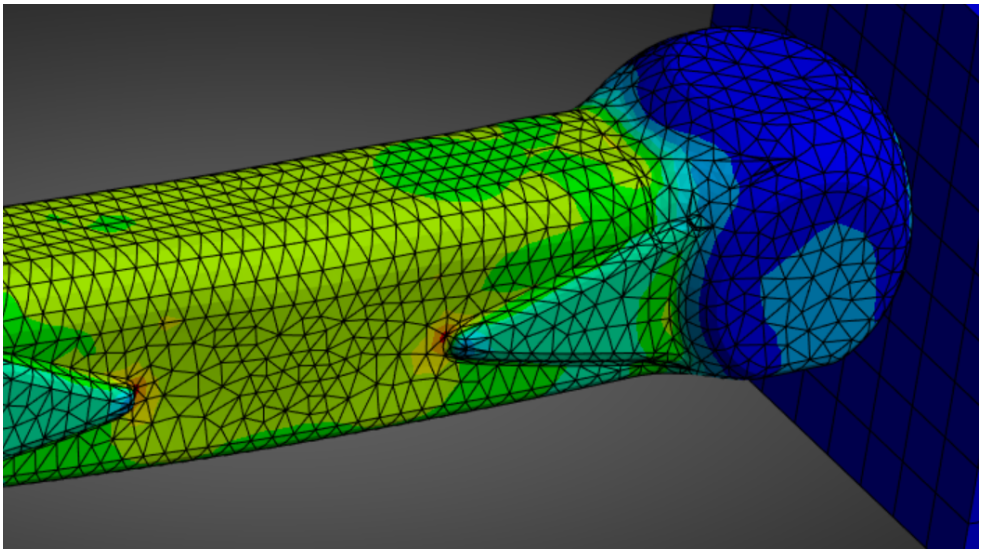

Figure 7.9: ”Master 14.5” shock test y-direction. (Source: Author’s own work)

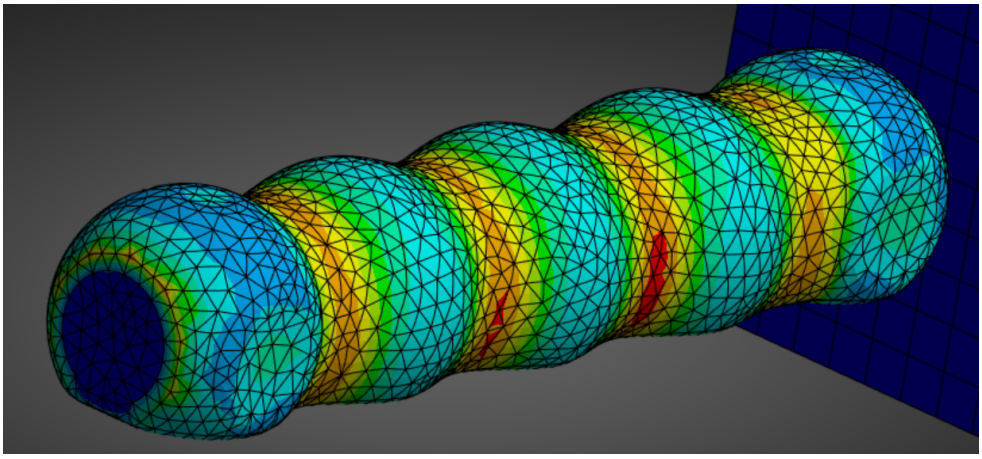

Figure 7.10: ”Master 15” shock test y-direction. One wall hidden. (Source: Author’s own work)

In the end, it was decided that ”Master 13.7” would be the concept moved forward with.

7.3 The usage of topology optimization

It ought to be stated that topology optimization was utilized in this process as well. At the earlier iterations, an optimization was applied for each test, with the goal of obtaining inspiration for future iterations. Two consequential results can be viewed in Figure 7.11 and Figure 7.12.

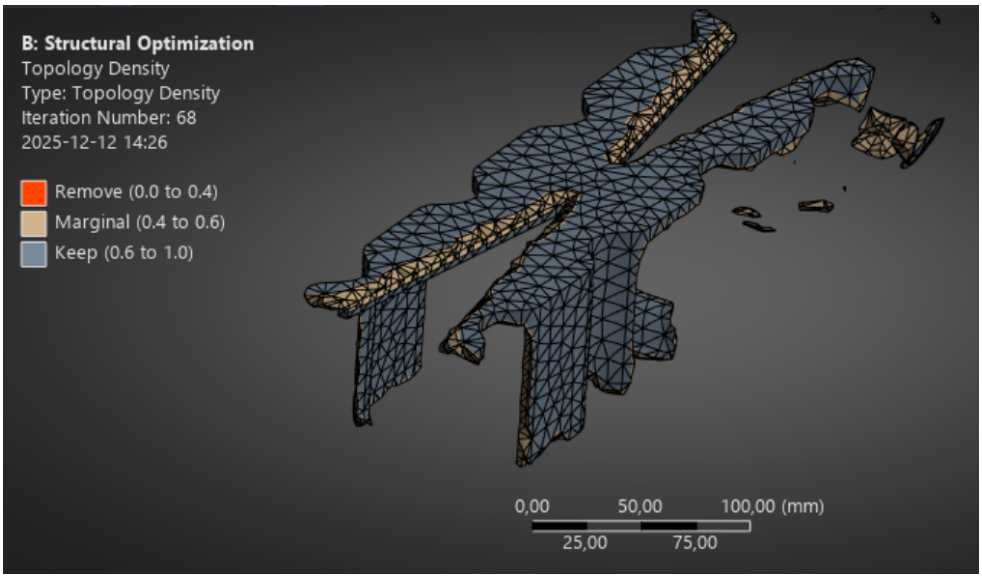

Figure 7.11: Topology optimization of y-direction shock test with ”Master 1”. (Source: Author’s own work)

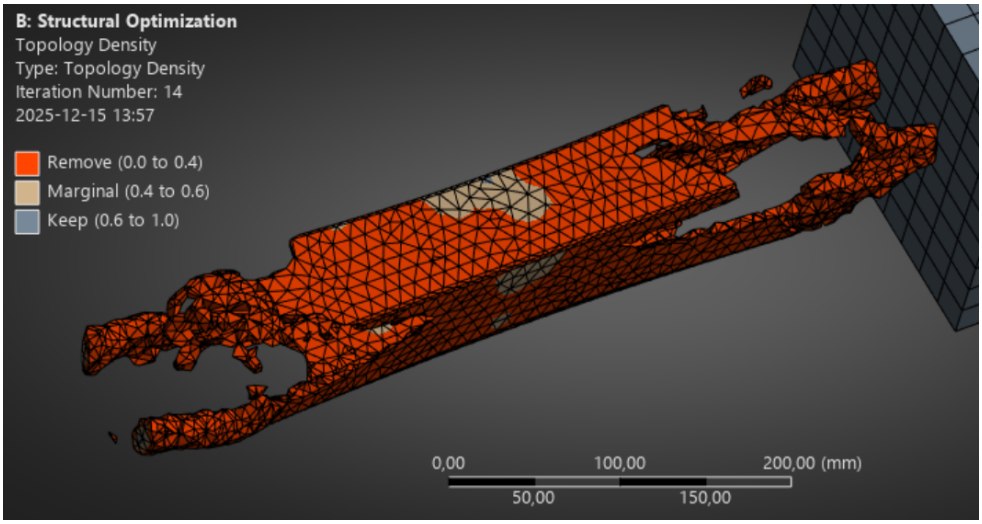

Figure 7.12: Topology optimization of y-direction shock test with ”Master 2”. (Source: Author’s own work)

Furthermore, during the quest to minimize the y-direction shock stresses, a new design space was created. Extra material was added at the tunnel part, leaving the ends as they were, see Figure 7.13. The result can be seen in Figure 7.14.

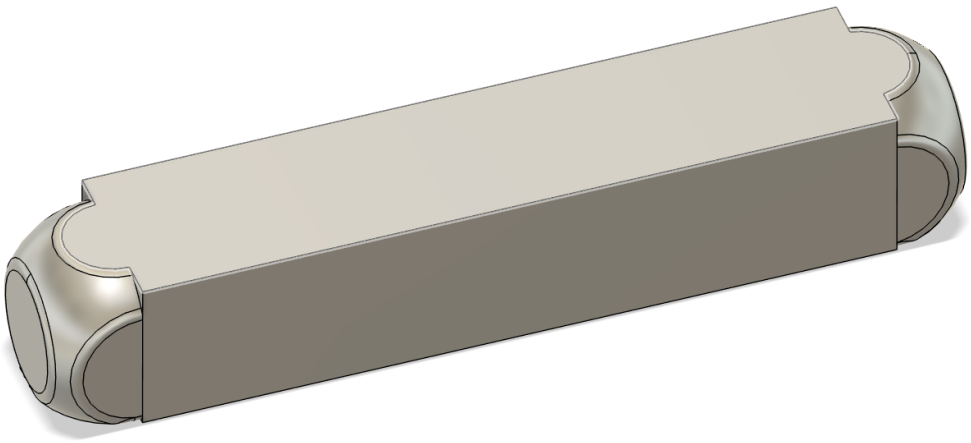

Figure 7.13: New design space. (Source: Author’s own work)

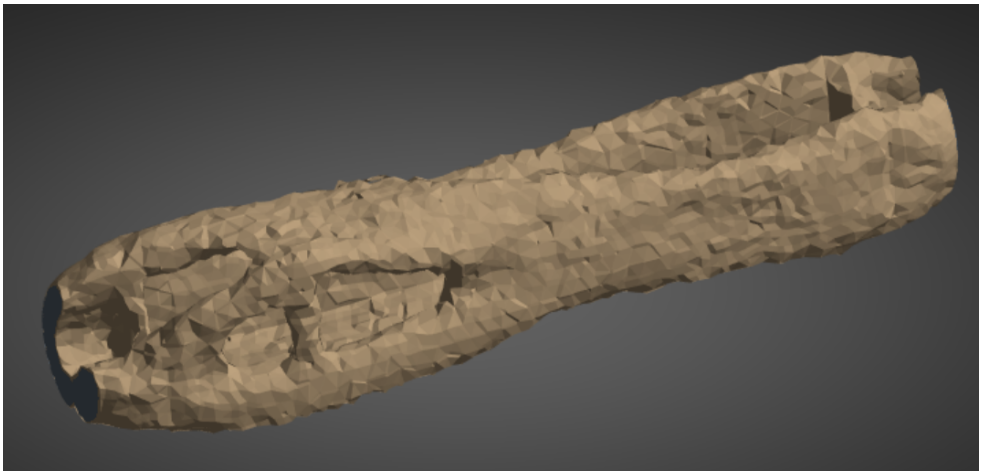

Figure 7.14: New design space topology optimization in the y-direction, results. (Source: Author's own work)

7.4 The ”Maestro” series

At this point, the author did not think that the actual topology optimization results had been utilized to their full potential. For this reason, another iteration series was initiated, named the ”Maestro” series. This series featured a starting design completely inspired by topology optimization results. Some influential results were Figure 7.14, Figure 6.22 and Figure 6.18. The resulting geometry, after some sketching, can be viewed in Figure 7.15. The outer part is the designed part, see Figure 7.16. The inner prism was deemed necessary as a protective casing for the battery, keeping ingress protection in mind.

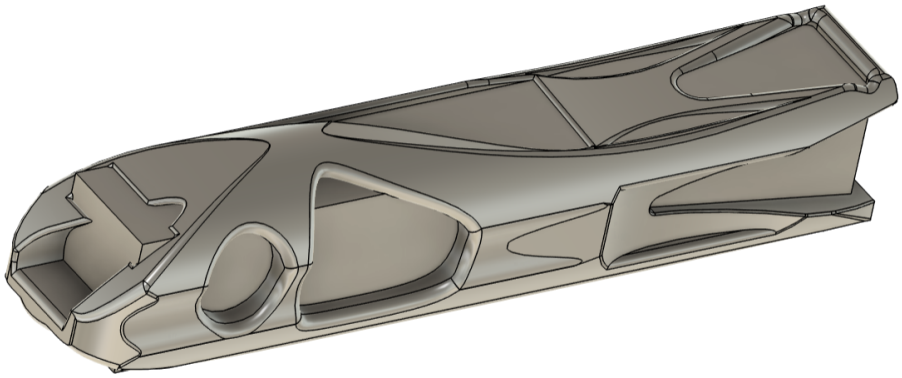

Figure 7.15: ”Maestro 1” including inner prism. (Source: Author’s own work)

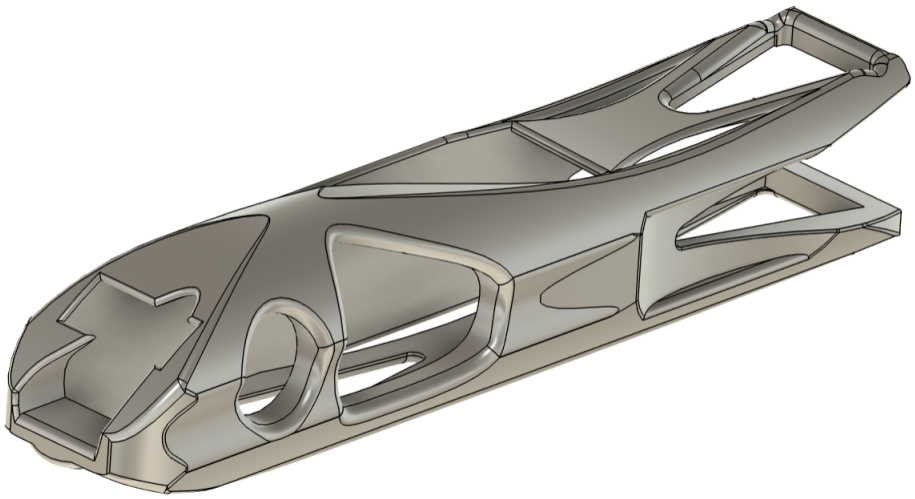

Figure 7.16: ”Maestro 2”, excluding inner prism. (Source: Author’s own work)

The resulting stresses for the Maestro were substantially larger than any test in the ”Master” series, see Table 7.2. For this reason, the ”Maestro” series was discontinued after two iterations.

Table 7.2: Results of the ”Maestro” series

Iteration	Mass (kg)	Drop test (MPa) (5mm/2mm/ 1mm)	Drop test(contact force)(5mm) (N)	Shock test (MPa)	Closest mode (Hz)
Maestro 1	0,939	58,932 / 69,8383 / 132,12	4702	x:1822,6 y:241,56 z:1171,8	358,48
Maestro 2 (Hollow)	0,809	41,435 / 64,04 / 79,657	2837,1	x:2882,1 y:225,14 z:2610,9	134,13 (multiple within range)

And so, to summarize, Master 13.7 was still the enclosure being moved forward with. A detailed render of the model can be viewed in Figure 7.17 below.

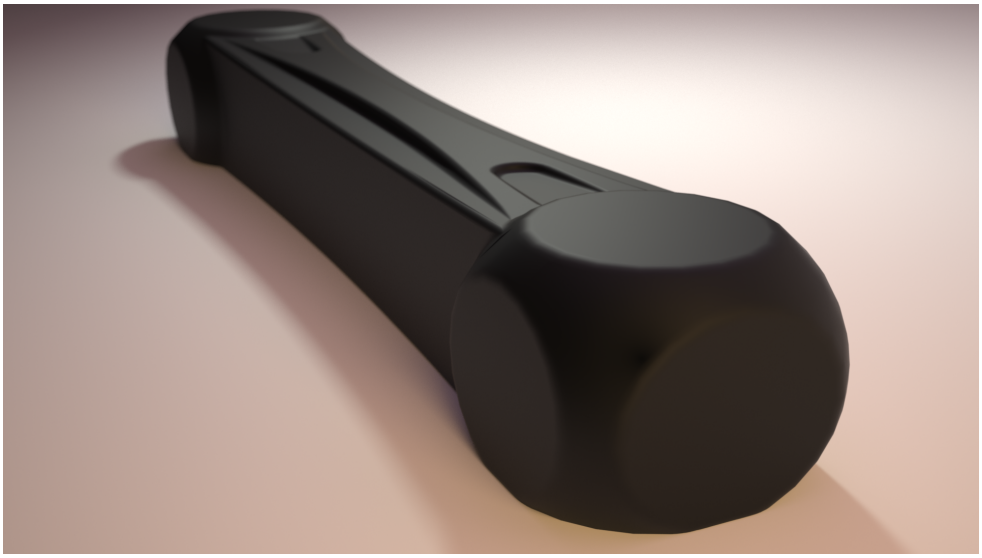

Figure 7.17: ”Master 13.7”, rendered in Maxwell Studios (Source: Author’s own work)

8 Inner Structure

The final portion of the process involved the design of the inner structure. The goal, which was motivated by the design brief, was to minimize weight without compromising structural integrity. To do so, besides the reinforcements already added, it was decided to utilize lattice structures.

8.1 Preparations

To insert a lattice throughout the whole model was considered not feasible. For this reason, the model was split up into one tunnel and two ends (see Figure 8.1). This way the ball-like ends, which carried a large proportion of the weight, could be latticed separately. The lattice was produced in ANSYS Discovery and the result looked like in Figure 8.2.

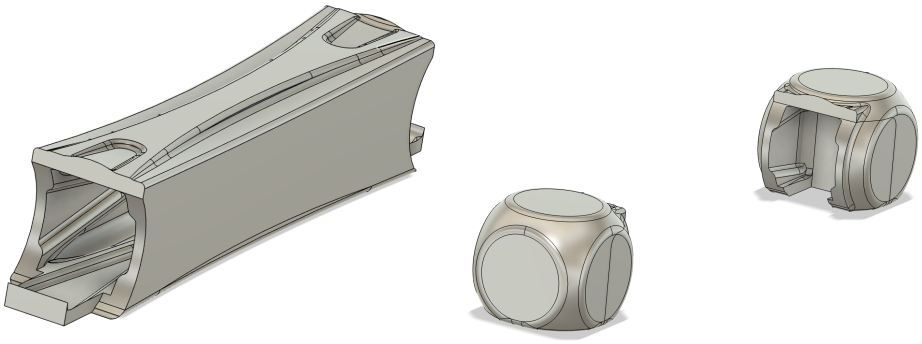

Figure 8.1: ”Master 13.7” split into pieces. (Source: Author’s own work)

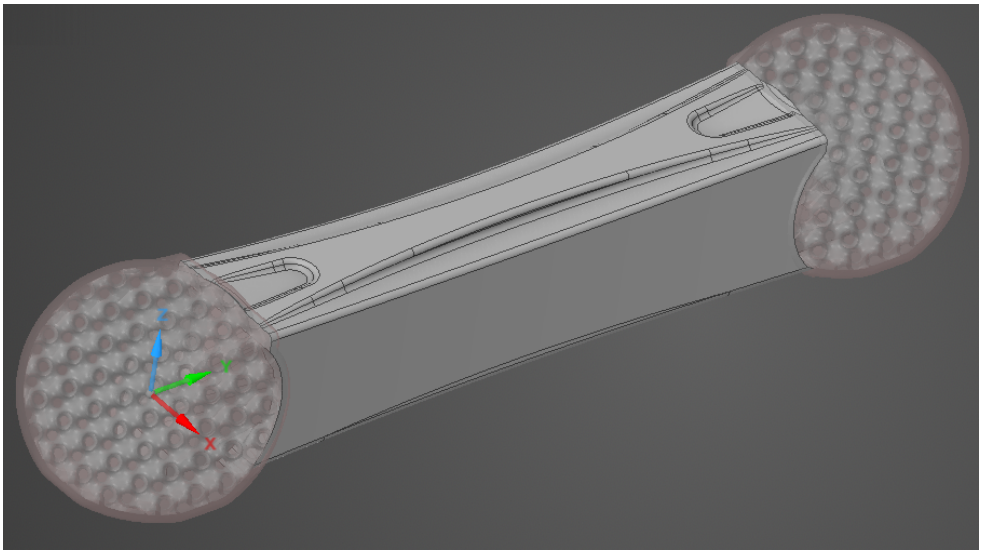

Figure 8.2: Latticed ”Master 13.7” in ANSYS Discovery. (Source: Author’s own work)

8.2 Testing and results

The testing was initially focused on cubic lattices, with the aim of testing the effects of various settings and measurements. It was also interesting to investigate the effect of lattice density and orientation. Diamond and cubic were used as they are bending-dominated, and could, in theory, have good energy absorption. Diamond is low stiffness, cubic is high. Gyroid was used in order to test surface-based lattices. The aspiration was to keep this section short.

SLS-holes were added in Meshmixer. All tests were meshed using patch-independent tetrahedrons, with great effort. Specific settings may be viewed in Appendix B.

One setting tested was using a boundary conforming lattice or not. Boundary conforming, like the name suggests, conforms to the outer boundary by adding a triangular lattice at the outskirts of the volume. Figure 8.3 shows the first cubic lattice, without a boundary conforming lattice, and ”remove partial segments” instead. Figure 8.4 shows the cubic lattice with boundary conforming. As can be seen in Table 8.1, the boundary conforming lattice had lower shock test stresses and higher drop test stresses compared to the first one.

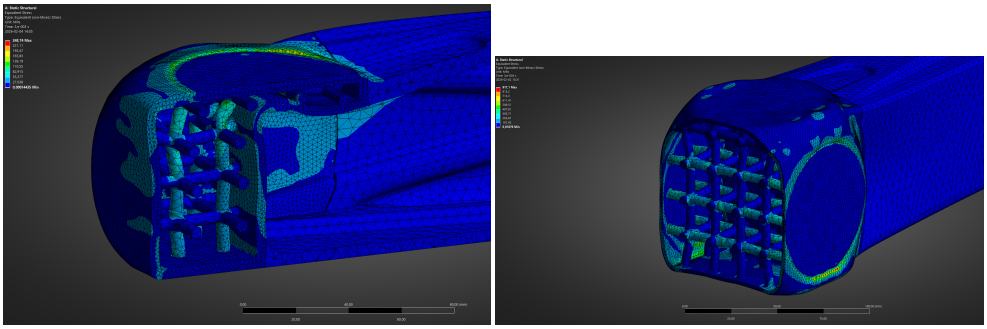

Figure 8.3: Left: First lattice z-direction shock test, section view. Right: First lattice x-direction shock test, section view. (Source: Author's own work)

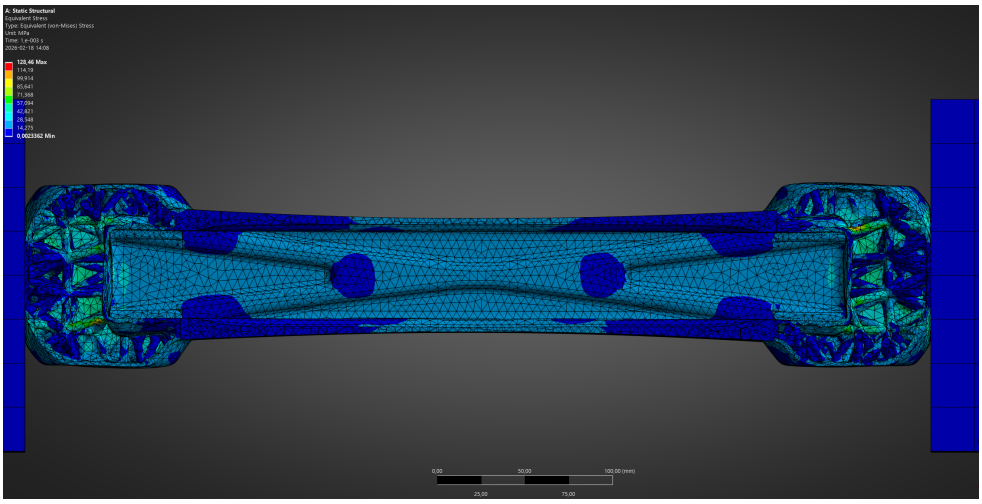

Figure 8.4: Second lattice (boundary conforming) y-direction shock test, section view. (Source: Author's own work)

The next test was a cubic lattice with a higher density, see Figure 8.5, having a fill percentage of 41,22%.

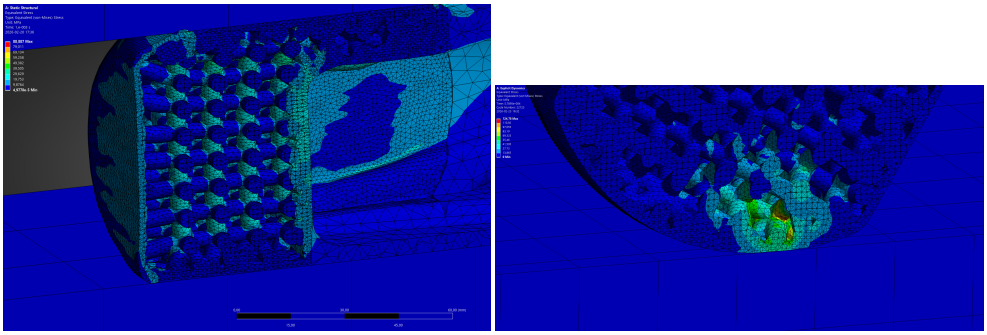

Figure 8.5: Left: Dense lattice z-direction shock test, section view. Right: Dense lattice drop test, section view. (Source: Author's own work)

The fourth and final cubic lattice was created at an angle. It was turned 45° around one axis, and 45° around an axis perpendicular to that one, creating the lattice seen in Figure 8.6. These angles were labeled θ and ϕ in Table 8.1. This test exhibited the lowest drop test stresses of all lattices.

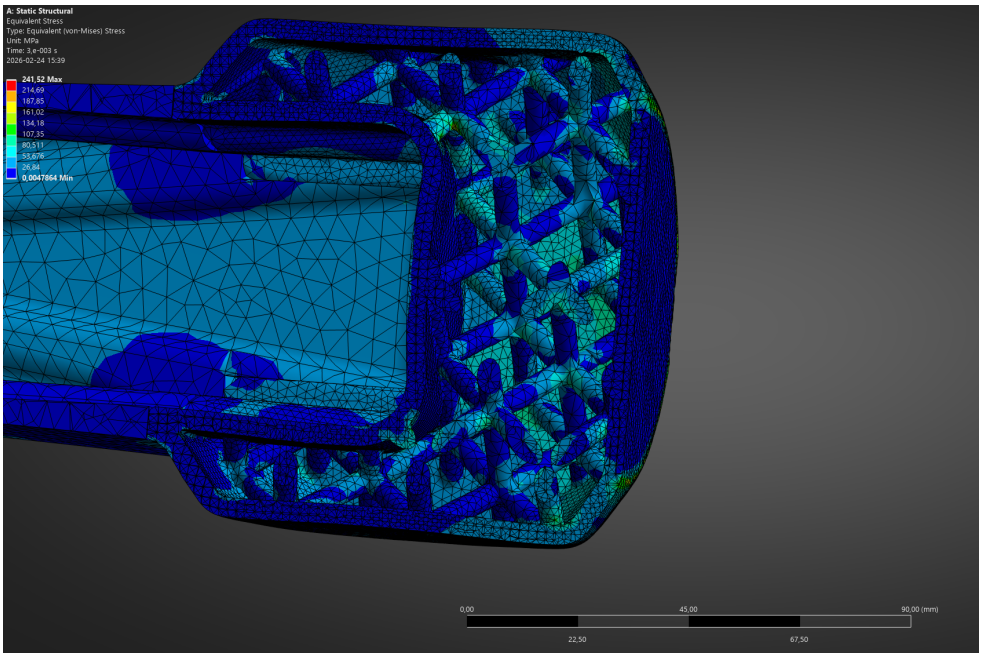

Figure 8.6: Rotated lattice y-direction shock test, section view. (Source: Author's own work)

The subsequent two lattices were a bit more ”exotic”. The first one was a gyroid lattice with a 30 mm period length. The results can be viewed in Figure 8.7, Figure 8.8 and Table 8.1.

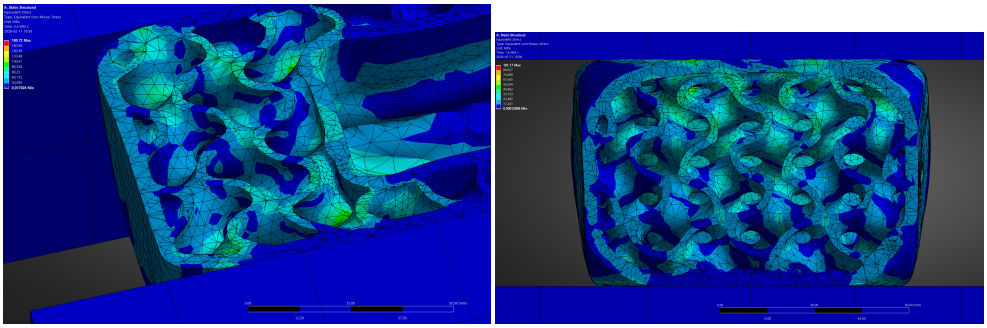

Figure 8.7: Left: Gyroid lattice x-direction shock test, section view. Right: Gyroid lattice z-direction shock test, section view. (Source: Author's own work)

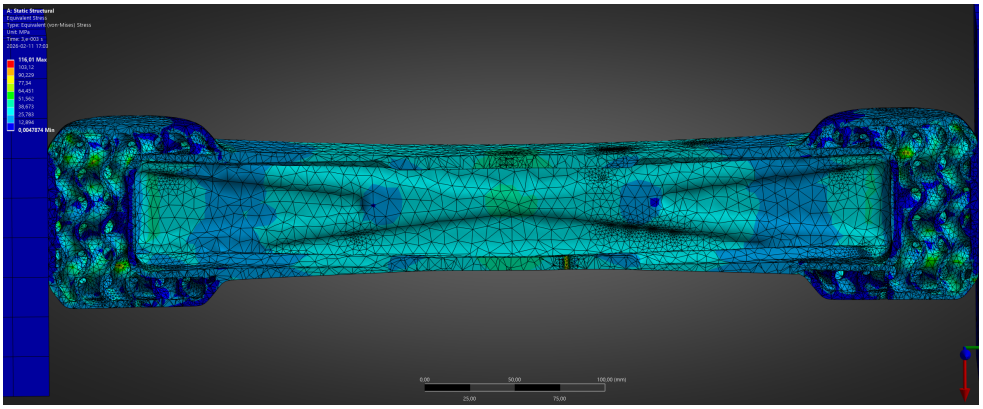

Figure 8.8: Gyroid lattice y-direction shock test, section view. (Source: Author's own work)

The final lattice was the diamond lattice, see Figure 8.9. This lattice was chosen due to its capability for high deformation and energy absorption. What ought to be remarked is the drop test result. As can be seen in Table 8.1, the test displayed a peak stress of 3261,2 MPa, causing the author to suspect wrongdoing. However, since no mistakes could be found on closer inspection, the result remained.

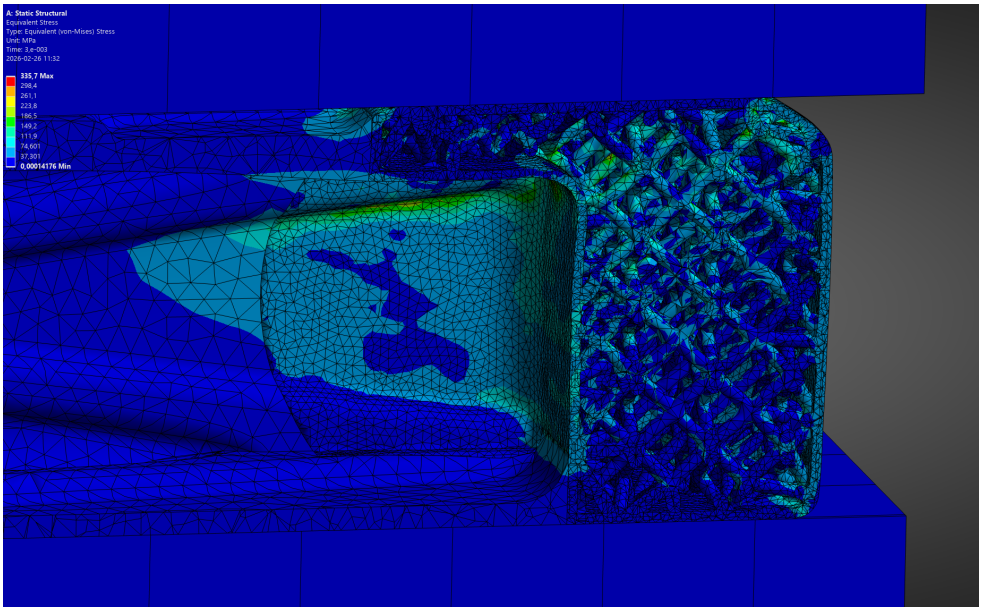

Figure 8.9: Diamond lattice z-direction shock test, section view. (Source: Author's own work)

Table 8.1: Lattice testing in Master 13.7

Lat.	Shell (mm)	Fill (%)	L (mm)	t (mm)	Ori.	Trim	m (kg)	Drop (MPa) + Contact (N)	Shock (MPa) (x,y,z)	Modal (Hz)
Cubic	2	12,53	20	5	$\theta = 0°$ $\phi = 0°$	R.P.S	0,855	97,086 899	x:917,1 y:370,4 z:248,74	204,00
Cubic	2	12,53	20	5	$\theta = 0°$ $\phi = 0°$	B.C	0,921	143,2 1895,6	x:148,04 y:128,46 z:172,8	418,65
Cubic	2	41,22	10	5	$\theta = 0°$ $\phi = 0°$	B.C	1,275	124,78 5517,4	x:151,32 y:95,817 z:88,887	395,54
Cubic	4	12,53	20	5	$\theta = 45°$ $\phi = 45°$	R.P.S	1,204	59,677 2420,9	x:266,96 y:241,52 z:350,51	291,79
Gyroid	4	20,57	30	2	$\theta = 0°$ $\phi = 0°$	None	1,098	91,261 6475,2	x:180,72 y:116,01 z:101,17	282,23
Diamond	2	14,65	15	3	$\theta = 0°$ $\phi = 0°$	B.C	0,916	3261,2 59688	x:372,15 y:195,54 z:335,7	305,55

As can be noted from the table, no latticed design had any modes in the 7–200 Hz range. It can also be noted that there were no stresses below 48 MPa.

8.3 Choice of lattice

As an analysis of the results, the values x_{drop} and x_{shock} were developed, allowing for comparison between the designs. The values were defined as:

$$x_{drop} = \frac{m_{lat.design}}{m_{Master13.7}} \sigma_{drop} \tag{8.1}$$

$$x_{shock} = \frac{m_{lat.design}}{m_{Master13.7}} \sigma_{shock,y} \tag{8.2}$$

It was reasoned that due to the awkward shape of the latticed volumes, which caused cramped areas, the stresses in x- and z- directions did not fairly represent the potential of the lattice. For this reason, as can be seen in (8.2), only the stresses in the y-direction were used for the shock test value.

Furthermore, the ratio between the mass of the latticed design and the original mass encourages lower masses.

When calculating this for all lattices, Table 8.2 below emerges.

Table 8.2: Comparative values for the different lattices

Lattice	x_{drop}	x_{shock}	**Average**
Cubic 1	49,54	188,997	119,27
Cubic 2	78,78	70,63	74,71
Cubic 3	94,91	72,88	83,89
Cubic 4	36,48	147,65	92,07
Gyroid	59,83	76,05	67,94
Diamond	1783,85	106,96	945,40

Because the gyroid lattice had the lowest values, it was deemed the most promising. The second lowest was the boundary conforming cubic lattice (Cubic 2).

9 Printing

The ”Master 13.7” model was subsequently SLS-printed, along with a sectioned version displaying the gyroid lattice. The printing was done using PA 1101, besides one scale model which was FDM-printed using PLA filament. The printed models can be viewed in Figures 9.1–9.3. SLS process pictures can be viewed in Figure 9.4.

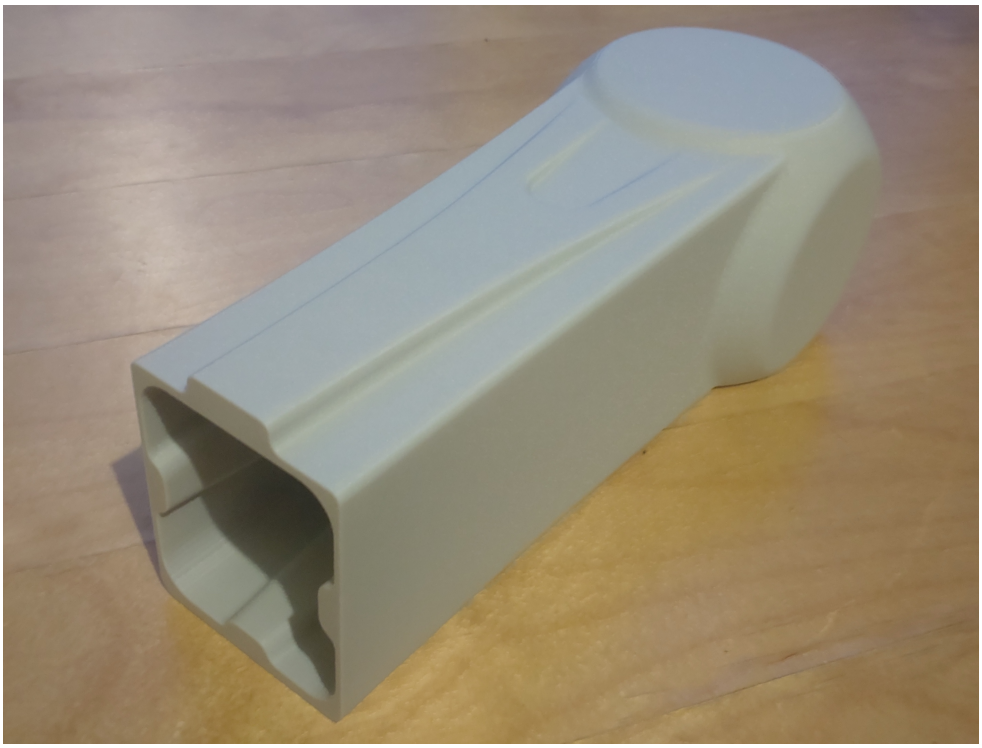

Figure 9.1: One half of ”Master 13.7” FDM-printed to scale. (Source: Author’s own work)

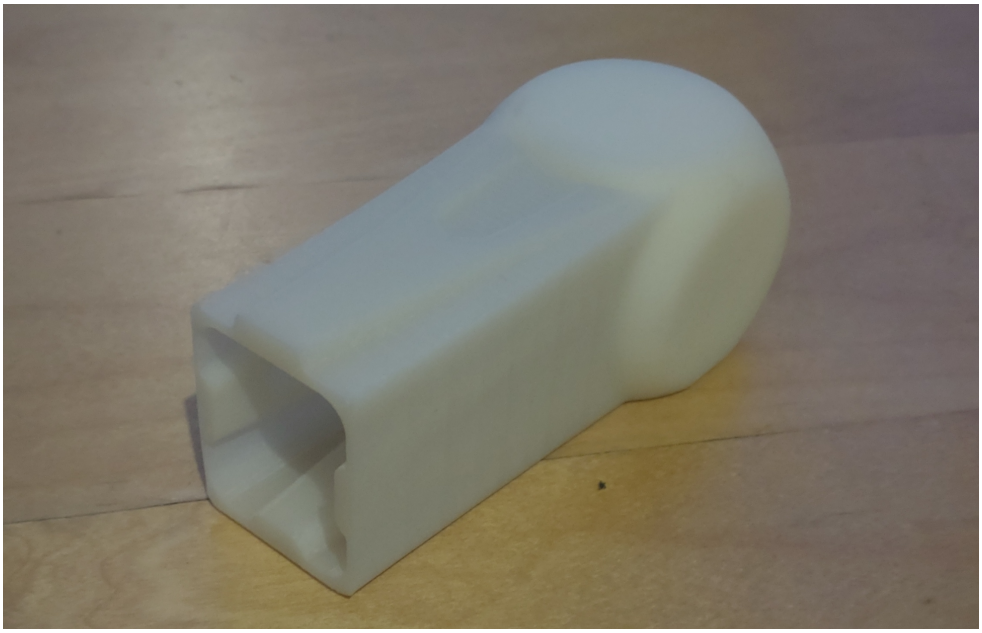

Figure 9.2: One half of ”Master 13.7” SLS-printed at 1/8th volume (1:2 length scale). PA1101. (Source: Author’s own work)

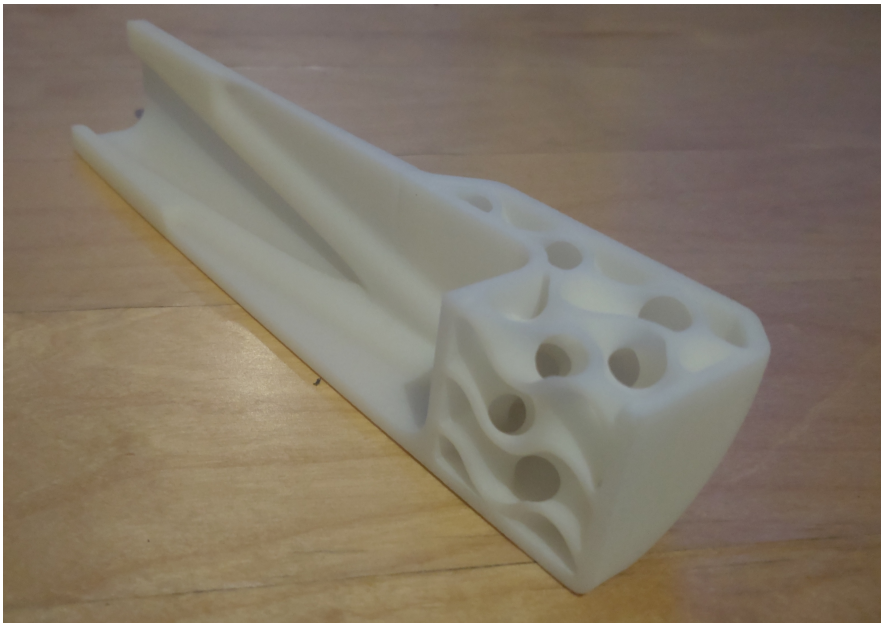

Figure 9.3: 1/8 slice of gyroid latticed ”Master 13.7”, printed using SLS, PA1101. (Source: Author’s own work)

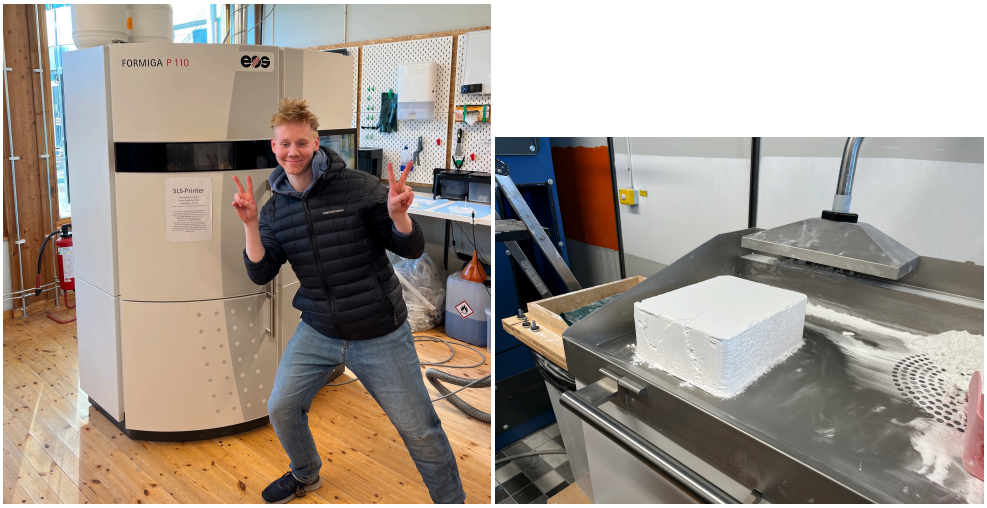

Figure 9.4: Left: The author posing in front of the SLS machine. Right: PA1101 powder before extracting the model. (Source: Author's own work)

10 Reflection and Discussion

10.1 Was the brief fulfilled?

In the end, the Master 13.7 model (without lattice) managed to match most of the criteria in the developed design brief, in simulations. It at least passed the FEM versions of the drop, shock and vibration tests set up for this project. While the thermal test was not verified properly, the high melting points of PA 2200 and PA 1101 give it a good chance of passing it. However, drastic temperature changes do still impact the mechanical properties of polymer materials, and can cause failures, such as crack formations. To further investigate this, a real test must be performed.

The design was also printable, both with lattice and without, and the mass was relatively low. That being said, the mass and printability criteria were not very specific, and improvements could be made with more work dedicated to these topics specifically. For one, more work could be done improving the lattices which in this project were not successful in removing mass without higher stresses.

The one part of the brief missing is testing with a battery containing the capabilities and components mentioned in section 3.5.2. And quite frankly, designing an enclosure with all parts, which also passes the shock tests, would be a demanding task. The attachment mechanism specifically, see Figure 3.2 for an example, would surely introduce multiple high stress areas. Having said that, it might as well be an issue of the tests being too rigid. As will be discussed in section 10.3, there is an argument to be made for a more lenient test where high stresses, and even breakage, is allowed in small amounts.

10.2 Was the purpose fulfilled?

As can be seen in Chapters 1–4, the brief was largely based on the problem formulation, which in turn was based on the purpose (along with constraints). Judging whether or not the purpose was fulfilled indicates if the brief was logically formulated, for one. More importantly, though, it also addresses the core objective of the project.

10.2.1 FEM and topology optimization within the process

One part of the purpose was to investigate the use of FEM and topology optimization in a design process. In a project such as this one, the use of FEM was helpful in many ways. For one, it eliminated the need for testing equipment for everything except final verification. But also, it allowed for a large amount of tests in a short amount of time, utilizing the template workflow described in section 6.2.1. The downside of FEM is of course that it is an approximation and real-life results will differ in expected and unexpected ways. In the context of the double diamond, FEM was used for converging on designs by means of testing, comparing and disqualifying. Both FEM and topology optimization were also used indirectly for divergence, since these results inform ideas and improvements. The benefit of using topology optimization was less clear. The difficulty in using it for such a project comes from the large number of criteria. At first glance it might seem as if it is only the three tests that need to be considered. However, there were also must-haves in the design which were implied by circumstances. For example, the enclosure must cover the whole battery, it needs a straight surface for the attachment mechanism and it should probably be symmetric. Add to this the dilemma of contact points being fixed (see section 6.4.4) and it becomes clear that getting a finished result just from topology optimization is not feasible. And the attempt to do so, the ”Maestro”, was not successful. The manner in which it was used instead in this project was as an inspiration and learning tool. By optimizing many types of models and design spaces, conclusions and design principles could be deduced and used for the following designs and iterations. The downside is the time needed and thought required to integrate it into the project. It is unclear if this effort was justified as it is possible that the conclusions gained would have been gained anyway.

10.2.2 Viable product?

The viability of the end product was not something treated in this project directly, however, it is relevant when evaluating whether or not an AM battery enclosure is promising. For one, the weight was higher than other products on the market, supposedly. That being said, with the extra weight comes extra robustness and longevity. Also, the extra weight added is still low compared to the weight of the whole e-scooter. The cost is another relevant factor in the viability. As mentioned in Chapter 9, printing half of Master 13.7 (without lattice) would cost 2269 kr at the university, according to the staff. This is higher than the price point of most e-scooter batteries including the battery pack. Having said that, the prices would of course be lower in mass production, using many SLS printers, and the cheaper PA 12. On the other hand, the FDM-printed part was significantly cheaper, costing only

around 150 kr for a whole model. PLA, the material often used for FDM, does, however, have lower yield strength on the layer direction. But if it was to be the case that the brief was too strict then FDM could be a promising alternative. Further investigation would have to be made from a business perspective in order to properly evaluate the viability. One needs to consider that injection molding is what these likely will be compared to.

10.2.3 AM in battery enclosure design

Based on the results in this project, the use of AM for e-scooter batteries cannot be ruled out. There is, however, a lot of work and testing left to do, especially due to the assumptions and approximations made in the simulations. In order to get a clearer answer, real-life testing must be carried out.

10.3 Discussing the Methodology

A major simplification made was the choice to exclude the battery and its weight. This was, as mentioned in section 6.2, done in order to simplify, since the weight of the battery was not known. This does, however, impact the load case and results significantly, and in hindsight, adding an estimated mass might have increased the accuracy. With a higher mass, the drop stresses can be expected to be higher. This does, however, depend on how the battery is fitted within the inner cavity, which affects how impact energy is transferred. A loose fitting battery would also not be affected by the shock test, since it would not take on any load. Finally, a higher mass should logically decrease the natural frequencies. However, the manner in which the battery is fitted is still important.

The way the brief was formulated also impacted the methodology greatly. For one, the brief demands that the enclosure at no point exceeds the yield stress. This disqualifies any enclosure which uses sacrificial material as protection. This is where the ”spike” design becomes an important example. Had this type of concept been allowed, then such a solution, with intentional breaking points, would be highly effective in protecting the battery. The IEC and UN standards are also not very clear on this, simply specifying ”no rupture”. Nevertheless, formulating the brief in such a lenient way would likely lead to all kinds of loopholes, thus complicating the FE analysis substantially. An argument could also be made for ignoring the IEC tests, as they are not mandatory in the same way the UN requirements are. This would make the tests even more forgiving. The rigidity of the tests also becomes relevant when comparing to the model inspired by a real product, see Figure 6.10. The fact that the model had such high stresses might

indicate that the tests were in fact too rigid. And if that is the case, then the simple rectangular, see Figure 6.11, could be strong enough, making it the obvious choice due to its simplicity. On the other hand, there is no real room for improvement on this concept, which is why it was not deemed promising for fulfilling the brief established in this project.

Here, the need for an actual test with proper machines, with an actual battery becomes apparent. Having actual test results would end most of the speculation and uncertainty. Furthermore, the accuracy of the FEA could be assessed in comparison to actual results.

Another issue with the methodology was with the lattices and their compatibility with the design. ”Master 13.7” was optimized with no lattice in mind. Furthermore, it passed the tests through being rigid. Adding a lattice in some ways undoes this work, disrupting the balance already established. Some of the lattices also rely on high deformation and energy absorption. As could be observed in many FE analyses, the ends often took all the stress, making the rest of the design pointless. The exception to this was the gyroid lattice which, as is seen in Figures 8.7 and 8.8, showed evenly distributed stresses.

10.4 Limitations and contributions

The research contributions from this project come both in the form of results and methodologies. The resulting ”Master 13.7” is presented as a potential e-scooter battery shape. Furthermore, all the FE simulations, including the lattice testing, provide a type of empirical data which can be expanded upon in the future.

The thesis also presents a methodology which includes all necessary aspects, along with the context from which these aspects came. The modified double diamond showcases how the double diamond can be reshaped for an optimization project. Furthermore, the optimization methodology itself provides a blueprint for design projects which only use computers.

In a wider sense, the thesis contributes an initial step in investigating the use of AM technology in battery enclosures, as a part of the collaboration between LTH and Glasgow University. While this master thesis specifically targets e-scooter batteries, its conclusions have implications for all LMT-batteries.

The thesis’ limitations stem primarily from simplifications made in the brief and the FEM tests. While making the project more manageable, these simplifications make the results more ambiguous and hard to interpret. Consequently, in conjunction with lack of physical tests, the thesis cannot provide a definite answer to the main

purpose. Furthermore, the project had quite a wide scope considering the time available, which led to some activities not being done in time.

10.5 Future improvements on the design

One immediate improvement would be of the ends. Their odd shape caused cramped areas for the lattices. As a result, it did not allow for much deformation and energy absorption. If they, on the other hand, were more separated from the tunnel, they could be more ball-shaped, almost like having two foam balls at the end.

More testing would also be done with the gyroid lattice. Making the period lengths lower, or changing the orientation might improve performance even further.

Further improvements would also involve incorporating the essential components into the design, some of which are required by EU regulation. Adding an attachment mechanism and a charging port would be a challenge if the brief is to still be fulfilled. Also, if it is to become a real product, the enclosure will also need a lid along with screws, for example, for its attachment.

Finally, more investigation into the ”Dragspel” concept could be made, seeing as it showed promise in the y-directional shock test.

10.6 Future Research

Future research could be about adding a business perspective. That way, one would get a clearer picture regarding whether or not AM has a place in battery enclosure design.

Other interesting research topics would involve investigating the use of lattice optimization, a feature provided in ANSYS.

Another one is a solution to the fixed contact point limitation described in section 6.4.4. It could be a solution where the point updates every iteration.

Finally, it would be interesting to investigate further how topology optimization could be used with a large amount of diverse criteria.

11 Conclusion

The main result of this master's thesis was the design concept ”Master 13.7”, which passed the established FEM tests. While this concept shows the ability to pass relevant regulations, a business perspective is needed in order to assess the actual viability. In particular, other manufacturing methods need to be compared in terms of cost. The final result also lacks the essential components specified in the brief. Hence, more research is required before the ”Master 13.7” is adopted into an actual product.

The modified double diamond successfully included the aspects necessary for this type of design process. While appending an optimization phase and a lattice phase, it maintained the philosophy of convergent and divergent thinking. Furthermore, the emphasis on testing led to the discovery of new design concepts which otherwise would have been overlooked.

The optimization phase of the diamond included a large number of simulations, iterations and testing. This procedure showcased what is possible for a low-budget project which uses only a computer. While both FEM and topology optimization played a key part in this process, the usefulness of the topology optimization was questioned. Hence, it might be relevant to inquire whether or not there might be better uses for this tool. The lattice structures, similarly, were rather ineffective in the project, being unsuccessful in improving the original ”Master 13.7” design. This indicates the need for an improved methodology as well as a greater focus on this part in particular.

In the context of the collaboration between LTH and Glasgow University, this thesis provides a starting point in terms of research and proposed methodology. The challenges discussed above clearly showcase the large scope this project attempts to undertake, and more work is required in order to get conclusive results. Determining AM's place in battery enclosure design requires improved methods, more research and proper testing. The assumptions, simplifications and approximate numerical methods used in this thesis are insufficient without physical testing to verify the results. And so, by further developing and improving the concepts in this thesis, clearer answers and better methodologies may be obtained. If this is done, the author finds it likely that additive manufacturing will expand into the world of battery enclosures.

References

[1] IEA. *Global EV Outlook 2025*. Available at https://www.iea.org/reports/global-ev-outlook-2025. [Online]. 2025.

[2] V. Mehranfar and C. Jones. “Exploring implications and current practices in e-scooter safety: A systematic review”. In: *Transportation Research Part F: Traffic Psychology and Behaviour* vol. 107 (2024). [Online], pp. 321–382.

[3] Philip J. Flores. “Not all green innovations are created equal: Consumer innovativeness and motivations in the adoption of shared micromobility”. [Online]. Doctoral dissertation. Lund, Sweden: Lund University School of Economics and Management, 2023.

[4] L Larsson. *Five years since electric scooters’ introduction in Sweden – here’s why people use them*. Accessed: 2026-01-12. Oct. 2023. URL: https://www.lusem.lu.se/article/five-years-electric-scooters-introduction-sweden-heres-why-people-use-them.

[5] S. Gössling. “Integrating e-scooters in urban transportation: Problems, policies, and the prospect of system change”. In: *Transportation Research Part D: Transport and Environment* 79 (Feb. 2020). [Online].

[6] S. AlKheder and Z. Albaghli. “Optimization of location-allocation for charging stations of shared electric scooters in Kuwait”. In: *Case Studies on Transport Policy* 22 (Dec. 2025). [Online].

[7] N. H. Dipu. “An overview of additive manufacturing technology: Generic steps, fundamental categories, advantages, disadvantages, and applications”. In: *Case Studies on Transport Policy* 2.4 (Dec. 2025). [Online].

[8] O. Deigel et al. *A Practical Guide to Design for Additive Manufacturing*. 152 Beach Road, #21-01/04 Gateway East, Singapore 189721, Singapore: Springer Nature Singapore Pte Ltd., 2019. ISBN: 978-981-13-8281-9.

[9] D. Thomas. “Costs, benefits, and adoption of additive manufacturing: a supply chain perspective”. In: *The International Journal of Advanced Manufacturing Technology* 85 (Nov. 2015). [Online], pp. 1857–1876.

[10] ASTM International. *Wohlers Report 2025 shows 9.1% AM industry growth*. Accessed: 2026-12-05. Mar. 2025. URL: https://www.astm.org/news/press-releases/wohlers-report-2025.

[11] W.K. Liu et al. “Eighty Years of the Finite Element Method: Birth, Evolution, and Future”. In: *Archives of Computational Methods in Engineering* 29.6 (June 2022). [Online], pp. 4431–4453.

[12] H. Werkle. *Finite Elements in Structural Analysis: Theoretical Concepts and Modeling Procedures in Statics and Dynamics of Structures*. Gewerbestrasse 11, 6330 Cham, Switzerland: Springer Nature, 2021. ISBN: 978-3-030-49840-5.

[13] J. Lógó and H. Ismail. “Milestones in the 150-Year History of Topology Optimization: A Review”. In: *Computer Assisted Methods in Engineering and Science* 27.2–3 (2020). [Online], pp. 97–132.

[14] C.A. Floudas and P.M. Pardalos. *Encyclopedia of Optimization*. 2nd ed. Springer, 2009. ISBN: 978-0-387-74759-0.

[15] Elgiganten. *Ninebot by Segway KickScooter batteri till ES1 och ES2 – N2GBAT190*. [Online]. Available: https://www.elgiganten.se/product/sport-fritid/elfordon/tillbehor-till-elsparkcykel/ninebot-by-segway-kickscooter-batteri-till-es1-och-es2-n2gbat190/N2GBAT190. Accessed: 2025-09-22.

[16] HX Electric Scooter. *X8 scooter battery*. [Online]. Available: https://hxescooter.com/product/x8-scooter-battery/. Accessed: 2025-09-22.

[17] Electric Pedal Power. *What’s inside an e-bike & electric scooter battery: How e-bike batteries work*. [Online]. Available: https://www.electricpedalpower.com.au/blogs/news/whats-inside-an-ebike-electric-scooter-battery-how-ebike-batteries-work. Accessed: 2025-12-10. Jan. 2024.

[18] Design Counsil. *The Double Diamond: A universally accepted depiction of the design process*. Accessed: 2025-09-30. Oct. 2019. URL: `https://www.designcouncil.org.uk/our-resources/archive/articles/double-diamond-universally-accepted-depiction-design-process`.

[19] D. Norman. *The Design of Everyday Things: Revised and Expanded Edition*. 250 West 57th Street, 15th Floor, New York, New York 10107: Basic Books, 2013. ISBN: 978-0-465-05065-9.

[20] K. T. Ulrich and S. D. Eppinger. *Product Design and Development*. 5th. London, United Kingdom: McGraw-Hill, 2012. ISBN: 978-0-07-340477-6.

[21] M. M. Casanovas. “Exploring Design Thinking Methodologies: A Comprehensive Analysis of the Literature, Outstanding Practices, and Their Linkage to Sustainable Development Goals”. In: *Sustainability* 17.15 (2025). [Online], p. 7142.

[22] T. Brown. “Design Thinking”. In: *Harvard Business Review* (June 2008). [Online].

[23] M. Kochanowska and W.R. Gagliardi. “The Double Diamond Model: In Pursuit of Simplicity and Flexibility”. In: *Perspectives on Design II*. [Online]. Cham, Switzerland: Springer, 2021, pp. 19–32.
[24] D. Godec et al. *A Guide to Additive Manufacturing*. Gewerbestrasse 11, 6330 Cham, Switzerland: Springer Nature Switzerland AG, 2022. ISBN: 978-3-031-05863-9.
[25] D. Bourell et al. “A Brief History of Additive Manufacturing and the 2009 Roadmap for Additive Manufacturing: Looking Back and Looking Ahead”. In: *US-TURKEY Workshop On Rapid Technologies* (2009).
[26] I.M. Alarifi. “Revolutionising fabrication advances and applications of 3D printing with composite materials: a review”. In: *Virtual and Physical Prototyping* 19.1 (2024).
[27] T.D. Ngo et al. “Additive manufacturing (3D printing): A review of materials, methods, applications and challenges”. In: *Composites Part B: Engineering* 143 (June 2018), pp. 172–196.
[28] Hubs (Protolabs Network). *What is FDM (fused deposition modeling) 3D printing*. [Online]. Available: https://www.hubs.com/knowledge-base/what-is-fdm-3d-printing/. Accessed: 2026-01-05.
[29] C. Zadeh et al. “Establishing a process-structure-property-performance framework for SLS additive manufacturing through integrated multiscale modeling”. In: *Materials Design* 257 (Sept. 2025).
[30] I. Gibson et al. *Additive Manufacturing Technologies*. 3rd. Gewerbestrasse 11, 6330 Cham, Switzerland: Springer Nature, 2021. ISBN: 978-3-030-56127-7.
[31] Hubs (Protolabs Network). *What is SLS 3D printing? A guide to selective laser sintering*. [Online]. Available: https://www.hubs.com/knowledge-base/what-is-sls-3d-printing/. Accessed: 2026-01-03.
[32] G. Colucci et al. “Additive Manufacturing of a PA11 Prototype Fabricated via Selective Laser Sintering for Advanced Industrial Applications”. In: *Polymer* 17 (Nov. 2025).
[33] M. Hassan et al. “3D printing in upcycling plastic and biomass waste to sustainable polymer blends and composites: A review”. In: *Materials Design* 237 (Jan. 2024).
[34] J. Zhao et al. “Bending-dominated to compression-dominated transition mechanism in additively-manufactured lattice structures”. In: *Materials Today Communications* 48 (Sept. 2025).
[35] A. Alghamdi et al. “Effect of additive manufactured lattice defects on mechanical properties: an automated method for the enhancement of lattice

geometry". In: *The International Journal of Advanced Manufacturing Technology* 108 (May 2020), pp. 957–971.
[36] M. Omidi and L. St-Pierre. "Mechanical Properties of Semi-Regular Lattices". In: *Materials Design* 213 (Jan. 2022).
[37] Y. Li et al. "High Mechanical Performance of Lattice Structures Fabricated by Additive Manufacturing". In: *Metals* 14 (Oct. 2024).
[38] M. Nasim and U. Galvanetto. "Mechanical characterisation of additively manufactured PA12 lattice structures under quasi-static compression". In: *Materials Today Communications* 29 (Dec. 2021).
[39] J. Mueller et al. "Energy Absorption Properties of Periodic and Stochastic 3D Lattice Materials". In: *Advanced Theory and Simulations* 2 (Aug. 2019).
[40] P.D. Fabbro et al. "Analysis of a Preliminary Design Approach for Conformal Lattice Structures". In: *Applied Sciences* 11 (Dec. 2021).
[41] S.M. Ahmadi et al. "Additively Manufactured Open-Cell Porous Biomaterials Made from Six Different Space-Filling Unit Cells: The Mechanical and Morphological Properties". In: *Materials* 8 (Apr. 2015).
[42] Z. Ozdemir et al. "Energy absorption in lattice structures in dynamics: Experiments". In: *International Journal of Impact Engineering* 89 (Mar. 2016).
[43] X. Yin et al. "Design and mechanical characterization of novel triply periodic minimal surface-based lattice structures with high strength and energy absorption". In: *Composite Structures* 382 (Apr. 2026).
[44] A.K. Roopa et al. "Mechanical and dynamic behavior of sustainable smart PLA polymeric-based 3D printed gyroid structures for vibration control applications". In: *Discover Sustainability* 7 (Dec. 2025).
[45] M.S. El-Asfoury et al. "Orientation driven design and mechanical optimization of gyroid TPMS lattice structures". In: *Scientific Reports* 16 (Jan. 2026).
[46] Z. Wang et al. "Orientation driven design and mechanical optimization of gyroid TPMS lattice structures". In: *Additive Manufacturing* 97 (Jan. 2025).
[47] M. Vafaeefar et al. "Experimental and Computational Analysis of Energy Absorption Characteristics of Three Biomimetic Lattice Structures Under Compression". In: *Journal of the Mechanical Behavior of Biomedical Materials* 151 (Mar. 2024).
[48] F. Awaja et al. "Cracks, microcracks and fracture in polymer structures: Formation, detection, autonomic repair". In: *Progress in Materials Science* 83 (Oct. 2016).
[49] EOS GmbH Electro Optical Systems. *PA2200 (PA12) Material Datasheet*. [Online]. Available: https://www.epfl.ch/schools/sti/ateliers/wp-content/uploads/2019/07/sls_PA2200_EOS-1.pdf. Accessed: 2025-10-10. July 2019.

[50] Professional Plastics. *Mechanical Properties of Plastic Materials*. [Online]. Available: https://www.professionalplastics.com/professionalplastics/MechanicalPropertiesofPlastics.pdf. Accessed: 2025-10-10.

[51] EOS GmbH Electro Optical Systems. *PA 1101*. [Online]. Available: https://www.vexmatech.com/assets/datasheets/sls/PA1101.pdf. Accessed: 2025-10-10. Nov. 2018.

[52] Ultimaker. *Ultimaker PLA Technical data sheet*. [Online]. Available: https://um-support-files.ultimaker.com/materials/2.85mm/tds/PLA/Ultimaker-PLA-TDS-v5.00.pdf. Accessed: 2025-12-10. Apr. 2022.

[53] MatWeb. *Overview of materials for Acrylonitrile Butadiene Styrene (ABS), Molded*. [Online]. Available: https://matweb.com/search/DataSheet.aspx?MatGUID=eb7a78f5948d481c9493a67f0d089646ckck=1. Accessed: 2025-12-10.

[54] *Regulation (EU) 2023/1542 of the European Parliament and of the Council of 12 July 2023 concerning batteries and waste batteries, amending Directive 2008/98/EC and Regulation (EU) 2019/1020 and repealing Directive 2006/66/EC, consolidated to 31 July 2025*. [Online]. Available: https://eur-lex.europa.eu/legal-content/EN/TXT/PDF/?uri=CELEX:02023R1542-20250731. Official Journal of the European Union (OJ L 191, 28.7.2023, p.1–117). Accessed: 2025-10-24.

[55] Side Project. *Fixing 36v electric scooter battery on the budget (Turboant x7 pro)*. YouTube video, Mar. 26, 2021. [Online]. Available: https://www.youtube.com/watch?v=uXHWH7Jpef8. Accessed: 2025-09-29.

[56] R.K. Chidambaram et al. “Structural assessment of electric two-wheeler battery enclosure: thermal and structural study”. In: *Journal of Thermal Analysis and Calorimetry* 150 (Aug. 2024), pp. 6939–6958.

[57] K.R. Ngoy et al. “Lithium-ion batteries and the future of sustainable energy: A comprehensive review”. In: *Renewable and Sustainable Energy Reviews* 223 (Nov. 2025).

[58] TÜV SÜD. *Lithium battery testing under UN DOT 38.3*. [Online]. Available: https://www.tuvsud.com/-/jssmedia/global/pdf-files/whitepaper-report-e-books/tuvsud-lithium-battery-testing-under-un-dot-38-3.pdf. Accessed: 2025-10-15.

[59] United Nations Economic Commission for Europe. *Manual of Tests and Criteria, 8th Revised Edition (ST/SG/AC.10/11/Rev.8), English*. [Online]. Available: https://unece.org/sites/default/files/2024-09/ST_SG_AC.10_11_Rev.8e_WEB.pdf. Nov. 27, 2023. Accessed: 2026-02-24.

[60] H. Rastan. *Sine Sweep Testing: A Practical Guide to Vibration Analysis*. [Online]. https://caeflow.com/vibration_and_acoustics/sine-sweep-vibration-analysis/. Jul. 27, 2025. Accessed: 2025-11-02.

[61] C. F. Lorenzo. *Variable-Sweep-Rate Testing: A Technique to Improve the Quality and Acquisition of Frequency Response and Vibration Data*. NASA Technical Note NASA-TN-D-7022. Cleveland, OH: NASA Lewis Research Center, Dec. 1970.

[62] IEC. *Who we are*. [Online]. https://www.iec.ch/who-we-are. Accessed: 2025-12-05.

[63] International Electrotechnical Commission. *IEC 62133-2, First edition, 2017-Secondary cells and batteries containing alkaline or other non-acid electrolytes — Safety requirements for portable sealed secondary cells, and for batteries made from them, for use in portable applications — Part 2: Lithium systems*. Geneva, Switzerland, 2017.

[64] IEC. *IP ratings*. [Online]. https://www.iec.ch/ip-ratings. Accessed: 2025-11-15.

[65] *Commission guidelines to facilitate the harmonised application of provisions on the removability and replaceability of portable batteries and LMT batteries in Regulation (EU) 2023/1542*. [Online]. https://eur-lex.europa.eu/eli/C/2025/214/oj/eng. Accessed: 2025-11-05.

[66] International Electrotechnical Commission. *Environmental testing — Part 2-78: Tests — Test Cab: Damp heat, steady state*. Geneva, Switzerland, 2001.

[67] ISO. *Space systems — Lithium ion battery for space vehicles — Design and verification requirements*. Geneva, Switzerland, 2024.

[68] ANSYS, Inc. *What is Finite Element Analysis (FEA)?* [Online]. Available: https://www.ansys.com/simulation-topics/what-is-finite-element-analysis. Accessed: 2025-12-20.

[69] N.S. Ottosen and H Peterson. *Introduction to the finite element method*. 1st. Prentice Hall, 1992. ISBN: 978-0134738772.

[70] M. Okeres and S. Keates. *Finite Element Applications: A Practical Guide to the FEM Process*. Gewerbestrasse 11, 6330 Cham, Switzerland: Springer Nature, 2018. ISBN: 978-3-319-67125-3.

[71] O.C. Zienkiewicz. *The Finite Element Method: Its Basis and Fundamentals*. 7th. Butterworth-Heinemann, 2013. ISBN: 978-1-85617-633-0.

[72] COMSOL. *The Finite Element Method (FEM)*. [Online]. Available: https://www.comsol.de/multiphysics/finite-element-method. Accessed: 2026-01-15. 2017.

[73] N.S. Ottosen et al. *Hållfasthetslära: allmänna tillstånd*. Studentlitteratur, 2007. ISBN: 978-91-44-05032-4.

[74] LS-DYNA Support. *What are the differences between implicit and explicit?* [Online]. Available: https://www.dynasupport.com/faq/general/what-are-the-differences-between-implicit-and-explicit/. Accessed: 2025-12-30.
[75] ANSYS, Inc. *What is Explicit Dynamics?* [Online]. Available: https://www.ansys.com/simulation-topics/what-is-explicit-dynamics. Accessed: 2025-12-15.
[76] J. He and Z.-F Fu. *Modal Analysis*. Gewerbestrasse 11, 6330 Cham, Switzerland: Springer Nature, 2001. ISBN: 0 7506 5079 6.
[77] P.W. Christensen and A. Klarbring. *An Introduction to Structural Optimization*. Springer, 2009. ISBN: 978-1-4020-8666-3.
[78] M. Becker. "Topology optimization using a dual method with discrete variables". In: *Structural Optimization* 17 (Aug. 1999), pp. 14–24.
[79] M.P. Bendsøe and O. Sigmund. *Topology Optimization: Theory, Methods, and Applications*. 2nd. Springer, 2018. ISBN: 978-3-662-05086-6.
[80] ANSYS, Inc. *3.2.1.1. Topology Optimization - Density Based Solution Methodology*. [Online]. Available: https://ansyshelp.ansys.com/public/account/secured?returnurl=//Views/Secured/corp/v242/en/mech_struct_opt/ds_topo_solvers.html. Accessed: 2026-01-10.
[81] K. Liu and A. Tovar. "An efficient 3D topology optimization code written in Matlab". In: *Struct Multidisc Optim* 50 (2014), pp. 1175–1196.
[82] K. Schittkowski and C. Zillober. "Sequential Convex Programming Methods". In: *Marti, K., Kall, P. (eds) Stochastic Programming. Lecture Notes in Economics and Mathematical Systems* 423 (1995).
[83] J. Duchi et al. *Sequential Convex Programming: Notes for EE364b, Stanford University*. 2018. [Online]. Accessed: 2026-01-10.
[84] O. Sigmund and K. Maute. "Topology optimization approaches: A comparative review". In: *Struct Multidisc Optim* 48 (2013), pp. 1031–1055.
[85] Q. Ni et al. "Sequential Convex Programming Methods for Solving Large Topology Optimization Problems: Implementation and Computational Results". In: *Journal of Computational Mathematics,* 23 (2005), pp. 491–502.
[86] ANSYS Inc. *Structural Optimization Analysis Guide*. [Online]. Available: https://ansyshelp.ansys.com/public/Views/Secured/corp/v251/en/pdf/Structural_Optimization_in_Mechanical.pdf.
[87] H. Sönnerlind. *Singularities in Finite Element Models: Dealing with Red Spots*. [Online]. https://www.comsol.com/blogs/singularities-in-finite-element-models-dealing-with-red-spots. 2015. Accessed: 2025-11-05.

Appendix A. Project time plan

The following figures show the initial project plan and how the project was eventually carried out.

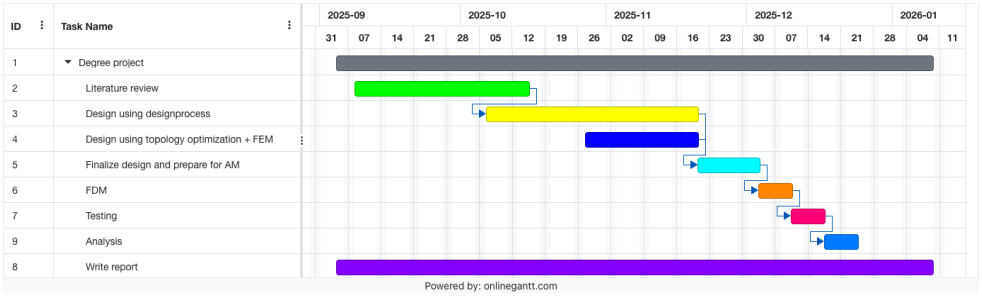

Figure A.1: Project plan.

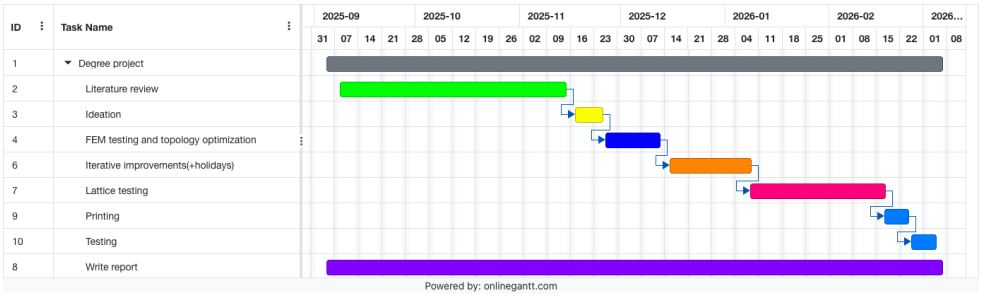

Figure A.2: Performed activities.

The large difference in time is due to not finishing in time for the presentation in January. For this reason, the project was extended until March. The actual plan also has different labels due to changes made in the project after the initial plan was made.

Appendix B. Specific settings

The following appendix contains settings for simulations which were particularly noteworthy or difficult. The computers used had 16 GB of RAM for the most part. Sometimes computers with 32 GB of RAM were also used.

B.1 Drop test, shock test and modal test

The following are the drop test settings used in explicit dynamics.

- ”Default” mesh. Face/edge meshing when having smaller mesh on contact area.
- Face/edge meshing when having smaller mesh on contact area.
- ”Frictionless” contact
- Drop height 1 m (equivalent to -4428,7 m/s in z-direction)
- ”Fixed support” on floor surface.
- Steps: 1. Step end time: 0,001 s.
- Output: von-Mises stresses & contact force (connect this to a graph)

The following are the shock test settings used in static structural.

- ”Default” mesh, 10 mm early on in the process, 5 mm later.
- ”Bonded contacts”
- ”Fixed support” on one wall.
- ”Displacement” on other wall, only free in the relevant direction.
- Acceleration according to eq. 6.1
- Steps: 1. Step end time: 0,003 (important since peak acceleration is at this time)
- Output: von-Mises stresses

The following are the vibration test settings used in modal.

- ”Default” mesh, 10 mm early on in the process, 5 mm later.
- No walls or floor.
- 10 modes to find is usually enough.

B.2 Meshing lattices

The following are some notes that were made about making the meshing for the two most difficult lattices work. The most common issue was the mesh filling in all the space and looking like Figure B.1.

B.2.1 Gyroid

- Repair STL file in Meshmixer.
- Export as one uniform part (Binary format)
- Import STL using ”geometry import” directly in ANSYS Mechanical (do not let it touch Spaceclaim or Discovery)
- Import walls (or floor) directly into ANSYS Mechanical as well.
- Body sizing, whole body, patch-independent tetrahedron, 1 mm minimum size.
- Face sizing, whole surface, default element, 5 mm size.

B.2.2 Dense lattice

- Add the split up model into ANSYS workbench.
- Add dense lattice in Discovery using ”shell”
- Repair model in Spaceclaim
- In Mechanical, mesh tunnel first: Body sizing, default element, 5 mm, mesh defeaturing on (in mesh settings)
- Freeze tunnel mesh.
- Meshing the ends: Patch-independent tetrahedron, mesh defeaturing off (obs. not the same as mesh-based defeaturing, which should be on), 1.5 mm minimum size, pinch tolerance 0,001 mm.

Note: This lattice had around 3 million elements and its drop test took 3 hours to simulate (despite being a 1 ms long step).

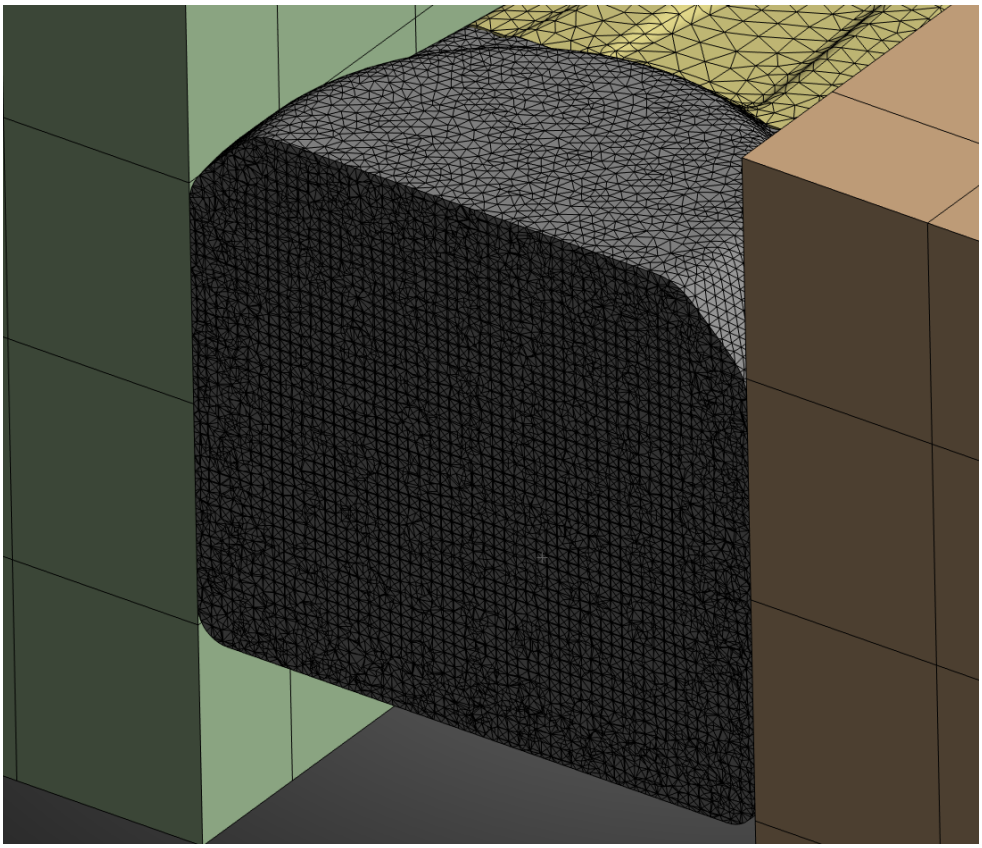

Figure B.1: Unsuccessfully meshed lattice in ANSYS Mechanical. Section view. (Source: Author's own work)